HETEROGENIZED TRANSITION METALS/COMPLEXES INTO THE CLAY MATRIX FOR LIQUID PHASE OXIDATION OF PHENOL DERIVATIVES

A THESIS SUBMITTED TO THE

UNIVERSITY OF PUNE

FOR THE DEGREE OF

DOCTOR OF PHILOSOPHY

(IN CHEMISTRY)

BY

Mr. Vikas S. Kshirsagar

Research Guide

Dr. Chandrashekhar V. Rode

CHEMICAL ENGINEERING AND PROCESS DEVELOPMENT DIVISION

NATIONAL CHEMICAL LABORATORY

PUNE 411 008, INDIA

July 2009

Certificate of the Guide

CERTIFIED that the work incorporated in the thesis entitiled ***"Heterogenized Transition Metals/Complexes into the Clay Matrix for Liquid Phase Oxidation of Phenol Derivatives"*** submitted by **Mr. Vikas S. Kshirsagar** was carried out by the candidate under my supervision/ guidance. Such material as has been obtained from other sources has been duly acknowledged in the thesis.

Dr. Chandrashekhar. V. Rode

(Supervisor/ Research Guide)

Declaration by the Candidate

I declare that the thesis entitled ***"Heterogenized Transition Metals/Complexes Into The Clay Matrix For Liquid Phase Oxidation Of Phenol Derivatives"*** submitted by me for the degree of Doctor of Philosophy is the record of work carried out by me during the period from 18-09-2006 to 30-06-2009 under the guidance of **Dr. C. V. Rode** and has not formed the basis for the award of any degree, diploma, associateship, fellowship, titles in this or any other University or other institution of Higher learning.

I further declare that the material obtained from other sources has been duly acknowledged in the thesis.

Date: Vikas S. Kshirsagar

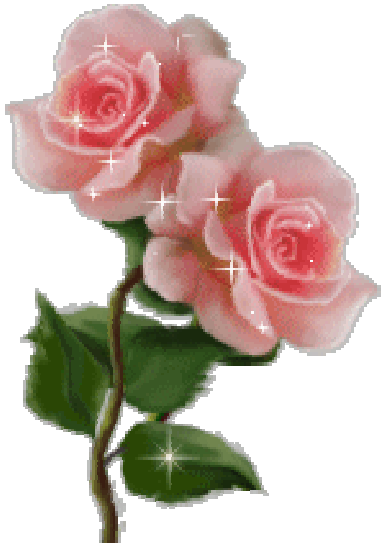

Dedicated

to my

Parents

Everyone has Problems -but Chemists have Solutions

Acknowledgement

I wish to express my sincere gratitude to my research guide, ***Dr. C. V. Rode****, Scientist, Chemical Engineering and Process Development Division, National Chemical Laboratory (NCL), Pune, for his constant support and encouragement during the course of this work. He has been a constant source of inspiration to me during my stay at NCL. I am grateful for his teaching and guidance. His enthusiastic attitude, innovative ideas and scientific knowledge have inspired me profoundly. I will be remaining ever grateful to him for his teaching, guidance, friendship and wonderful personality. It has been an intellectually stimulating and rewarding experience to work with him. I truly feel privileged to have joined his research group.*

I would like to thank head of the Chemical Engineering and Process Development Division, Dr. B. D. Kulkarni, for providing me all the divisional facilities required for my research work.

I would like to thank Dr. S. Sivaram, Director, NCL, Pune, for allowing me to carry out research and providing all infrastructural facilities at NCL. I am grateful to Council of Scientific and Industrial Research (CSIR), New Delhi for awarding me the research fellowship.

I take this opportunity to express my deepest sense of gratitude towards Mr. P. B. Jadkar for his timely help, constant support and valuable guidance.

I would like to thank Dr. M. Shirai and Dr. A. Yamaguchi AIST, Sendai, Japan for EXAFS analysis and very useful scientific discussions.

I express my gratitude to Dr. R. C. Chikate of Abasaheb Garware College, Pune who has been a source of inspiration for me.

I owe my special thanks to all scientific and non scientific staff of NCL. I would like to thank Dr. K. R. Patil, Dr. C. S. Gopinath, Dr. A. K. Nikumbh, Dr. Rane, Dr. P. N. Joshi, Dr. Vaidya, Mr. Raheja, Mr. Patane, Mr. Kamble, Mr. Dure, Mr. Wanjale, Mr. Shinde, Mr. Narvade, Mr. R. K Jha, Ms. Violet, for their help and cooperation in completing my research work successfully.

I also wish to thank my seniors and my friends, Dr. (Mrs) M. M. Potdar, Dr. Indresh, Dr. Sunil Tonde, Dr. Shrikant, Dr. Manisha K, Dr. Yogesh, Dr. Charu, Dr. Amit, Dr. Nitin, Dr. Sunil Shinde, Dr. Abhishek, Dr. Snageeta, Dr. Shashi, Dr. Debu, Dr. Bibhas, Dr. Nandu, Dr. Kapil, Dr. Mahesh D., Dr. Rashmi, Dr.Ankush, Dr. Sachin S., JP, Mahesh, Ajit, Vivek, Amit, Makarand, Savita, Sandeep, Piplad, Samadhan, Rajamani, Amol, Ajay G., Rasika, Pravin, Mahadev, Sachin, Narayan, Nitin, Ajay Jha, Ms. Mandakini, Ms. Prema, and all other research scholars

and friends in NCL who are not named in person, for their valuable suggestions and helping hand.

Words are not enough to express my love and gratitude to my family members. It gives me great pleasure to thank my parents, my sister, my brothers for always providing unconditional support and helping me over the years. And my dear wife, thank you for being patient and supportive all the time particularly during the tough writing stage of the thesis.

Vikas Shripat Kshirsagar

TABLE OF CONTENTS

CHAPTER I

INTORDUCTION

CHAPTER III

COBALT INTERCALATED MONTMORILLONITE CATALYST

CHAPTER IV

COBALT SAPONITE CATALYST

CHAPTER V

NANO STRUCTURED SPINEL COBALT OXIDE CATALYST

CHAPTER VI

REACTION KINETICS OF LIQUID PHASE AIR OXIDATION OF *P*-CRESOL TO *P*-HYDROXYBENZALDEHYDE

List of Figures

List of tables

List of Schemes

ABBREVIATIONS

BE	Binding energy
BET	Brunauer-Emmett-Teller
CT	Charge transfer
DRUV	Diffuse reflectance UV-Visible spectroscopy
DTA	Differential thermal analysis
FWHM	Full width at half maximum
FT-IR	Fourier- transform infrared Spectroscopy
HRTEM	High resolution transmission electron microscopy
MFC	Mass flow control
PID	Proportional integral derivative
PHB	*p*-Hydroxybenzaldehyde
PHBAcid	*p*-Hydroxy benzoic acid
PHBAlc	*p*-Hydroxy benzyl alcohol
P-XRD	Powder X-ray diffraction
Salen	N, N'-ethylenebis(salicylideneamine)
Salophen	N, N'-phenylenebis(salicylideneamine)
SEM	Scanning electron microscopy
SAED	Selected area electron diffraction
TEM	Transmission Electron Microscopy
Temp.	Temperature
TOF	Turnover frequency
TON	Turnover Number
TG	Thermogravimetry
UV-Vis	Ultra Violet Visible Spectroscopy
XAFS	X-ray Absorption Fine Structure spectroscopy
XANES	X-ray Absorption Near Edge Structure
XPS	X-Ray Photoelectron Spectroscopy
XRD	X-ray diffraction

Abstract

Heterogenized Transition Metals/Complexes into the Clay Matrix for Liquid Phase Oxidation of Phenol Derivatives

Introduction: The catalysis has wide ranging applications in chemical industry and has a major impact on the quality of human life as well as economic development. The catalytic reactions are generally classified as homogeneous or heterogeneous depending on the physical state of the catalyst. The overall performance of a catalytic process is determined by conversion of the reactant or turn over number, selectivity of the desired product and the catalyst life.

Among various catalytic processes, oxidation of organic substances is one of the most important methods for producing diverse chemicals from oil derivatives and vegetable raw materials [1-2]. In the production of fine chemicals it is imperative that the reactions are selective. The traditional oxidation methods often involve the use of stoichiometric amounts of inorganic oxidants, such as chromates, which clearly cause serious effluent problems [3-4]. In addition, these reactions usually require high temperatures and pressures, which consume a lot of energy and cause lower selectivities. These drawbacks can be overcome by developing catalytic processes for oxidation. From an industrial point of view oxidation catalysis poses three challenges: a) activation of molecular oxygen, b) avoid over oxidation of the substrate, and c) overcome the lack of functionality in the feedstock.

Oxidation of various phenol substituted derivatives such as *o*-cresol, *p*-cresol, *m*-cresol, 3,4-dimethoxy toluene, *p*-cresyl isobutyrate, *p*-cresyl acetate, *p*-phenoxy toluene, *p*-cresyl

methyl ether, *p*-cresidine, 2-nitro-*p*-cresol etc. leads to the variety of chemical products. The resulting oxidation products viz. hydroxy-substituted aromatic alcohols, aldehydes or ketones and acids are important intermediates in the manufacture of pharmaceuticals, agrochemicals, polymeric resins and artificial flavours. One such example is the oxidation of *p*-cresol which gives *p*-hydroxy benzyl alcohol and *p*-hydroxybenzaldehyde. Derivatives of *p*-hydroxy benzyl alcohol and *p*-hydroxybenzaldehyde (PHB) are important intermediates for the manufacture of vanillin, a widely used flavoring agent, trimethoxybenzaldehyde, various agrochemicals and pharmaceuticals such as semi synthetic penicillin, amoxicillin, antiemetic drug trimethobenzamide [5-7]. *p*-Hydroxybenzaldehyde is also used as an additive for metal plating brighteners, electroplating, in perfumes and in liquid crystals[8]. Several reports have appeared on oxidation of *p*-cresol using both homogeneous as well as heterogeneous cobalt catalysts [9]. Heterogeneous catalysts are preferred due to their inherent advantages such as easy recovery and their amenability for continuous processing. Recently, catalysts containing cobalt and/or some other metals such as copper or manganese supported on molecular sieves, carbon, resins, zeolite silicious materials and clays have been reported. In case of zeolite catalysts such as CoAPO-5 and CoAPO-11, the catalyst was found to dissolve in the reaction media while in other cases leaching of cobalt was found to be > 50% under reaction conditions which demands use of large excess of catalyst (up to 8 mol %) loading in the process. Hence developing/designing new stable solid catalysts for liquid phase oxidation of *p*-cresol and similar derivatives is still a challenge in the area of oxidation catalysis.

In this thesis we have successfully developed variety of novel solid catalysts involving metal-Schiff complexes intercalated into montmorillonite clay, Co-saponite catalyst and nano structured cobalt oxide catalyst for selective liquid phase oxidation of *p*-cresol derivatives.

The specific objectives of this work are given below.

OBJECTIVES OF PRESENT INVESTIGATION

- Preparation of metal complexes by conventional methods and immobilization of these metal complexes into the clay matrix.
- Preparation of clay materials with various composition and properties
- Preparation of nanostructured cobalt oxide materials by co-precipitation and digestion method.
- Detailed characterization of catalyst materials using various techniques such as (Brunauer- Emmett-Teller (BET), UV-Visible spectroscopy, FTIR, XPS, XRD, TGA, extended X-ray absorption fine structure (EXAFS), TEM, SEM, and AAS.
- Catalyst activity testing of the above prepared catalysts for the oxidation reactions of substituted phenol derivatives.
- Optimization of reaction conditions for the best catalysts.
- Kinetics of liquid phase air oxidation of *p*-cresol by Co_3O_4.
- Interpretation of activity results based on the characterization data.

The thesis is divided into seven chapters with appropriate references at the end of each chapter.

Chapter 1 provides in brief the concept of catalysis, types of catalysis, green chemistry concept and general introduction to the oxidation reactions. A summary of literature on oxidation of phenol substituted derivatives using homogeneous, heterogeneous and heterogenized homogeneous catalysts and catalyst characterization is also given in this chapter. At the end of this chapter the scope and objectives of this thesis are given.

Chapter 2 gives detailed experimental procedures used for oxidation reactions such as Parr reactor setup, and atmospheric oxidation setup.

Chapter 3 explains the synthesis of different Schiff's bases, Schiff base complexes and their intercalation into montmorillonite and saponite clays. This chapter also focuses on detailed characterization by various techniques to confirm the intercalation of the metal complexes into the interlamellar spaces of the clay. These prepared catalysts were tested for their activity for liquid phase air oxidation of the phenol substituted derivatives such as *p*-cresol *m*-cresol, *o*- cresol. Cobalt is one of the most studied oxygen activating metals. Many of its chelate compounds are known to reversibly bind oxygen to form superoxo- or peroxo-type complexes. Co(salen) is a Schiff's base complex discovered by Tsumaki in 1930 which can bind dioxygen reversibly. Under oxidation conditions, soluble Co-salen complexes usually form either mononuclear superoxo or inactive dinuclear μ-oxo type complexes with dioxygen. The formation of inactive μ-oxo dimer can be avoided by immobilization of various metal complexes in zeolite framework or their intercalation into the clays. However, intercalation of metal complexes into the interlamellar spaces of clay materials would be more appropriate because it can offer

shape selectivity as well as diffusion in only two-dimensional space instead of three dimensional volume.

In our study, two-dimensional montmorillonite and saponite clay were chosen as a host framework for intercalation of Co-salen type complexes. Various types of cobalt Schiff complexes were prepared and intercalated with those clays. In order to prove the intercalation, the heterogenized catalysts were thoroughly characterized by Fourier−transform infrared (FT−IR) spectrum, ultraviolet−visible (UV−vis) spectrum, X-ray diffraction (XRD), thermogravimetry analysis (TGA), scanning electron microscope (SEM), X-ray photoelectron spectroscopy(XPS), atomic absorption spectroscopy (AAS), and extended X-ray absorption fine structure (EXAFS).

This heterogeneous catalyst was found to give a five fold higher TON than the homogeneous cobalt salen complex for liquid phase air oxidation of *p*-cresol. A total selectivity ≥ 90 % to the oxidation products could be achieved with this solid catalyst by eliminating the undesired coupling side products in air oxidation of *p*-cresol under ambient pressure conditions. Different Schiff bases were screened and their activity was tested for oxidation of cresol derivatives [10, 11].

Chapter 4 discusses the novel synthesis of cobalt saponite catalyst, their characterization and activity evaluation for *p*-cresol oxidation. Smectites are one of the most common phyllosilicates types of clays used as solid catalysts for several types of reactions due to their specific characteristics, such as a high specific surface area, cation exchange or hydration capacities. Saponite clay is an example of trioctahedral smectite in which the charge imbalance due to isomorphic substitutions in the structure layers is compensated

by cations placed in interlamellar position. Therefore, Co-saponite obtained can be viewed as a nanocomposite (100nm) of Co phases over aluminosilicate support as a catalyst for oxidation reactions. Co-saponites with varied cobalt compositions were prepared and characterized by BET, XRD, DRUV, XPS techniques.

XPS studies showed octahedrally and tetrahedrally coordinated divalent cobalt species in Co-saponite and it's coordination with lattice oxygen. The nitrogen adsorption-desorption isotherm for Co-saponite sample showed Type I istherm. The pore size distribution of Co-saponite catalyst by BJH adsorption adsorption desorption method confirmed the microporous (average pore size 1.7-2 nm) nature of catalyst. UV-visible spectroscopy proves divalent cobalt species was octahedrally and tetrahedrally coordinated in Co-saponite.

Highest conversion of 92% of p-cresol was achieved with Co-saponite catalyst at 827 kPa of oxygen pressure giving 92% selectivity to p-hydroxybenzaldehyde. Formation of benzoic acid could be significantly minimized as well as formation of non oxidation products were also completely suppressed using our catalyst. Activation energy calculated from the Arrhenius plot was found to be 42 kJ/mole.

XPS studies of the fresh and used catalyst along with the oxidation experiments with Co-saponite without oxygen, support that the liquid phase *p*-cresol oxidation proceeds probably through Mars-van Krevelen pathway involving the lattice oxygen and the subsequent re-oxidation of the vacant sites by molecular oxygen[12, 13].

Chapter 5 is concerned with the synthesis of spinel nano structured cobalt oxide catalyst by simultaneous co-precipitation and digestion method. These nanoparticles were found

to be highly active for air oxidation of *p*-cresol under mild conditions while the selectivity to the oxidation products could be altered by changing the digestion time during the preparation of the catalyst. The catalysts were characterized by TEM, XPS, XRD and BET surface area. The surface area of cobalt oxide nano particles was found to be 95m^2/g while that of bulk cobalt oxide was only 9m^2/g. XRD peaks were indexed on the basis of spinel structure with the space group of Fd3m. The lattice parameter obtained, a = 8:072A˚, is in good agreement with the reported value for Co_3O_4 powder. The HRTEM image of Co_3O_4 particles indicates rod-type aggregates (diameter: 4–5 nm, length: 20–30 nm) that are formed from 2–3 nm primary particles. XPS spectrum exhibiting the Co $2p_{3/2}$ and Co $2p_{1/2}$ doublet core level peaks at binding energies (BE) of 780.2 and 795.3 eV with a difference of 15.1 eV indicate the presence of both Co^{2+} and Co^{3+} species in the catalyst. This redox couple of cobalt is responsible for catalyzing the oxidation reaction. Catalyst reuse experiments showed the same activity as that for the fresh catalyst. Reproducibility of catalyst preparation with respect to its physico-chemical characterization as well as the activity measurement for oxidation was found to be excellent [14].

Chapter 6 presents the experimental study on the kinetics of liquid phase oxidation of *p*-cresol to *p*-hydroxybezaldehyde has been investigated using insoluble cobalt oxide (Co_3O_4) catalyst at oxygen partial pressures in the range 0.1-1.5 MPa, reaction temperatures 333-393 K, p-cresol concentrations 0.49-1.53 kmol/m^3 and catalyst loadings 0.38-3.03 kg/m^3. The effects of oxygen partial pressure, reaction temperature, p-cresol concentration and catalyst loading on the initial rate of reaction have been studied. The

initial rate varied linearly with catalyst loading up to 1.5 kg/m^3 beyond which it was independent of the catalyst loading while first order dependence was observed with variation in oxygen partial pressure. A rate expression proposed by considering Langmuir-Hinshelwood (LH) type mechanism, based on the initial rate data is given below.

$$r = \frac{wk_1 K_A C_A C_B}{(1 + K_A C_A)} \qquad \textit{Model I}$$

A batch reactor model was also developed based on the kinetics studied and the concentration time profile predicted by the model was in good agreement with the experimental data. The activation energy for the liquid phase oxidation of p-cresol was found to be 39.6 kJ/mol [15].

Chapter 7 summarizes the work presented in all the chapters and general conclusions arrived from the discussed results.

References

1. J. Ebner and D. Riley in *Active Oxygen in Chemistry*, J. S. Valentine, A. Greenberg and J. F. Liebman, Eds., Chapman and Hall, London, vol.1, **1995**.
2. I.P. Skibida and A. M. Sakharov, *Catal. Today* **1996**, *27*, 187.
3. R. A. Sheldon, I. W. C. E. Arends and A. Dijksman, *Catal. Today* **2000**, *57,* 157.
4. R. A. Sheldon, J. K. Kochi, *Metal Catalyzed Oxidations of Organic Compounds*, academic Press, new York, **1981**.
5. A. J. Poss, R. K. Belter, *J. Org. Chem.* **1988**, *53,* 1535.
6. T. Sigeru, T. Hideo, S. Takasi, A. Mitstio, *J. Org. Chem.*, **1979**, *44*, 3305.

7. D. V. Rao, F. A. Stuber, *Synthesis*, **1983**, *4*, 308.
8. S. Mitchell, *Kirk-Othmer Encyclopedia of Chemical Technology,* 4th ed.; Willy-Interscience: New York, **1998**; vol. 13, pp 1030-42.
9. C. V. Rode, M. V. Sonar, J. M. Nadgeri, R. V. Chaudhari, *Org. Process Res. Dev.* **2004**, *8*, 873.
10. C. V. Rode, V. S. Kshirsagar, J. M. Nadgeri, K. R. Patil *Ind. Eng. Chem. Res*. **2007**, *46*, 8413.
11. V. S. Kshirsagar, A. C. Garade, K. R. Patil, A. Yamaguchi, M. Shirai, C. V. Rode *accepted* in *Appl. Catal. A: Gen.* **2009.**
12. V. S. Kshirsagar, A. C. Garade, K. R. Patil, M. Shirai, C. V. Rode, *Top. Catal.* **2009,** *52***,** 784.
13. V. S. Kshirsagar, A. C. Garade, K. R. Patil, R. K. Jha, C. V. Rode, *Ind. Eng. Chem. Res.* **2009**, (Doi: *10.1021/ie801941e*)
14. V. S. Kshirsagar, S. Vijayanand, H. S. Potdar, P. A. Joy, K. R. Patil, C. V. Rode *Chem. Lett*. **2008**, *37*, 310.
15. V. S. Kshirsagar**,** J. M. Nadgeri, P. R. Tayade, C. V. Rode *Appl. Catal. A: general* **2008**, *339,* 28.

1.1. Catalysis

Berzelius invented the term 'Catalysis' in 1835 to characterize the phenomenon in which the addition of a small amount of a foreign substance caused a large increase in the chemical change without itself getting consumed. The word 'catalysis' came from the two Greek words, the prefix, *cata* meaning down, and the verb *lysein* meaning to split or break. The catalyst breaks down the normal forces that inhibit reactions of the molecules; a widely accepted definition of catalyst being, 'a substance that increases the rate of approach to equilibrium of a chemical reaction without itself being substantially consumed in the reaction process'. Catalysis has been an intriguing concept since then and continuing efforts have been on to understand and utilize this phenomenon for practical purposes that has resulted in numerous inventions during this century, leading to improving the quality of human life. In fact, life has evolved through the metabolic reactions that are catalyzed by enzymes, which are known as nature's catalysts [1, 2]. The contribution of chemical industry based on catalytic production of variety of chemicals and fuels to the global economy is worth over 10 trillion dollars per year [3]. Nearly 95% of all the manufacturing processes practiced in the chemical industry today are based on the catalysis in one form or the other, amounting to more than 20% of the GDP of developed nations. Thus, catalysis has a major impact on the quality of human life as well as economic development. Recently, Professor Gerhard Ertl, the German physicist was awarded the 2007 Nobel Prize in Chemistry for his efforts to understand the mechanisms of heterogeneous catalytic reactions, which involved the investigations of reactions on metal surfaces [4]. Figure 1.1 shows the plot of reaction co-ordinate versus energy. There is a

distinction between catalyzed and non-catalyzed reaction in terms of energy of activation. As shown in this Figure, the catalyzed reaction requires less energy of activation as compared to the non-catalyzed reaction.

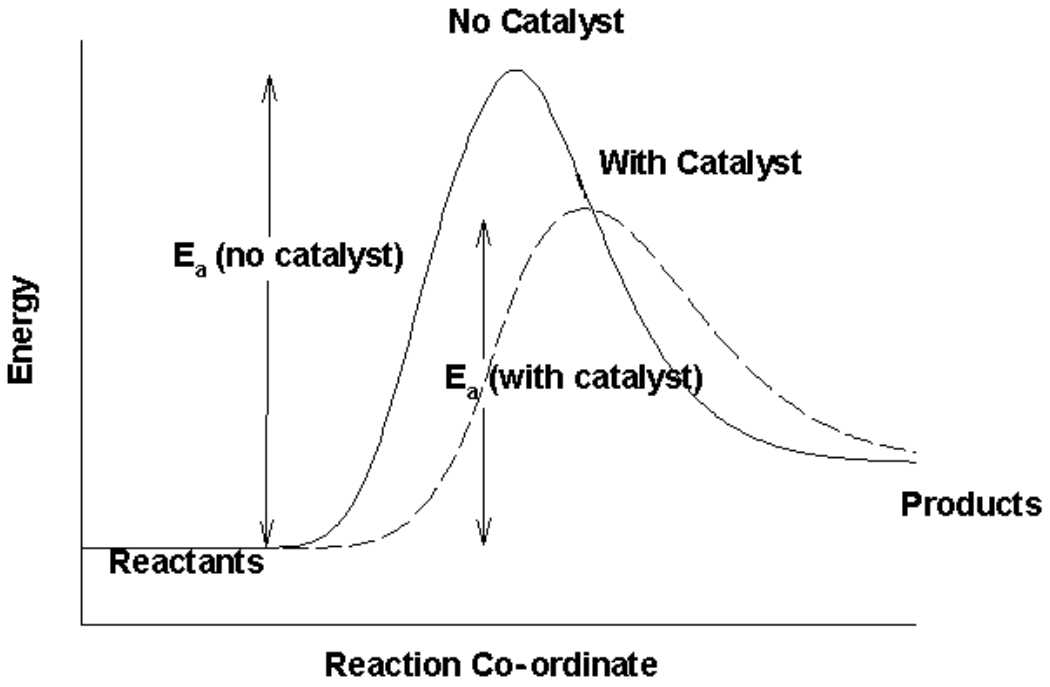

Figure 1.1. Pictorial representation of a catalytic reaction

1.2. Green chemistry

A process or a technology is called “green” if it uses raw materials efficiently, use of toxic and hazardous reagents and solvents can be avoided and formation of waste or undesirable byproducts is minimized [5]. Catalytic routes often satisfy these criteria. This can be well illustrated by the selective oxidation of ethylene to ethylene epoxide, an important intermediate for ethylene glycol (antifreeze) and various polyethers and polyurethanes.

The old non-catalytic route for ethylene oxide (called as epichlorohydrin process) follows a three-step synthesis

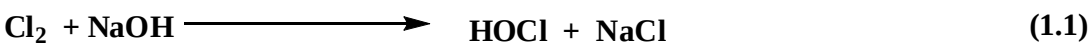

(1.1)

(1.2)

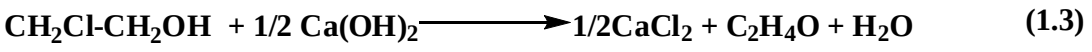

(1.3)

Or in total:

(1.4)

Scheme 1.1. Oxidation of ethylene to ethylene oxide.

Hence, for every molecule of ethylene oxide, 1.5 molecules of inorganic salts are formed, creating a serious waste disposal problem that was traditionally solved by dumping it in a river. Such practice is of course now totally unacceptable and banned by legislature.

The catalytic route, however, is much cleaner and simpler, although it does produce a small amount of CO_2. By using silver as a catalyst, promoted along with small amounts of chlorine, ethylene oxide is quantitatively obtained directly from C_2H_4 and O_2 with around 90% selectivity to ethylene oxide and ~ 10 % of the

ethylene ending up as CO_2. Now a days all production facilities for ethylene oxide are based on catalytic oxidation of ethylene.

Catalysis has played a vital role in developing new, environmentally benign technologies to replace several stoichiometric synthetic routes often involving toxic, corrosive and costly reagents and associated with generation of inorganic waste products. In oil refineries, various processes for the production of liquid fuels and for converting a wide variety of feed stocks to high value products are all based on catalytic routes and a pioneering work on various aspects of catalysis has been done in this field [6, 7].

Usually, catalysts are categorized as homogeneous and heterogeneous, depending on their physical form in which they are present in the respective catalytic process. A broad classification of catalysis is shown below.

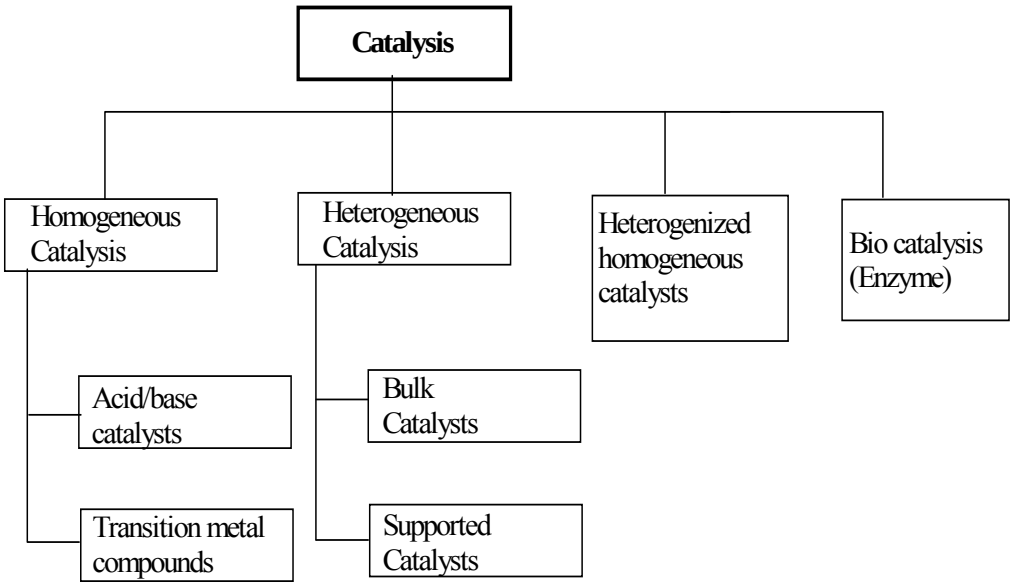

Figure 1.2. Classification of catalysis

1.3. Homogeneous catalysis

Homogeneous catalysis, by definition, refers to a catalytic system in which the substrates and the catalyst are in one phase, most often the liquid phase. More recently a narrower definition is being used, according to which homogeneous catalysis involves (organo) metallic complexes as the catalysts [8]. Homogeneous catalysts are more reactive in general, mainly due to the absence of phase boundaries, diffusion limitations and physisorption phenomenon. Soluble metal complexes as homogeneous catalysts provide selective synthetic routes under mild operating conditions for valuable chemicals from basic organic precursors e.g. ethylene to acetaldehyde by Wacker catalyst [9]. Some of the important reactions catalyzed by transition metal complexes are hydrogenation, oxidation, hydroformylation, carbonylation, and carbon-carbon bond formation reactions such as Heck reaction, co-polymerization and ring opening metathesis [10]. Important examples of commercial applications of homogeneous catalysis are: hydroformylation of olefins to aldehydes/alcohols, oxidation of *p*-xylene to terephthalic acid, hydrocyanation of butadiene to adiponitrile, ethylene oligomerization [11], oxidation of ethylene to acetaldehyde by $PdCl_2/CuCl_2$ [12] etc. Though homogeneous catalysis plays an extremely important role in highly efficient processes, yet there are some serious drawbacks such as catalyst-product separation from the reaction mixture and re-usability of the catalyst. These shortcomings have led the researchers to design and investigate new stable and easily separable catalyst systems.

1.4. Heterogeneous catalysis

Heterogeneous catalysts are those which act in a different phase than that of the reactants. Mostly these are solid materials interacting with the substrate molecules either in a liquid or gaseous phase. The Heterogeneous catalysts have numerous industrial applications in the chemical, food, pharmaceutical, automobile and petrochemical industries [13], and it has been estimated that 90 % of all chemical processes use heterogeneous [14].

The first industrially important heterogeneous catalytic process introduced in 1875, used platinum to oxidize SO_2 to SO_3, for the synthesis of sulfuric acid [15]. Another important discovery in that period was the early studies of alcohol dehydration over alumina and alcohol oxidation on platinum metal.

In nineteen twenties, heterogeneous catalysis by solid acids and supported metals was widely applied in oil refining and petrochemicals. In contrast, fine chemicals manufacture was dominated by synthetic organic chemists who adhered to stoichiometric methodologies. The pressure of environmental legislation has, in the last decade, provided an important stimulus for the development of clean, catalytic methodology.

The main advantage of a heterogeneous catalytic process is that it can be operated continuously in a reactor for long duration, at times up to few years.

Hence, developing a heterogeneous catalyst for any process is very important, as it has a major advantage of its easy recovery from the reaction mixture, thus offering a simpler handling and preventing the loss of active catalyst function as compared to the homogeneous catalyst [16].

A chemical reaction catalyzed by a solid catalyst, mainly occurs at the catalyst surface that involves the active sites (or active centers). Hence the activity of a solid catalyst is directly proportional to the specific surface area of a solid a solid per unit weight or per unit volume. However the sizes of catalyst particles used in industrial applications mainly depend on the type of reactor used. For example in fine chemical industry, batch slurry type reactors are employed and in our work also we have studied the catalyst activity in slurry reactors. In such reactors, weight fractions of catalyst generally range between 0.05 to 2.5 % (w/w).

Some of the important characteristics of a good solid catalyst are:

- It should have highest selectivity to the desired product.
- It should give reasonable rates of reaction, in terms of conversion and/or productivity per unit time.
- It should be stable and give consistent performance over a long period of reaction time to have the economically viable.

Obviously these characteristics are fundamentally related to the adsorption-desorption phenomena and interaction of adsorbed molecules on the catalyst surface. From these perspectives we have attempted to design the novel efficient solid catalysts for the liquid phase oxidation of *p*-cresol.

1.5. Heterogenization of homogeneous catalysts

Many homogeneous catalytic systems, though have many attractive properties, viz. high selectivity and activity, yet cannot be commercialized because of difficulties associated with the catalyst-product separation from reaction system, thermally

sensitive nature and reusability of the catalyst [16]. Hence, the homogeneous reactions that have been commercialized either involve volatile substrates and products or do not contain thermally sensitive organic ligands. Heterogenization of the homogeneous catalysts has been a very active area of catalysis research, in order to combine together the advantages of easy recovery of the solid catalyst and the specificity of the homogeneous catalyst. The term heterogenization refers to a process, whereby a homogeneous transition metal complex (including free metal particles, biological molecules, organic species etc.) is either immobilized, or anchored, or incorporated or encapsulated or intercalated in an inert organic (polymer) or inorganic support. These heterogeneous catalysts have a lot of advantages over their homogeneous analogues such as,

i. Fixed-bed and continuous flow operations,
ii. Complete commercial utility on a large scale due to the economic benefits over batch operations and/or expense of catalyst recovery and recycle,
iii. Maintaining high selectivity and conversion (turn over frequency) of their homogeneous analogues
iv. Preventing other side reactions e.g. dimerization, alkylation and aggregate formation of the catalyst complex, which normally occurs in solution.

1.6. Bio-catalysis

Bio-catalysis can be defined as utilization of natural catalysts, such as protein enzymes, to perform various chemical transformations. This involves catalysts in the form of enzymes, whole cells etc. These are considered as ideal catalysts, as they can

be operated in aqueous medium at or below room temperature and atmospheric pressure and with nearly 100 % selectivity. These catalysts have been used for various reactions such as oxidation, reduction, etc [17]. A specially designed mutant of *Candida antarctica* was found to be an effective bio-catalyst for the Michael addition of acrolein with acetylacetone at 20°C in absence of any solvent [18].

1.7. Selectivity in heterogeneous catalysis

The selectivity in chemical transformations is broadly classified as;

- Regioselectivity
- Chemoselectivity
- Stereo / Enantioselectivity
- Atom Economy
- E factor

1.7.1. Regioselectivity The selective reaction of one functional group in the presence of same functional groups situated at different positions of substrate.

e.g. hydrogenation of 1-phenylethane-1,2diol to 2-phenyl ethanol.

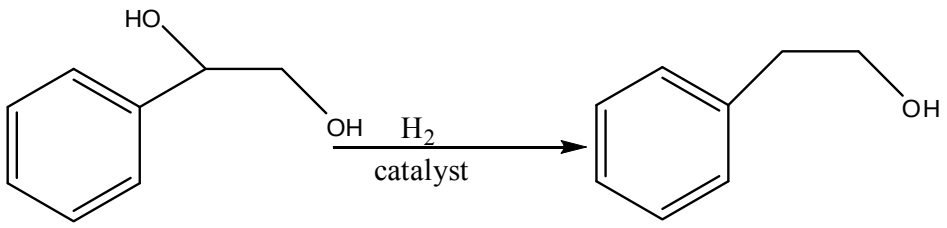

(1.5)

1.7.2. Chemoselectivity: It can be defined as a situation where two different chemical reactions can occur, giving two different products.

e.g. Oxidation of *p*-cresol to *p*-hydroxybenzyl alcohol or benzaldehyde.

1.7.3. Stereoselectivity

Sterioselectivity can be defined as reaction of one stereoisomer in presence of another isomer

E.g. Selective hydrogenation of maleic acid in presence of fumaric acid

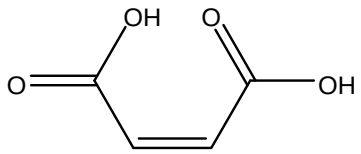

Maleic acid

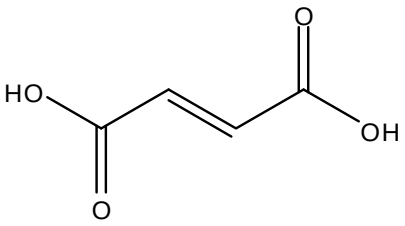

fumaric acid

1.7.4. Atom Economy

The atom economy or atom efficiency concept was first introduced by Barry Trost in 1991[19]. It is calculated by the ratio of number of atoms ended up in the product to number of atoms from the reactant.

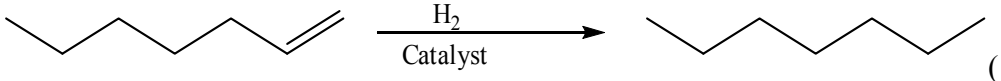

(1.6)

Scheme 1.2. Hydrogenation of 1-heptene to heptane

In above reaction the atom economy is 100%.

Due to increasing environmental awareness in recent years, there is a growing need for high atom utilization, low-salt processes, which can be achieved by catalytic routes for industrially important reactions involving oxidations, hydrogenations, carbonylations, etc.

1.7.5. E factor: E factor can be defined as the ratio of mass units of waste formed to the mass units of product formed.

Synthetic methods can be made efficient if the reactions involved are both selective (chemo-, regio-, diastereo-, and/or enantio-) and economical in terms of atom utilization (maximum number of atoms of reactants appearing in the products). Transition metal-catalyzed catalyzed process is one of the approaches to achieve this long-term goal.

1.8. Oxidation

The chemical term ‘oxidation’ can be defined as the take-up of oxygen by organic and inorganic materials or removal of hydrogen from a substrste [20]. The development of processes for oxidation of organic substances is a goal that has long been pursued, since it is one of the most important methods for producing diverse chemicals from oil derivatives which are basically only hydrocarbons [21, 22]. Various process options for oxidation processes are shown in Figure 1.2 [23].

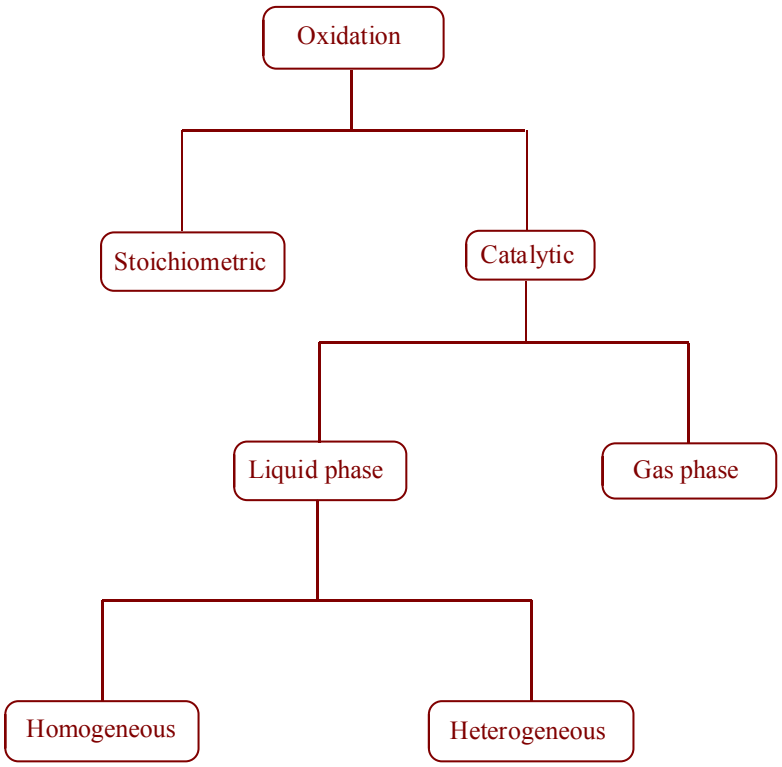

Figure 1.3. Classification of oxidation reactions

Well known examples of reagents used in stoichiometric (or even excess) quantities for oxidation reactions are given in Table 1.1 which are now becoming prohibitive by legislature all over the world, due to the generation of huge quantities of inorganic wastes posing a serious effluent disposal problem [21].

Table 1.1. Various oxidants used in liquid phase oxidations [24, 25]

Sr. No.	Name of oxidizing agent	Drawbacks
1	Pyridinium chlorochromate	Relatively acidic reagent (more acidic than PDC and Collins) - can cause problems with acid labile groups

2	Collins's reagent(CrO_3.2 pyridine)	Requires a large excess of reagent for complete reaction.
3	Pyridinium dichromate	Work-up can be messy on large scale. Often require a large excess.
4	aq. sulfuric acid, acetone, chromic acid	toxic and mutagenic, requires in stoichiometric quantities
5	Potassium permanganate, potassium dichromate, lead tetra acetate	Not very chemoselective, which limits its use. Hazardous nature e.g. Pb, Cr.
6	Sodium chlorite	Requires in stoichiometric
7	Osmium tetra oxide	Osmium tetra oxide is very expensive and highly toxic

Table 1.2 shows comparison between catalytic and stoichiometric oxidation reaction. Catalytic oxidations provide an environmentally acceptable and cheap process as compared to stoichiometric oxidations.

Table 1.2. Comparison between catalytic and stoichiometric oxidation

Catalytic oxidation (O_2)	Stoichiometric oxidation
Advantages ➢ Cheap oxidant ➢ No effluent problem Disadvantages ➢ Limited scope	Advantages ➢ Broad scope Disadvantages ➢ Expensive and hazardous oxidants ($K_2Cr_2O_7$, $KMnO_4$, $Pb(OAc)_4$, etc. ➢ Generation of large amounts of inorganic wastes posing a serious effluent disposal problem. ➢ Tedious work up for recovery of pure product. ➢ Selectivity not upto the mark

Depending on the reactant phase, the catalytic oxidation is classified in two types as liquid and gas phase. In gas phase oxidation, substrate concentrations are much lower and radical chain oxidation pathway is less favored. Gas phase oxidation generally operates through Mars-van Krevelen mechanism (scheme 1.3a) while in liquid phase, the oxidation follows a free radical pathway as represented by scheme 1.3b.

Gas phase (Mars-van Krevelen mechanism)

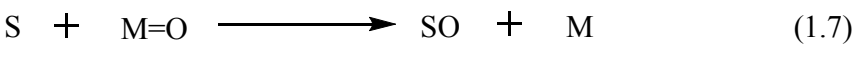

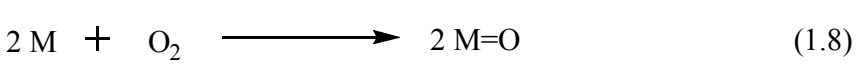

Scheme 1.3a. Gas phase oxidation.

Liquid phase

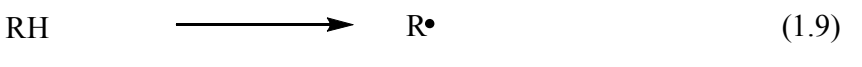

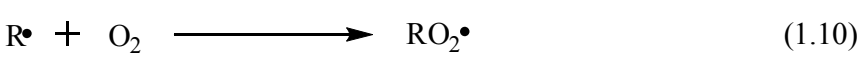

Scheme 1.3b. Liquid phase oxidation

Among various substrates, selective oxidation of sp^3 hybridized carbon of inactive hydrocarbons to industrially important intermediates still remains a major challenge [26-30]**.** There are several large scale industrial vapor phase oxidation processes in operation nevertheless, it has certain disadvantages such as very high operating temperature and the formation of a large amount of carbon dioxide, contributing to the global warming. Further, the conversion has to be kept low to attain a high

selectivity of aldehydes, and the low concentration of substrates in the feed stock mixture poses the problem of recovery. In case of vapor phase oxidation of toluene with oxygen, carried out at temperature > 473 K and under 0.5– 2.5 MPa pressure [31-34]**,** these conditions seem to be too harsh for improving the selectivity to benzaldehyde. Generally, the conversion has to be kept at less than 4% to attain 70% selectivity of benzaldehyde and to avoid the formation of carboxylic acids, phenols, and decomposition to carbon oxides (CO_2 and CO) and tar [35, 36]**.** However, any diffusion limitations are expected to be much less severe in gas-solid systems as compared to liquid-solid systems [37].

Liquid-phase oxidations are also operated commercially e.g. *p*-xylene to terephthalic acid, cyclohexane to cyclohexanol/cyclohexanone and adipic acid, n-butane to acetic acid etc. Oxidation of isobutane to *tert*-butyl hydroperoxide (TBHP)/*tert*-Butanol, di-isopropyl benzene to hydroquinone, epoxidation of propylene to propylene oxide, oxidation of alcohols to aldehydes, *p*-cresol to *p*-hydroxybenzaldehyde, 2-hydroxybenzylalcohol to salicylaldehyde, 4-hydroxy-3-methoxy benzyl alcohol to vanillin. Due to relatively milder reaction conditions, liquid phase oxidations are easy to operate while giving the quantitative conversions of the substrate. Since, liquid phase oxidation operates through free radical pathway; it is always associated with the formation of coupling as well as over oxidation products. This is even more imperative in the production of fine chemicals since the recovery of the desired oxidation product of highest purity is required due to their applications in health care, fragrance and flavours, pharmaceutical formulations [38, 39]**.** From this perspective, designing a solid catalyst system capable of operating via Mars-van Krevelen

mechanism in liquid phase becomes a challenging task. In the present work, we have made an attempt to demonstrate that Mars-van Krevelen mechanism is also operating for liquid phase air oxidation of *p*-cresol using our solid catalyst (Co-saponite) (chapter 4).

1.8.1. Molecular oxygen as an oxidizing agent

Table 1.3 lists various oxygen donors used in catalytic oxidation reactions [23]**.** Among various oxidants (Table 1.3), although H_2O_2 has the highest active oxygen content, it is usually used as 50% aqueous solution hence occupy large reactor volume and its storage and handling conditions are rather stringent. Also, H_2O_2 is again a secondary oxygen donor like others, since it is prepared from oxygen as a primary source of oxygen.

Table 1.3. Oxygen donors [40]

Donor	Active oxygen (%)	By-product
H_2O_2	47	H_2O
N_2O	36.4	N_2
O_3	33.3	O_2
t-BuO_2H	17.8	t-BuOH
CH_3CO_3H	21	CH_3CO_2H
$C_5H_{11}NO_2$	13.7	$C_5H_{11}NO$
$NaClO_2$	35.6	NaCl
NaClO	21.6	NaCl

NaBrO	13.4	NaBr
$KHSO_5$	10.5	$KHSO_4$
$NaIO_4$	10	$NaIO_3$
HNO_3	25.4	HNO_2
PhIO	7.3	PhI

In this respect, atmospheric air becomes the most abundant and cheapest primary oxygen donor without having any waste disposal problem. It is well known that biologically some of the enzymes perform selective oxidations of complex organic molecules at very mild conditions [41, 42]. Several synthetic transition metal complexes are able to mimic these enzymes and reversibly bind and activate molecular oxygen [43-45]. Thus, for the past few decades there has been a growing interest in transition metal catalyzed activation of O_2 for organic oxidations [21, 36, 41, 43, 46-50].

There are two forms of molecular oxygen in gas phase as dioxygen (O_2) and trioxygen (O_3) formed by electric discharge passed through oxygen molecule. Molecular oxygen contains in its ground state two unpaired electrons, which are localized on the degenerate antibonding π_{2p} orbitals: the ground state thus is a triplet state (Figure 1.4) which requires high energy of activation to react with singlet organic molecules. This symmetry barrier can be overcome by activating oxygen to the singlet state. Molecular oxygen may be activated in different ways. Thermal excitation of the molecules from triplet state of oxygen to singlet state of oxygen requires considerable activation energy. However oxygen may also be activated

chemically, by bonding it to an appropriate centre which may be the transition metal atom in the coordination complex or the surface of solid e.g. transition metal oxide.

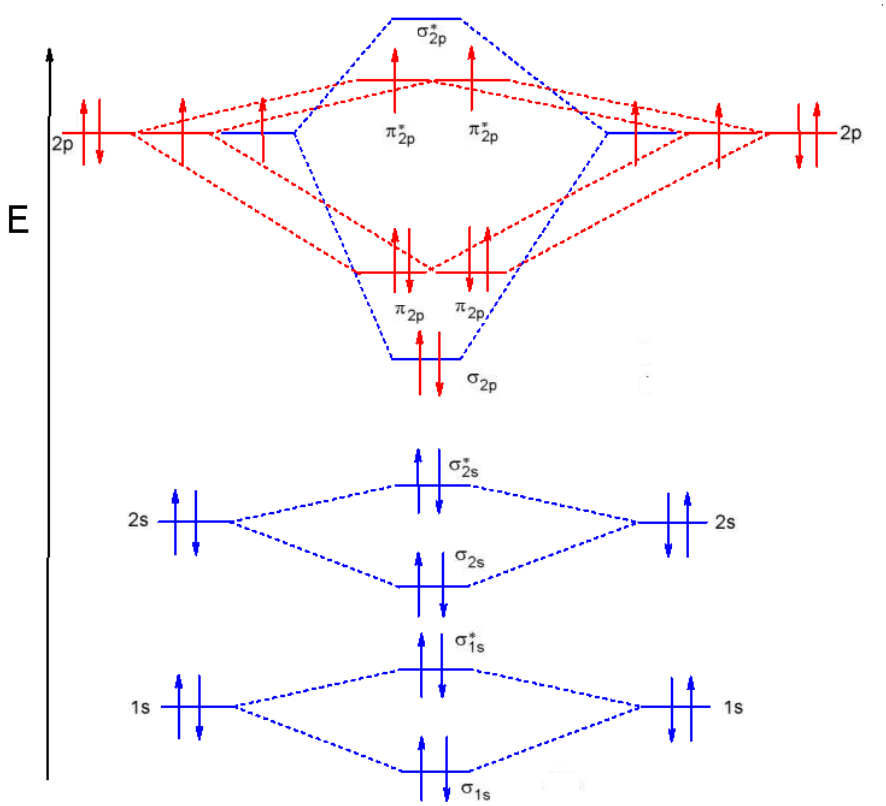

Figure 1.4. Molecular orbital diagram of oxygen

In the present work, chemical activation of molecular oxygen has been attempted by several solid catalysts hence, some theoretical background on this aspect is summarized in the following section.

1.8.2. Activation of oxygen by transition metal complexes

Metal complexes in low oxidation states can interact with dioxygen in successive steps in which electrons are transferred from the metal to dioxygen forming successively superoxo, μ-peroxo, oxo, and μ-oxo complexes

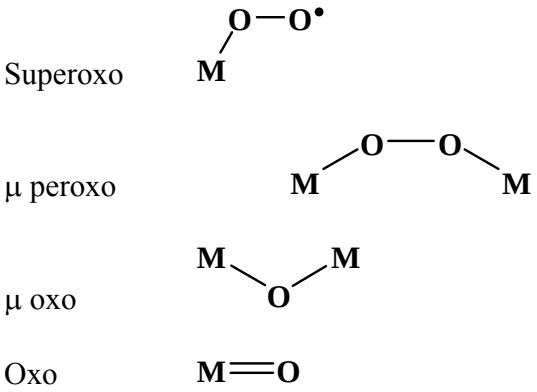

Figure 1.5 Binding of oxygen with the metals [51].

Many transition metal complexes are reported to catalyze the oxidation reactions.

1. Ruthenium compounds are widely used as catalysts in many reactions e.g. $RuCl_3.nH_2O$, $RuCl_2(Ph_3P)_3$ used in aerobic oxidation of allylic and benzylic alcohols under mild conditions [52].
2. $Pd(OAc)_2$-NaOAc was reported for aerobic oxidation of alcohol. [53].
3. In 1984, Semmelhack reported the first practical Cu-catalyzed aerobic oxidation of alcohols by10 mol% CuCl and 10 mol% TEMPO under oxygen atmosphere [54].
4. Various cobalt complexes usually referred to as synthetic dioxygen carriers are known to interact reversibly with dioxygen under ambient conditions [55-57]**.** The oxidations of cyclohexane and *p*-xylene by dioxygen in air are chain reactions involving organic free-radicals; these are considered as homolytic processes. In these systems, cobalt (III and II) and/or manganese (III and II) ions catalyze the initiation steps. Reactions of this type, in which the organic substrates are directly oxidized by air or by pure dioxygen, are often classified as autoxidation processes [58]. Among all transition metals, cobalt is most

commonly used for activating dioxygen. Paramagnetic transition metal ions have the ability to donate unpaired electrons and at the same time receive and donate electron density (π-backbonding), which enables the paramagnetic ($^3O_2$) oxygen molecule to bind reversibly with these metal ions.

1.9. Catalytic oxidation

1.9.1. Catalytic oxidation by Co complexes

Cobalt forms numerous compounds and complexes of industrial importance. Cobalt is one of the most studied oxygen activating metals. Many of its chelate compounds are known to reversibly bind oxygen to form superoxo- or peroxo-type complexes as shown above in Figure 1.5.

Alfred Werner was the first one to observe more than hundred years ago that cobalt reacted with oxygen in air, which caused its complexes to change colour [59]. The formed complex was a dinuclear, peroxo-bridged cobalt-oxygen species, which is the first characterized compound in which molecular oxygen is bound to a metal ion. Since then cobalt and its reactions with oxygen have been under intense study, especially the mononuclear cobalt complexes with Schiff base- or porphyrin type ligands [60]. Salen is the most commonly used chelating ligand in coordination chemistry and homogeneous catalysis. Salen is a Schiff base prepared from salicylaldehyde and ethylene diamine. As shown in Scheme 1.4

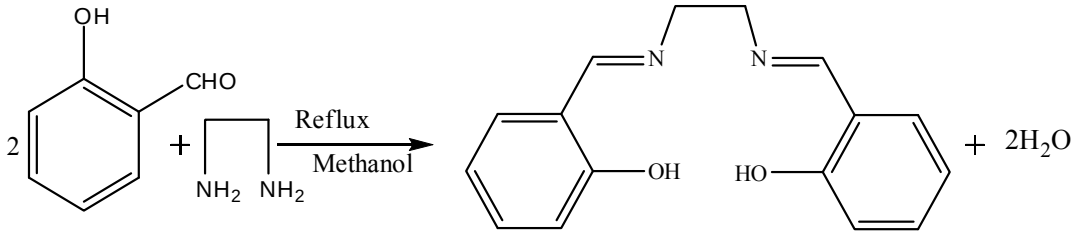

Scheme 1.4. Salen preparation

As an anionic tetradendate ligand, salen resembles other quasi-planar ligands including those that are macrocyclic, such as porphyrinate, corrin, and bis(dimethylglyoximate). The first report of a synthetic reversible cobalt-oxygen carrier was made by Tsumaki in 1938 [61]. He showed that the darkening that had been observed by Pfeiffer and co-workers in 1933 [62], when red-brown crystals of the cobalt (II) Schiff base complex Co(salen) were exposed to the atmosphere, was due to the reversible absorption of molecular oxygen. The cobalt (II) species most widely used as catalysts in oxidation by O_2 are complexes with salen, porphyrin, phthalocyanine, acac, dimethylglyoximato, amine, pyridine, cyclidene and carboxylato ligands.

1.9.2. Intercalation of metal complexes into the clay material

As discussed above metal complexes such as Co(salen) usually form either mononuclear superoxo- or dinuclear μ–oxo type complexes with dioxygen [63]. Such complexes in solution give poor selectivity to the desired product, since a variety of oxygenated products are formed because of the highly reactive nature of free radicals generated during the course of oxidation. In addition, fast deactivation of the metal function due to the formation of μ-oxo dimmers [64] and carryover of trace metal impurities into the product stream during catalyst separation protocol are two critical

issues in case of homogeneously catalyzed liquid phase oxidations . In order to overcome these disadvantages [65-67], metal complexes can be anchored onto or inside solid supports such as inorganic oxides (silica, alumina, microporous zeolites, mesoporous M41S and macroporous clay type materials), carbon, carbon nano tube, fullerene or polymers [68]. The major problem here is that the bonds between metal and ligand are often broken and reformed during catalytic reactions, leading to leaching of the metal from the catalyst in the product, thus decreasing the reaction rate and activity. Reduced leaching was observed when a catalyst is encapsulated inside the zeolite pores (ship-in-a-bottle approach) or of mesoporous MCM-41 type materials [69-70]. Several polymer and inorganic oxide-anchored complexes have been developed with catalytic activities as good as those of homogeneous complexes [71-72]. However, there are no reports on immobilization of cobalt complexes into the interlamellar space of clay materials which can offer diffusion in only two-dimensional space instead of three-dimensional volume. This increases the encounter frequencies between reactants, leading to enhancement in reaction rates at very mild conditions as well as reduction of the extent of undesired reactions [73].

Clays are silicate minerals of aluminium and magnesium hydroxide. They are crystalline materials of very fine particle size ranging from 150 to < 1 micron (colloidal forms). Clays have been also used as green catalysts for several industrially important reactions [74-77]. Clays are classified on the basis of layer type (1:1 or 2:1), layer charge and type of interlayer into eight major groups. Further subdivision into subgroups and species is made on the octahedral sheet type, chemical composition, and the geometry of superposition of individual layer and interlayers.

Saponite and hectorite are examples of trioctahedral smectites and montmorillonite, biedellite and nontronite are the dioctahedral smectites. Main features of saponite type smectite are, cation exchange capacity, swelling properties, transverse layer rigidity, acidity of clays. The general formula for saponite clay is, $[Na^{+}_{x} (M^{2+}_{6})\{Si_{8-x}Al_{x}\} O_{20} (OH)_{4}]$ where M can be Mg, Ni, Zn, Co, etc. Modified smectite (acid activated) clays have proven to be more effective and reasonably inexpensive supports than other supports for transition metals used in various types of reactions carried out in the liquid phase [78]. In addition to their high surface area, their laminar structure confers size or shape selectivity to molecules and hence facilitates interaction with the active sites of metals. The surface hydroxyl groups of saponites, by donating or accepting the protons help in stabilizing the intermediates; for example, cationic hydride intermediate which would otherwise lose protons are stabilized on the surface of saponite due to mobile protons. This is possible because of the negative charge on the oxygens of the clay surface and delocalization of the protons. Interlayer space in clays can be effectively used for exchanging cationic metal complex catalysts and thus novel heterogeneous catalysts can be developed in which the catalytic activity of the complex can be studied in constrained environment of clays. Pinnavaia et al. has studied the selectivity behavior of cationic rhodium phosphine precursors in hectorite clay for hydrogenation of olefins and acetylenes [79].

In our work we have developed metal Schiff bases intercalated into the montmorillonite clay as efficient solid catalysts for liquid phase oxidation of *p*-cresol. Montmorillonite, the main component of bentonite, is a layered silicate mineral that

belongs to the montmorillonite/smectite group of clay minerals. As shown in Figure 1.6 montmorillonite clay consists of three layers: a silicon tetrahedron, an aluminum octahedron, and another silicon tetrahedron. The unit structure is a very thin platelet (about 10A [1 nm] thick and 0.1 to 1μ wide). In montmorillonite, some of the Al ions are substituted by magnesium ions, resulting in a negative charge on the two large surfaces of montmorillonite platelets. This negative charge is neutralized by an interlayer of cations (e.g., Na^{+}, K^{+}, Ca^{2+}, and Mg^{2+}) that separates adjacent layers of platelets. This structure makes montmorillonite chemically stable. The specific characteristics of montmorillonite are due to various actions of its surface negative charge and interlayer cations.

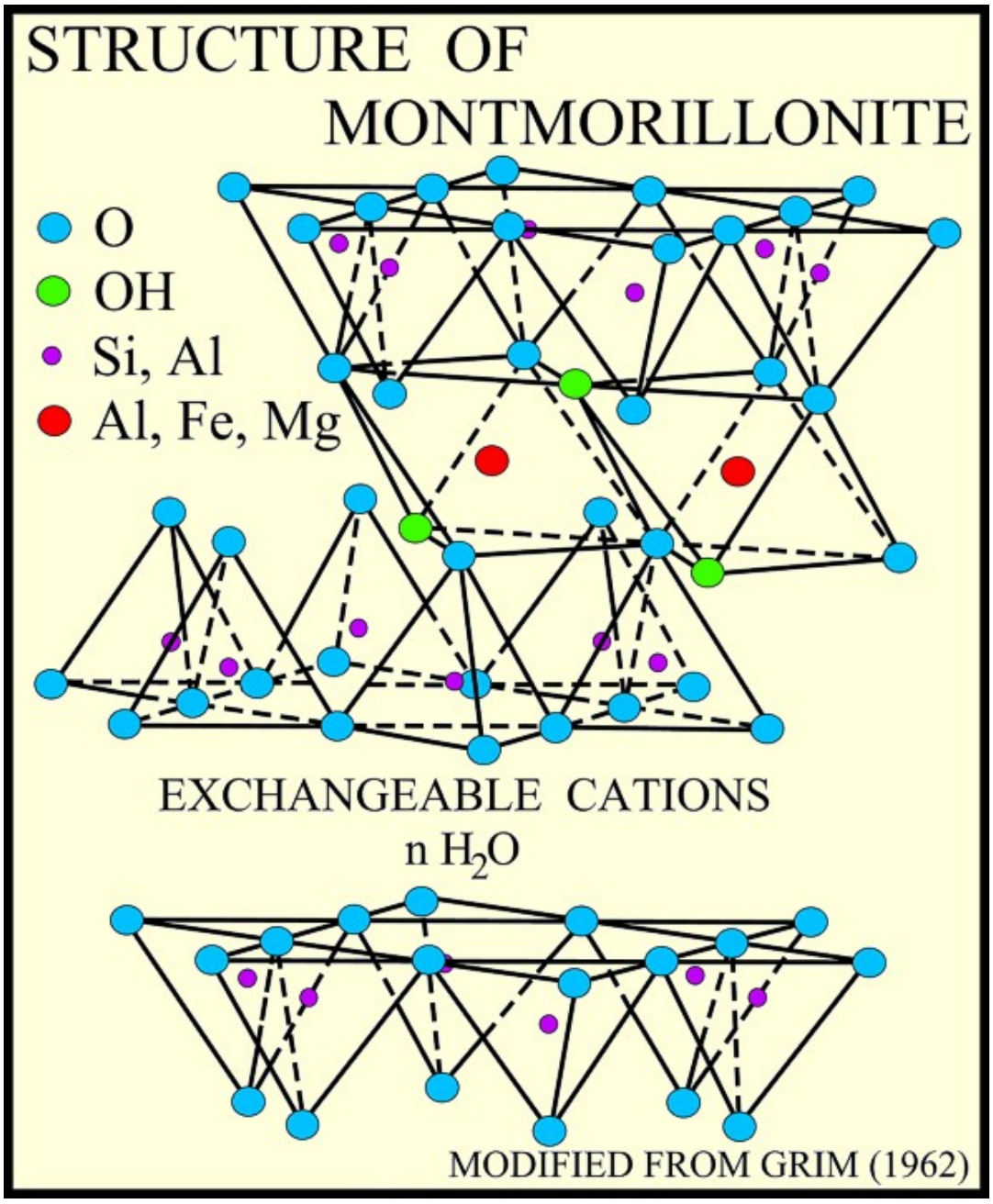

Figure 1.6. Structure of montmorillonite clay.

1.10. Oxidation of aromatic side chains

Catalysis for 'green chemistry' has been nicely illustrated for the production of aromatic acids via oxidation of hydrocarbon oxidation of the side chain of an

aromatic ring. Classical method for such oxidation involved the use of chlorine or nitric acid (Schemes 1.13-1.15) which now has been largely replaced by catalytic oxidations with dioxygen.

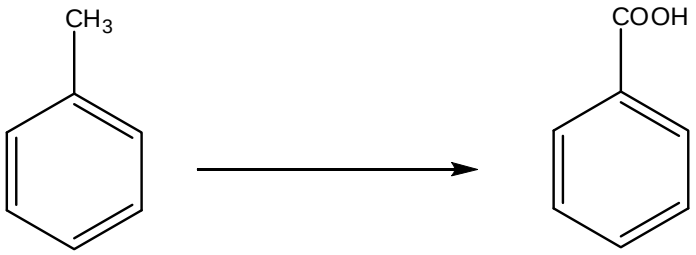

(1.12)

1) Chlorination + Hydrolysis, atom utilization = 36%

$$ArCH_3 + 3\ Cl_2 \longrightarrow ArCCl_3 + 3\ HCl \quad (1.13)$$

$$ArCCl_3 + 2\ H_2O \longrightarrow ArCOOH + 3\ HCl \quad (1.14)$$

2) Nitric acid oxidation, atom utilization = 56%

$$ArCH_3 + 2\ HNO_3 \longrightarrow ArCOOH + 2\ NO + 2\ H_2O \quad (1.15)$$

3) Catalytic aerobic oxidation, atom utilization= 87%

$$ArCH_3 + 1.5\ O_2 \longrightarrow ArCOOH + H_2O \quad (1.16)$$

Figure 1.6. ‘Classical’ versus ‘green’ aromatic side-chain oxidation.

Oxidation of hydrocarbon with dioxygen is more facile when the C─H bond is activated through aromatic or vinylic group adjacent to it. The homolytic C─H bond

dissociation energy decreases from ca. 100 kcal mol^{-1}(alkyl C─H) to ca. 85 kcal mol^{-1} (allylic and benzylic C─H) feasible.

1.10.1. Oxidation of cresols

The alkyl groups of cresols are sensitive to oxidation. Oxidation of phenol substituted derivatives such as *o*-cresol, *p*-cresol, *m*-cresol, 3,4-dimethoxy toluene, *p*-cresyl isobutyrate, *p*-cresyl acetate, *p*-phenoxy toluene, *p*-cresyl methyl ether, *p*-cresidine, 2-nitro-4-methyl phenol etc. is an important step for the variety of chemical products. The resulting oxidation products viz. hydroxy-substituted aromatic aldehydes or ketones are important intermediates in the manufacture of pharmaceuticals, agrochemicals, polymeric resins and artificial flavours. Derivatives of *p*-hydroxy benzyl alcohol and *p*-hydroxybenzaldehyde (PHB) are an important intermediate for the manufacture of vanillin, a widely used flavoring agent, trimethoxybenzaldehyde, various agrochemicals and pharmaceuticals such as semi synthetic penicillin, amoxicillin, antiemetic drug trimethobenzamide [80-81]. *p*-Hydroxybenzaldehyde is also used as an additive for metal plating brighteners, electroplating, in perfumes and in liquid crystals [82]. Depending on the oxidizing agent, reaction conditions, and position of the methyl group, the oxidation of side alkyl group which occur by free radical mechanisms, lead to a large number of compounds such as hydroquinones, quinols, quinones, cyclic ketones, furans, dimeric and trimeric cresols, and toluyl ethers. . After the hydroxyl group has been protected by esterification or etherification, the methyl group can be selectively oxidized to a formyl group (e.g., with manganese dioxide or oxygen) or to a carboxyl group (with acid permanganate

solution). Unlike *m*-cresol, *o*- and *p*-cresols can be directly oxidized with oxygen to give *o*- and *p*-hydroxybenzaldehyde, e.g., in the presence of catalytic amounts of iron tetraarylporphines [83-84]. Alkali fusion of the cresols in the presence of lead oxide or manganese dioxide produces the corresponding hydroxybenzoic acids directly. A detailed literature summary on the oxidation of cresols is presented in Table 1.4.

Table 1.4. Summary of literature on oxidation of phenol substituted derivatives.

Sr. No.	Catalyst/Reagent Used	Substrate	Oxidant	Reaction conditions	Ref.
1	Cetyl pyridinium bromide(CPBr)	*p*-cresol	Chloramine T		85
2	Acetic anhydride	*p*-cresol	Ozone		86
3	Mn(II) acetate, acetic unhydride	*p*-cresol	Ozone		87
4	Polymer supported Schiff base cobalt complex	*p*-cresol	Oxygen	O_2 flow 120ml/min, *p*-cresol 10.8 g, NaOH 14.0g, catalyst 1.2g, methanol 55mL, Reaction Temp 348 K, R.T. 15h	88
5	Manganese acetate, potassium bromide, mineral acid,	*p*-cresol	Ozone	278 K,	89
6	Acetic acid and iron phosphate	*p*-cresol			90
7	CuMn-oxide/C	*p*-cresol	O_2		91
8	5%Pd/C, $CoCl_2$	*p*-cresol,	O_2	373 K, Acetic acid and NaOH, time, 8h,	92
9	Co-Mn/Al_2O_3 and C, Ag, Fe, Ni, Zn and Ce as a promoter,	*o*-cresol	O_2 /air		93
10	Co_3O_4	*p*-cresol	Air	373 K, 3h, High pressure	94
11	Mn_2O_3 sulfuric acid,	*p*-cresol		318 K,	95
12	Supported noble metal Au, Ru, Rh, Pd, Ir, and Pt	*o*-cresol			96
13	CuMn	*p*-cresol			97

14	Co(II) phthalocyanine	*p*-cresol		328-353 K	98
15	Cerium complexes	3,5 dimethoxy *p*-cresol			99
16	$CoCl_2$,	*p*-cresol			100
17	CuCo/C	*o*-cresol			101
18	$Co(OAc)_2$, 2%NH4Br as cocatalyst	*m*-cresol	O_2	10hrs, 353 K	102
19	Cooxide/Resin	*p*-cresol		348 K, 8h,	103
20	Cosalen encapsulated in zeolite	*p*-cresol	Air		104
21	$Co(OAc)_2$ $4H_2O$-$CuSO_4$ $5H_2O$	*p*-cresol	Air	333-340 K , atmospheric pressure	105
22	Co salt	*p*-cresol	O_2	313- 373 K 8-14h,	106
23	Cobaltosic oxide/resin	*p*-cresol	Air		107
24	Cerium complexes	2,6-dimethoxy-*p*-cresol	O2		108
25	CoCuAl hydrotalcite	*p*-cresol			109
26	CoCuAl hydrotalcite	*p*-cresol			110
27	Cobalt sulfophthalocyanine/C	*p*-cresol	O_2	12 h, 333 K,	111
28	$CoCl_2$,	*p*-cresol	Oxygen containing gases	341-343 K, 12h,	112
29	Copper chloride and Cobaltous chloride	*p*-cresol	O_2		113
30	CoCuAl hydrotalcite	*p*-cresol			114
31	Co_3O_4, CeO_2, mixed oxide	*p*-cresol			115
32	$Co(AcO)_2$, $Mn(OAc)_2$ and NaBr	*p*-,*o*-cresol etc.	O_2		116
33	Pd/TiO_2, ZrO_2, ZSM-5, MCM-41	*o*-cresol, *m*-xylene			117
34	Metalloporphyrin immobilised in supercages of NaCoX	*p*-cresol and styrene			118

	molecular sieve				
35	$CoFe_2O_4$,	*p*-cresol			119
36	Metalloporphyrin immobilised in supercages of NaCoX molecular sieve	*p*-cresol and styrene			120
37	Cobalt cerium complex oxide	*p*-cresol			121
38	CoAPO-5	*p*-cresol		333 K,	122
39	Co_3O_4, CeO_2, mixed oxide	*p*-cresol			123
40	Fe, Mn chelates(porphyrin) $Cu(NO_3).3H_2O$	*o*-cresol	O_2	343 K, 30h,	124
41	$CoCl_2$, CoAPO-5 and CoAPO-11	*p*-cresol	O_2	313-353 K,	125
42	Ni complexes	Cresols and methylanisoles			126
43	CoAPO-11, CrAPO-11	*p*-cresol	O_2	10 h, 328 K ,	127
44	Cobalt powder and Cobalt hydroxide	*p*-cresol			128
45	Colloidal SiO_2, and (V_2O_5,+K_2O+Cs_2O+SO_3)	*p*-cresol			129
46	TiO_2 photocatalytic oxidation				130
47	Cerium four coordinated hydroxo ligand	*p*-cresol		2-5 h, 313-393 K,	131
48	Immobilized microorganism, (Enterobacter cloacae IFO 13535)	*p*-cresol		303 K, 30 h, product was *p*-hydroxybenzoic acid	132
49	Co-Mn-Oxide/resinD3520	*p*-cresol			133
50	Pd-Ge/Carbon	*p*-cresol	O_2	Acetic acid, H_20, potassium acetate, 373 K	134
51	Pseudomonas putida KS-0180 (FERM P-12880). Bacteria	*p*-cresol		Product was pHBAcid	135

	And KS0160				
52	Cerium catalyst	*p*-cresol	O_2	393 K ,	136
53	Zeolite ZSM-12	*p*-cresol	H_2O_2		137
54	Cobalt(II) oxide/D3520(macroporous divinylbenzene-styrene copolymer	*p*-cresol			138
55	OsO_4	*m*-cresol		Alkaline medium,	139
56	Cerium(IV)	*o*-cresol			140
57	$CoCl_2$	*p*-cresol	Air		141
58	$FeCl_3$,	*p*-cresol	O_2	1 atm, 333 K, NaOH	142
59	Ammonium metavanadate and KNO_3/celite	*p*-cresol	Air and steam	Gas phase, 673 K,	143
60	Methylhydroxylase from denitrifying bacterium (PC-07)	*p*-cresol		Anaerobic oxidation	144
61	$CoCl_2.6H_2O$, And $FeCl_3.6H_2O$, $NiCl_2$,	*p*-cresol	O_2	1.2atm, 333 K , 1 h,	145
62	Mn, Ni, Cr, Co salts	*p*-cresol	O_2	Isolation of PHB	146
63	bis-(4-methylpyridineisoindolinato)cobalt(II) acetate, phthalocyaninatocobalt(II), and sulfophthalocyaninatocobalt(II) (II).	*p*-methylphenols(cresols)	O_2	333 K ,	147
64	C-meso-5,7,7,12,14,14-hexamethyl-1,4,8,11-tetraazacyclotetradecane nickel(III), ([Ni(III)L])	*p*-cresol			148
65	Fe tetraphenylporphine (FeTPP as FeTPPCl)(sic), $CuCl_2$, and $(NH_4)_2Ce(NO_3)_6$	*p*-cresol	O_2	7 h, 343 K	149

66	$Co(OAc)_2.4H_2O$	*p*-cresol	Air	43 h	150
67	$Co(OAc)_2.4H2O$, $Ce(OAc)_3.H2O$	*p*-cresol	O_2	368 K	151
68	$Co(OAc)_2$	*p*-cresol		338 K	152
69	Microorganism and Fe(III)	*p*-cresol etc			153
70	blue copper protein (azurin) or ferroceneboronic acid (III) as mediator.	*p*-cresol			154
71	Cerium(IV)	m-cresol			155
72	$Cu(OAc)_2$ and $Co(OAc)_2$	*p*-cresol	O_2		156
73	$KMnO_4$	*o*-cresol			157
74	Co_3O_4	*m*-cresol			158
75	$CoCl_2$	*p*-cresol	O_2	333- 338 K,	159
76	PC-07	*p-cresol and nitrate as* e^- *acceptor*			160
77	$CoCl_2$, activated charcoal	*p*-cresol	O_2	10 h, NaOH, MeOH	161
78	AgOAc and $Pd(OAc)_2$	2,6-dialkyl-*p*-cresol			162
79	Ac_2O and H_2SO_4	*m*-cresol acetate			163
80	$Co(OAc)_2.H_2O$, NH_4Br	*m-tosylate toluene*	Air	373 K 10 h	164

Oxidation of methyl group of *p*-cresol is a challenging process since the phenolic hydroxyl group interferes in the oxidation process and only tarry products were formed [165]. The oxidation of *p*-cresol after protecting the phenolic group also gave only tarry products. It is important to note that concentration of alkali which protects

the phenolic should be optimized. Several reports have appeared on use of both homogeneous as well as heterogeneous catalyst systems for the liquid phase oxidation of *p*-cresol nevertheless, developing an improved solid catalyst for *p*-cresol oxidation still remains a challenge [85-92, 94, 95,97, 98, 103-107, 109-115, 119-123, 126-138, etc.]. In this work, we report several novel solid catalysts for liquid phase oxidation of *p*-cresol under mild conditions [166-171]

1.11. Quantitative measurement of a catalyst performance

The overall performance of a catalytic reaction is determined in several ways such as TON (Turnover number), TOF (Turnover frequency h^{-1}), conversion, yield, selectivity and rate of reaction. These are defined as follows.

***1.11.1. TON*:** It is the ratio of moles reactant reacted per mole catalyst. It is a measure of catalyst stability and activity.

***1.11.2. TOF (time^{-1})*:** It is defined as number of moles reactant reacted per mole catalyst per unit time. It is a measure of catalyst efficiency.

1.11.3. Conversion

Consider a chemical reaction,

$$A + B \rightarrow C + D \qquad (1.17)$$

Percent conversion of A is defined as the percentage of reactant 'A' that is consumed in the reaction.

$$\% \text{ Conversion } = \frac{\text{initial conc. of A - final conc of A}}{\text{initial conc. of A}} \times 100$$

1.11.4. Yield

$$A + B \rightarrow C + D \qquad (1.17)$$

Where C is desired product

$$\% \text{ Yield} = \frac{\text{moles of 'A' reacted to produce C}}{\text{moles of 'A' totally reacted}} \times 100$$

1.11.5. Selectivity

Consider a chemical reaction,

$$A + B \rightarrow C + D + E \qquad (1.18)$$

Where C is the desired product

$$\% \text{ Selectivity} = \frac{\text{conc. of C}}{\text{conc. of substrate consumed}} \times 100$$

1.12. Kinetics of heterogeneous catalytic reactions

Liquid phase oxidation reactions is a three phase system involving a reaction between the gas and liquid phase reactants in presence of a solid catalyst as represented below:

$$A + nB \xrightarrow{\text{Catalyst}} nC$$

Where the species A is generally a reactant present in the gas phase and B is a nonvolatile reactant present in the liquid phase, with the reaction occurring at the surface of a solid catalyst.

Various steps taking place for this reaction to occur are:

a) Transport of A from bulk gas phase to the gas-liquid interface.

b) Transport of A from gas-liquid interface to the bulk liquid.

c) Transport of A and B from bulk liquid to the catalyst surface.

d) Intraparticle diffusion of the reactants in the pores of the catalyst.

e) Adsoprtion of the reactants on the active sites of the catalyst.

f) Surface reaction of A and B to yield products.

The intrinsic kinetics of a reaction is a characteristic of that system and its study is important for both understanding the reaction pathway as well as forming a basis for design and scale up purposes. For a solid catalyzed gas-liquid reaction, the overall rate is dependent on the external and intraparticle mass transfer and intrinsic kinetics of the reaction. General aspects of kinetic modeling of a heterogeneous catalytic reaction are briefly summarized here while a detailed study of kinetics of *p*-cresol oxidation in particular, is given in chapter 6.

1.12.1 Power law model

Kinetics of a reaction empirically can be represented by Power Law model in which the rate of a reaction is given by the overall rate constant and the reaction orders.

For example consider the reaction

$$A + B \longrightarrow P \qquad (1.19)$$

In this model it assumed that the rate of reaction is proportional to some powers of the concentrations of the reactants

$$r = k_{mn} C_A^m C_B^n \qquad (1.20)$$

Where k_{mn}, m, n, are the arbitrary constants valid for a particular system in the range of variables investigated. Here m and n are the reaction orders with respect to A and

B respectively, and k_{mn} is the rate constant in $cm^3/mole)^{m+n-1}$ $(cm^3/g)s^{-1}$, C_A and C_B are the concentration of A and B respectively.

***1.12.2. Langmuir-Hinshelwood rate models*:** This approach of studying the kinetics of a heterogeneously catalyzed reaction is more realistic since the reaction of dissolved species A and B occurs on the surface of the catalyst through adsorption of the atoms or molecules of the reactants on the active centers of the catalyst. For the reaction to occur, the steps involved are given in section 1.14

1.12.2.1. Single site L-H model: Let θ be the fraction of surface that is covered and (1- θ) be the fraction that is bare. The rate of adsorption is then $k_{1p}(1- \theta)$ where p is the gas pressure and k_1 a constant. The rate of desorption is equal to $k_{-1}\theta$. At equilibrium, rates are equal and hence

$$\theta/(1- \theta) = k_1 p/k_{-1} \qquad (1.20)$$

From which θ can be written as

$$\theta = kp/(1 + kp) \qquad (1.22)$$

As an example: Consider the reaction

$$A \longrightarrow B \qquad (1.23)$$

$$A + s \longrightarrow As \qquad (1.24)$$

$$As \longrightarrow Bs \qquad (1.25)$$

$$Bs \longrightarrow B + s \qquad (1.26)$$

The rate of reaction is proportional to θ and hence can be written as

$$r = \frac{kC_A}{1 + KC_A} \qquad 1.25$$

Where C_A is the concentration of A.

1.12.2.2. Dual site L-H model

Competitive adsorption: The case of two substances getting adsorbed on neighboring sites is of considerable importance. Let the fraction covered by A be θ and that by B be θ′. Then the fraction bare is (1−θ− θ′). The substances are assumed to be adsorbed without dissociation. The rate of adsorption of A is

$$r_1 = k_1 p(1 - \theta - \theta') \qquad (1.28)$$

And the rate of desorption is

$$r_{-1} = k_{-1}\theta \qquad (1.29)$$

At equilibrium, these rates are equal and

$$\theta/(1 - \theta - \theta') = Kp \qquad (1.30)$$

Where $K=k_1/k_{-1}$

Similarly,

$$\theta'/(1 - \theta - \theta') = K' p' \qquad (1.31)$$

From these equations

$$\theta' = Kp/(1 + Kp + Kp') \qquad (1.32)$$

And

$$\theta' = K' p'/(1 + Kp + Kp') \qquad (1.33)$$

As an example, consider the reaction

$$A + B \longrightarrow P \qquad (1.34)$$

The reaction is between adsorbed A and adsorbed B.

The different steps involved are

$$A + s \longrightarrow As \qquad (1.35)$$

$$B + s \longrightarrow Bs \qquad (1.36)$$

$$As + Bs \longrightarrow Ps + s \qquad (1.37$$

$$Ps \longrightarrow P + s \qquad (1.38)$$

The reaction is proportional to θ and θ□ covered by A and B.

The rate of reaction is therefore,

$$R = \frac{kKK'pp'}{\left(1 + Kp + K'p'\right)^2} \qquad (1.39)$$

In terms of concentration

$$R = \frac{kAB}{\left(1 + KA + K'B\right)^2} \qquad (1.40)$$

Where *A* and *B* are concentrations of A and B respectively.

Comparison between Power law and L-H type kinetic models is given below.

Power law kinetic model	L-H type kinetic model
➢ Mathematically simple and more convenient for fitting the experimental data, but it does not explain the mechanistic aspects of adsorption and surface reaction. ➢ May represent the data over a limited range of concentration.	➢ More suitable for correlating the data over a wider range of concentrations. ➢ More realistic as the sequence of adsorption, surface reaction and desorption steps are better recognized in the models.

➢ May fail in reactions proceeding consecutively as the reactant and intermediate competitively adsorbed, and the reaction order may change.	

1.13. Objectives of the present investigation

The major objective of this thesis was to design and develop various solid catalysts for the selective liquid phase air oxidation of alkyl side chain of *p*-cresol. For achieving this goal, the total work was systematically divided into the following milestones.

- Preparation of metal complexes by conventional methods and their immobilization of these metal complexes into the clay matrix.
- Preparation of clay materials with various composition and properties
- Preparation of nanostructured cobalt oxide materials by co-precipitation and digestion method.
- Detailed characterization of catalyst materials using various techniques such as (Brunauer- Emmett-Teller (BET), UV-Visible spectroscopy, FTIR, XPS, XRD, TGA, extended X-ray absorption fine structure (EXAFS), TEM, SEM, and AAS.
- Catalyst activity testing of the above prepared catalysts for the oxidation reactions of substituted phenol derivatives under the both atmospheric and elevated pressure conditions.

- Optimization of reaction conditions for the best catalysts.
- Kinetics of liquid phase air oxidation of p-cresol by Co_3O_4.
- Interpretation of activity results based on the characterization data.

1.14. References

1. S. Lippard and J. Berg, *Principles of Bioinorganic Chemistry*, University Science Books, **1994**.
2. W. Kaim, B. Schwederski, *Bioinorganic Chemistry: Inorganic Elements in the Chemistry of Life*, John Wiley & Sons, **1994**.
3. R. J. Farranto, C.H. Bartholomew (Eds.) *Fundamentals of Industrial Catalytic Processes*, Blackie Academic and Professional, London, **1997**.
4. G. Ertl, *Surf. Sci*. **1994**, *299-300*, 742.
5. P. T Anastas, J. C. Warner, "*Green Chemistry: Theory and Practice*", Oxford university press, New York, **1998**
6. R. A. Sheldon, *Chem. Ind.* **1992**, *27*, 903.
7. G. W. Parshall, *Homogeneous Catalysis*, John Wiley: New York, **1980**
8. W. N. M. Piet van Leeuwen, in *Homogeneous Catalysis Understanding the Art* Kluwer academic Publishers **2004**
9. C. D. Frohling, C. W. Kohlpaintner, in *Applied Homogeneous Catalysis with Organometallic Compounds*, Volume 1, Eds.: Cornils, B; Herrmann, W. A., Wiley-VCH: Weinheim, **1996**, p. 27.
10. C. Pariya, K. N. Jayaprakash, A. Sarkar *Coord. Chem. Rev*. **1998**, *168*, 1

11. G. W. Parshall, S. D. Ittel, *Homogeneous Catalysis*; John Wiley: New York, **1992**.

12. R. Jira, *Ethylene and its industrial derivatives*, Miller S.A. (Ed.), Ernest Benn Ltd. **1969**, p. 650.

13. J. N. Armor, *Appl. Catal. A* **2001**, *222*, 407

14. National Research Council Panel on New Directions in Catalytic Sciences and Technology, *Catalysis Looks to the Future*, National Academy Press, Washington D. C., **1992**, p.1

15. S. M. George *Chem. Review*, **1995**, *95*, 3.

16. J. Manassen, in *Catalysis, Progress in Research,* Eds.: Basolo, F; Burwell Jr., R. E., Plenum Press: New York, **1973**, p. 177.

17. (a) B. Schulze, M. G. Wubbolts *Curr. Opin. Biotechn.*, **1999**, *10*, 609.

    (b) P. Villeneuve, J. M. Muderhwa, J. Graille, J. H. Michael *J. Mol. Catal. B: Enz.* **2000**, *9*, 113.

18. M. Svedendahl, K. Hult, P. Berglund, *J. Am. Chem. Soc*. **2005**, *127*, 17988.

19. (a) B. M. Trost, *Science* **1991**, *254*, 1471.

    (b) B. M. Trost, *Angew. Chem. Int. Ed.* **1995**, *34*, 259.

20. R. A. Sheldon, in *The Activation of Dioxygen and Homogeneous Catalytic Oxidation*, D. H. R. Barton, A. E. Martell and D. T. Sawyer, Eds., Plenum Press, New York, **1993**.

21. J. Ebner , D. Riley in *Active Oxygen in Chemistry,* J. S. Valentine, A. Greenberg and J. F. Liebman, Eds., Chapman and Hall, London, vol.1, **1995.**

22. P. Skibida, A. M. Sakharov, *Catal. Today* **1996**, *27*, 187.

23. R. A. Sheldon, In *Catalytic Oxidation: Principles and Applications*: R. A. Sheldon, van Santen, Eds.; World Scientific: Singapore, **1995**; p 177
24. S. V. Ley, A. Madin in *Comprehensive Organic Synthesis*, Eds. B. M. Trost and I.Fleming, Pergamon, Oxford, **1990**, vol. *7*, pp 251.
25. F. A. Luzzio, *Org. React*. **1998**, *53*, 1.
26. R. A. Sheldon, H. van Bekkum, *Fine Chemicals through Heterogeneous Catalysis*, Wiley-VCH, Weinheim, **2001**, p 1.
27. J. M. Thomas, R. Raja, G. Sankar, R. G. Bell, *Nature* **1999**, *398*, 227.
28. S. S. Stahl, *Angew. Chem. Int. Ed*. **2004**, *43*, 3400.
29. C. Limberg, *Angew. Chem. Int. Ed*. **2003**, *42*, 5932.
30. A. D. Sadow, T. D. Tilley, *Angew. Chem. Int. Ed*. **2003**, *42*, 803.
31. C. Subrahmanyam, B. Louis, F. Rainone, B. Viswanathan,A. Renken, T. K. Varadarajan, Catal. Commun. **2002**, *3*, 45.
32. A. Martin, U. Bentrup, A. BrPckner, B. LPcke, *Catal. Lett*. **1999**, *59*, 61.
33. F. Konietzni, H.W. Zanthoff, W. F. Maier, *J. Catal*. **1999**, *188*, 154.
34. A. Martin, U. Bentrup, G.-U. Wolf, *Appl. Catal. A* **2002**, *227*, 131.
35. F. Bruhne, E. Wright, *Ullmann's Encyclopedia of Technical Chemistry*, 6th edn., **1998**, Electronic Release (benzaldehyde entry).
36. F. Konietzni, U. Kolb, U. Dingerdissen, W. F. Maier, *J. Catal*. **1998**, *176*, 527.
37. A. K. Suresh, M. M. Sharma, T. Sridhar, *Ind. Eng. Chem. Res.* **2000**, *39*, 3958.

38. R. A. Sheldon, I. W. C. E. Arends and A. Dijksman, *Catal. Today* **2000**, *57*, 157.

39. D. Riley, M. Stern, J. Ebner, in *The Activation of Dioxygen and Homogeneous Catalytic Oxidation*, D. H. R. Barton, A. E. Martell and D. T. Sawyer, Eds., Plenum Press, New York, **1993**.

40. R. A. Sheldon, J. Dakka, *Catal Today* **1994**, *19*, 15.

41. W. Kaim, B. Schwederski, *Bioinorganic Chemistry: Inorganic Elements in the Chemistry of Life*, John Wiley & Sons, **1994**.

42. S. Lippard, J. Berg, *Principles of Bioinorganic Chemistry, University Science Books*, **1994**.

43. R. Sheldon, *Metalloporphyrins in Catalytic Oxidations*, Marcel Dekker, Inc., New York, **1994**.

44. R. D. Jones, D. A. Summerville and F. Basolo, *Chem. Rev.* **1979**, *79*, 139.

45. M. Costas, M. P. Mehn, M. P. Jensen, L. Que, Jr., *Chem. Rev*. **2004**, *104*, 939.

46. R. A. Sheldon, in *The Activation of Dioxygen and Homogeneous Catalytic Oxidation*, D. H. R. Barton, A. E. Martell and D. T. Sawyer, Eds., Plenum Press, New York, **1993**.

47. K. Karlin and Z. Tyeklár, in *Bioinorganic Chemistry of Copper*, Eds., Chapman&Hall, *1993*.

48. Y. Cui, R. Patt, R. Chen and J. Gratzl, *J. Mol. Catal. A: Chem.* **1999**, *144* 411.

49. R. Hage, J. E. Iburg, J. H. Koek, R. Martens, J. Kerschner, E. L. M. Lempers, R. J. Martens, U. S. Racheria, S. W. Russell, T. Swarthoff, M. R. P van Vliet, J. B. Warnaar, L. van der Wolf, B. Krijnen, *Nature* **1994**, *369*, 637.

50. R. Sheldon and J. Kochi, *Metal-Catalyzed Oxidations of Organic Compounds*, Academic Press, **1981**.

51. , J. E. Huuhey, E. A. Keiter, R. A. Keiter Eds., *Inorganic Chemistry: Principles of Structure and Reactivity* HarperCollins College Publishers, New York, **1993**.

52. M. Matsumoto, S. Ito, *J. Chem Soc. Chemm. Commun*. **1981**, 907

53. T. F. Blackburn, J. Schwartz, *J. Chem. Soc. Chem. Commun*. **1977**, 157

54. M. F. Semmelhack, C. R. Schmid, D. A. Cortes, C. S. Chou, *J. Am. Chem. Soc*. **1984**, *106*, 3374.

55. R. D. Jones, D. A. Summerville, F. Basolo, *Chem Rev*. **1979**, *79*,139.

56. E. C. Niederhoffer, J. H. Timmons, A. E. Martell, *Chem Rev*. **1984**, *84*, 137.

57. D. H. Busch, N. W. Alcock, *Chem Rev*. **1994**, *34*, 585

58. A. K. Suresh, M. M. Sharma and T. Sridhar, *Ind. Eng. Chem. Res*., **2000**, *39*, 3958.

59. A. Werner and A. Mylius, Z. *Anorg. Allg. Chem*. **1898**, *16*, 245

60. E. Niederhoff, J. Timmon and A. E. Martell, *Chem. Rev*. **1984**, *84*, 137.

61. T. Tsumaki, *Bull. Chem. SOC. Jpn.*, **1938**, *13*, 252.

62. P. Pfeiffer, E. Brieth, E. Lubbe. and T. Tsumaki, Justus Liebigs *Ann. Chem*., **1933**, *84*, 503.

63. R. J. Motekaitis and A. E. Martell, *Inorg. Chem*. **1988**, *27*, 2718.

64. R. A. Sheldon, In *Catalytic Oxidation: Principles and Applications*: R. A. Sheldon, van Santen, Eds.; World Scientific: Singapore, **1995**;p 177.

65. Y. Iwasawa: in *Tailored Metal Catalysts* D.Reidel Publishing Comp., Holand, **1986**.

66. A. Kozlov, K. Asakura and Y. Iwasawa, *Micro. Meso. Mater*.**1998**, *21*, 571.

67. M. Ichikawa, *Platinum Metals Review*. **2000**, *44*, 3.

68. I. W. C. E. Arends, R. A. Sheldon, *Appl. Catal. A: gen.* **2001**, *212*, 175.

69. D. E. De Vos, M. Dams, B. F. Sels, P. A. Jacobs, *Chem. Rev*. **2002**, *102*, 3615.

70. A. Corma, *Chem. Rev*. **1997**, *97,* 2373.

71. D.C. Bailey, S.H Langer, *Chem. Rev*. **1981**, *81*, 109.

72. B.C. Gates, *Stud. Surf. Sci. Catal*. **1986**, *29*, 4153.

73. S. Cheng, *Catal. Today* **1999**, *49*, 303.

74. R.E. Grim, 2nd ed., *Clay Mineralogy*, McGraw-Hill, New York, **1968**.

75. M. Balogh, P. Laezlo, *Organic Chemistry Using Clays*, Springer, Berlin, **1993**.

76. J.M. Thomas, W.J. Thomas, in: *Principles and Practice of heterogeneous catalysis*, VCH, Weinheim, **1997**, p. 624.

77. J.J. Fripiat, in: G. Ertl, H. Knozinger, J.Weitkamp (Eds.), *Handbook of Heterogeneous Catalysis*, VCH, Weinheim, **1997**, P .387

78. J. H. Clark, A. J. Butterworth, S. J. Tavener, A. J. Teasdale, S. J. Barlow, T. W. Bastock, K. Martin, *J. Chem. Technol. Biotechno.*, **1997**, *68*, 367

79. T.J. Pinnavaia R.Raythatha, J.G.S.Lee,L.J.Halloran, J.F.Hoffman, *J. Am. Chem. Soc*. **1979**, *101*, 6891.

80. T. Sigeru, T. Hideo, S. Takasi, A. Mitstio, *J. Org. Chem*., **1979**, *44,* 3305.

81. D. V. Rao, F. A. Stuber, *Synthesis*, **1983**, 4308

82. S. Mitchell, *Kirk-Othmer Encyclopedia of Chemical Technology*, 4th ad.; Willy-Interscience: New York, **1998**; vol. 13, pp1030.

83. A. Schnatterer, H. Fiege, Bayer AG, *EP 330036*, **1989**

84. A. Schnatterer, H. Fiege, K.-H, Neumann Bayer AG, *EP 451650*, **1991**

85. S. Geetha, *Journal of Indian Council of Chemists*, **2007**, *24*, 79.

86. A. G. Galstyan, G. O. Sedikh, G. A. Galstyan, *Ukrainskii Khimicheskii Zhurnal*, **2007**, *73*, 104.

87. A. G. Galstyan, G. O. Sedikh, G. A. Galstyan *Kinet. Catal.*, **2008**, *49*, 186.

88. G. Xin-ying, Z. Da-yang, *Shenyang Huag. Xuey. Xuebao*, **2006**, *20*, 241.

89. A. A. Sedykh, A. G. Galstyan, *Russ. J. Appl. Chem.*, **2006**, *79*, 123.

90. Y. Zhu, J. Li, X. Yang, Y. Wu, *Cuihua Xuebao*, **2005**, *26*, 261.

91. F. Wang, G. Yang, W. Zhang, W. Wu, J. Xu, *Adv. Synth. Catal.* **2004**, *346*, 633.

92. B. Barton, C. G. Logie, B. M. Schoonees, B. Zeelie, *Org. Proc. Res. Dev.* **2005**, *9*, 62.

93. J. Xu, F. Wang, *CN1475307* **2004.**

94. C. V. Rode, M. V. Sonar, J. M. Nadgeri, R. V. Chaudhari, *Org. Pro. Res. Dev.* **2004**, *8*, 873.

95. H. Jian-ling, S. De-sheng W. Zun-yao *Dangdai Huagong*, **2004**, *33*, 4.

96. T. Hayashi, *JP 2005104940 A2* **2005**, 12 pp.

97. F. Wang, G. Yang, W. Zhang, W. Wu, J. Xu *Chem. Comm.* **2003**, *10*, 1172.

98. Z. Cai, W. Yang, Z. Zhang *CN 1319581 A* **2001**, 11 pp

99. T. Yoshikuni, *J. Mol. Catal A: Chem.* **2002**, *187*, 143.

100. A. Wolf, C. Krueger, R. Langer A. Klausener *DE 10219030 A1* **2003**, 8 pp.

101. F. Wang, J. Xu, S. Liao, *Chem. Comm.* **2002**, *6,* 626..

102. J. Liu, P. Yi, *Zhongguo Kuangye Daxue Xuebao*, **2000**, *29*, 550.

103. G. Zhenghong, S. Y. Jing, W. Siping, Y. Ping, *Appl. Cat. A: Gen.* **2001**, *209*, 27.

104. T. Joseph, C. S. Sajanikumari, S. S. Deshpande, S. Gopinathan *Indian J. Chem., Sect. A*: **1999**, *38*, 792.

105. Y. She, Y. Huang, X. Wang, X. Song, Y. Chen, J. Yang, *Beijing Gongye Daxue Xuebao*, **1999**, 25, 114.

106. H. Kang, H. Yuezhen H. Yuecong *CN 1249298* A **2000**,3.

107. C. Zhiyu, S. Yajing, G. Zhenghong, Y. Ping, *Tianjin Daxue Xuebao*, **1998**, *31*, 783.

108. T. Yoshikuni, Y. Sasaki, *Kyoiku Kenkyu Ronbunshi*, **1998**, *7*, 133.

109. Y. Liu, K. Zhu, S. Liu, X. Yie, Y. Wu, *Yingyong Huaxue*, **1998**, *15*, 15.

110. Y. Liu, S. Liu, K. Zhu, X. Ye, Y. Wu *Appl. Catal., A,* **1998**, *169*, 127.

111. H. Li, K. Shenglu, *Hecheng Huaxue*, **1997**, *5*, 404.

112. K. Ishizawa, O. Gyokuzan, H. Nakatsu, *JP 10287608 A2* 2 **1998,** 5 pp.

113. Y. Ji, Wei, Xianyong *Meitan Zhuanhua*, **1998**, *21*, 85.

114. Y. Liu, K. Zhu, S. Liu, X. Yie, *Yingyong Huaxue*, **1998**, *15*, 11.

115. C. Liu, Y. Fan, Y. Chen, *Shiyou Jiagong*, **1997**, *13*, 43.

116. S. G. Koshel, V. V. Voronenkov, G. N. Koshel, E. K. Rudkovskii, T. B. Krestinina, *Russ. J. Org. Chem.,* **1997**, *33*, 1044.

117. S. Cho, D. S. Kim, S. I. Woo, *Korean J. Chem. Eng*., **1997**, *14*, 479.

118. X. Wang, S. Gao, C.S. Ca, L. X. Yu, G. Jing-Fu; S. Shu-Ju; C. Xi-Zhang, *Chem. Res. Chin. Univ*. **1998**, *14*, 111.

119. Liu, Changkun *Gongneng Cailiao*, **1997**, *28*, 427.

120. W. Xing-Qiao, G. Shuang; C. Chang-Sheng, Y. Lian-Xiang, G. Jing-Fu, C. Xi-Zhang, *J. Porphyrins Phthalocyanines*, **1998**, *2*, 209.

121. C. Liu, Y. Fan, Y. Chen, *Gongneng Cailiao*, **1997**, *28*, 316.

122. V. Vo, N. Ba Xuan, N. Van Phat, C. Van Minh, P. Hu'u Dien *Tap Chi Hoa Hoc*, **1996**, *34*, 59.

123. C. Liu, Y. Fang, Y. Chen, *Bopuxue Zazhi*, **1997**, *14*, 45.

124. A. Schnatterer, H. Fiege, K. H. Neumann, *Eur. Pat. Appl. EP 451650 A1* **1991**, 15 pp

125. M. P. J. Peeters, M. Busio, P. Leijten, J. H. C. van Hooff, *Appl. Catal., A*, **1994**, *118*, 51.

126. D. Meirstein, Y. Usan, *Israeli IL 79763 A1* **1991**, 18 pp.

127. J. Dakka, R. A. Sheldon, *Neth. Appl. NL 9200968 A* 1994, 8 pp

128. Y. Kamiya, N. Okabayashi, N. Kamiyama, *Sekiyu Gakkaishi*, **1994**, *37*, 52.

129. Y. Asami, *JP 07031882 A2* 1995.

130. V. Brezova, E. Brandsteterova, M. Ceppan, J. Pies, *Chem. Commun*. **1993**, *58*, 1285.

131. T. Yoshikuni, *J. Chem. Technol. Biotechnol*. **1994**, *59*, 353.

132. M. Ishikura, D. Takeuchi, T. Iizuka, K. Uehara, *JP 07059582 A2* **1995** 6 pp.

133. K. Yang, M. Zhang, *Lizi Jiaohuan Yu Xifu*, **1993**, *9*, 402.

134. M. Costantini, D. F. Laucher, Eric *Eur. Pat. Appl. EP 577476 A1* **1994**, 18 pp.

135. K. Uehara, M. Ishikura, D. Takeuchi, *JP 05336980 A2* **1993** .

136. T. Yoshikuni, *J. Mol. Catal.* **1992**, *72*, 29.

137. N. K. Mal, A. Bhaumik, R. Kumar, A. V. Ramaswamy, *Catal. Lett*. **1995**, *33*, 387.

138. K. Yang, J. Li, M. Zhang, *Lizi Jiaohuan Yu Xifu*, **1990**, *6*, 328.

139. A. K. Singh, S. Saxena, M. Saxena, R. Gupta, R. K. Mishra, *Indian J. Chem., Sect. A* **1988**, *27*, 438.

140. J. P. Singh, S. J. S. Sirohi, M. Aishwati, Miss., *J. Indian Chem. Soc*. **1987**, *64*, 440..

141. S. N. Sharma, S. B. Chandalia, *J. Chem. Technol. Biotechnol*. **1990**, *49*, 141.

142. H. Kamimura, *JP 62135443 A2* **1987**, 2 pp.

143. I. Nakamura, N. Saito, K. Takatsu, *JP 01100141 A2* **1989**

144. I. D. Bossert, G. Whited, D. T. Gibson, L. Y. Young, *J. Bacteriol*. **1989**, *171*, 2956.

145. H. Kamimura, *JP 62153240 A2* **1987**, 3 pp..

146. F. Roehrscheid, *DE 3525848 A1* **1987**, 4 pp.

147. P. Campo, P. Cocolios, P. Dognin, H. Ledon, *EP 323290 A1* **1989**, 11

148. Y. Uzan, D. Meyerstein, *Isr. J. Chem.* **1986**, *27*, 280.

149. A. Schnatterer, H. Fiege, *EP 330036 A1* **1989**, 16 pp.

150. M. Osu, M. Suzuki, T. Tokumaru, M. Yahata, K. Nishizawa, Y. Horikawa, *JP 63264435 A2* **1988**, 8 pp.

151. T. Yoshikuni, *JP 63104937 A2* **1988,** 5 pp.

152. M. Osu, M. Suzuki, T. Tokumaru, M. Yahata, K. Nishizawa, Y. Horikawa, *JP 62263139 A2* **1987**, 3.

153. D. R. Lovley, D. J. Lonergan, *Appl. Environ. Microbiol*. **1990**, *56*, 1858.

154. H. A. O. Hill, B. N. Oliver, D. J. Page, D. J. Hopper, *J. Chem. Soc., Chem. Commun*. **1985**, 21, 1469.

155. R. G. Varma, R. L. Yadav, *J. Pure Appl. Sci*. **1983**, *16*, 135.

156. T. Miyazaki, H. Uzawa, A. Furukawa, H. Kaneda, *JP 61024535 A2* **1986** , 5 pp.

157. Z. S. Makarova, I. B. Repinskaya, *Zh. Org. Khim*. **1982**, *18*, 1022.

158. Z. Bulgaranova, D. Klisurski, D. G. Dimitrov, *Vissh. Khim.-Tekhnol.* Inst., Sofia, 1979, 25, 124.

159. A. T. Au, *US 4471140 A* **1984**, 3 pp.

160. I. D. Bossert, L. Y. Young, *Appl. Environ. Microbiol*. **1986**, *52*, 1117.

161. A. T. Au, C. W. Jung, *US 4453016 A* **1984**, 3 pp.

162. T. Itahara, T. Sakakibara, *Bull. Chem. Soc. Jpn*. **1979**, *52*, 631.

163. I. V. Vygodskaya, V. Y. Kugel, F. I. Novak, A. N. Bashkirov, *Neftekhimiya*, **1978**, *18*, 409.

164. S. Nagao, T. Takahashi, *JP 54109941* **1979**, 5 pp.

165. E. Marko, L. Triendl, *Catal. Lett.* **1992**, *46*, 345.

166. C. V. Rode, V. S. Kshirsagar, J. M. Nadgeri, K. R. Patil *Ind. Eng. Chem. Res*. **2007**, *46*, 8413.

167. V. S. Kshirsagar, J. M. Nadgeri, P. R. Tayade, C. V. Rode *Appl. Catal. A: gen*. **2008**, *339*, 28.

168. V. S. Kshirsagar, S. Vijayanand, H. S. Potdar, P. A. Joy, K. R. Patil, C. V. Rode, *Chem. Lett*. **2008**, *37*, 310.

169. V. S. Kshirsagar, K. R. Patil, M. Shirai, C. V. Rode, *Top. Catal*. **2009**, *52*, 784.

170. V. S. Kshirsagar, A. C. Garade, K. R. Patil, R. K. Jha, C. V. Rode, *Ind. Eng. Chem. Res* **2009**.(doi 10.1021/ie801941e).

171. V. S. Kshirsagar, A. C. Garade, K. R. Patil, A. Yamaguchi, M. Shirai, C. V. Rode *accepted* in *Appl. Catal. A: Gen.* **2009**.

2.1. Materials

p-Cresol, *o*-cresol, *m*-cresol were supplied by Loba Chemie while sodium hydroxide was obtained from Merck. Analytical grade as well as HPLC grade methanol was obtained from M/s Runa Chemicals, India. Commercially available montmorillonite was obtained from Sigma-Aldrich, Banglore, India. Cobalt acetate, salicyladehyde, ethylene di-amine, *o*-phenylenediamine, and acetophenone were purchased from S.d. fine chemicals, India. Sodium silicate, aluminuim nitrate, magnesium nitrate, urea, sodium hydroxide, were purchased from Merck limited, India. Air compressed in the cylinders used for the oxidation reactions was purchased from M/s Inox Ltd. Mumbai.

2.2. Catalyst preparation

Various solid catalysts used for liquid phase oxidation of *p*-cresol were: (i) Co and Mn based Schiff bases intercalated into clays; (ii) Cobalt saponites; and (iii) nanostructured spinel cobalt oxide.

Detailed methods of preparation of these catalysts are given below.

2.2.1. Intercalated catalyst

Clay intercalated catalyst samples used in this work were prepared stepwise:

i. Preparation of synthetic clays
ii. Preparation various Schiff base ligands
iii. Preparation various Co and Mn Schiff bases
iv. Preparation of Co and Mn Schiff bases intercalated into clay material.

Synthetic clay samples were prepared by making the slurry of sodium silicate (17.96 g, 0.063 moles), aluminium nitrate (3.12 g, 0.017 moles) and sodium hydroxide (0.39 g, 0.018 moles) in de-ionized water and stirring for half an hour at 363 K. After being mixed homogeneously, magnesium nitrate (15.82 g, 0.062 moles) and urea (15.01 g, 0.249 moles) were added. The whole mixture was stirred for 12 h. Then the mixture was cooled to room temperature, filtered and washed with distilled water and kept overnight in aluminium nitrate solution. Then it was filtered, washed with distilled water and the residue was kept 10h for drying at 383 K.

2.2.1.1. Schiff base ligand preparation

Several Schiff bases were prepared by the reported condensation method as per the scheme 2.1 [1]. In a typical preparation of salen Schiff base, stoichiometric amount of salicylaldehyde (2.44 g, 0.02 moles) dissolved in methanol (25 mL) was added drop by drop to ethylene diamine solution (0.6 g, 0.01 moles in 25 mL methanol). The contents were refluxed for 2 h and bright yellow crystals of N, N'-ethylenebis(salicylideneamine)[salen] were obtained which were separated by filtration, washed and dried in vacuum. The crude product was then recrystallized from methanol to yield pure salen with melting point as 400 K (reported m.p. 401 K).

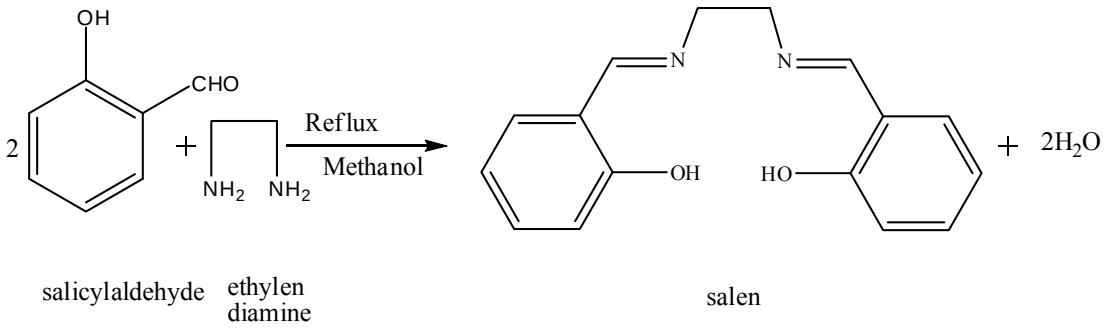

Scheme 2.1. Preparation of salen

Other Schiff bases, 1) N, N'- phenylenebis(salicylideneamine) [salophen],

2) N, N'-ethylenebis(acetophenoneamine) [acene],

and 3) 1,4-N,N'- phenylenebis(salicylideneamine) [1,4 salophen] were prepared by following the condensation method similar to that used for the salen except by changing the relevant carbonyl and amino precursors as shown in Schemes 2.2 to 2.4.

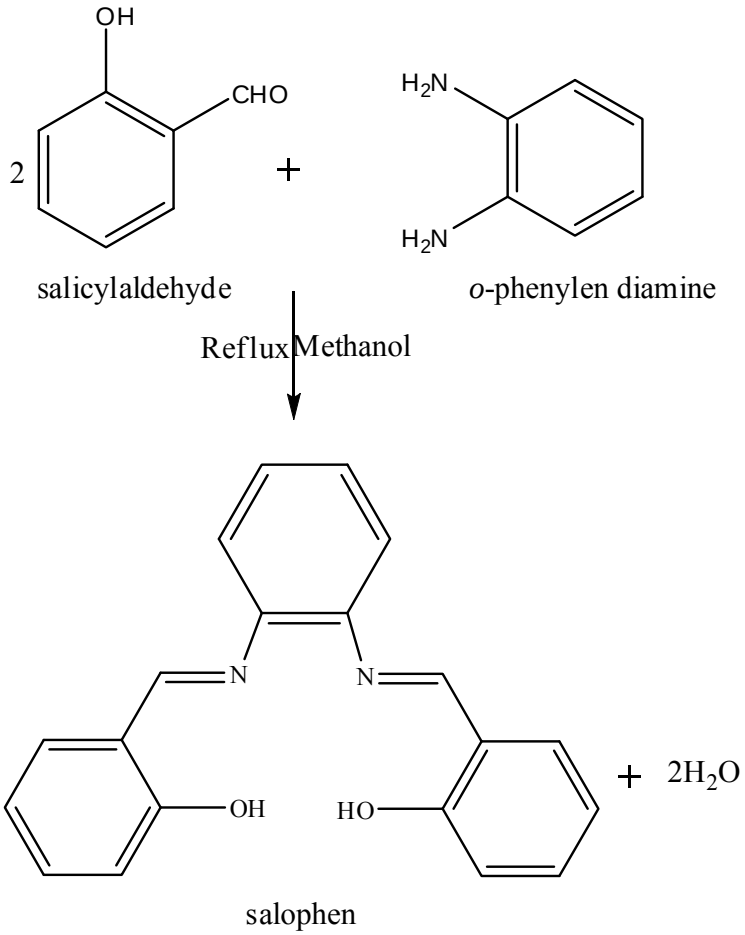

Scheme 2.2. Salophen preparation

Color : Saffron
Melting point : 436 K

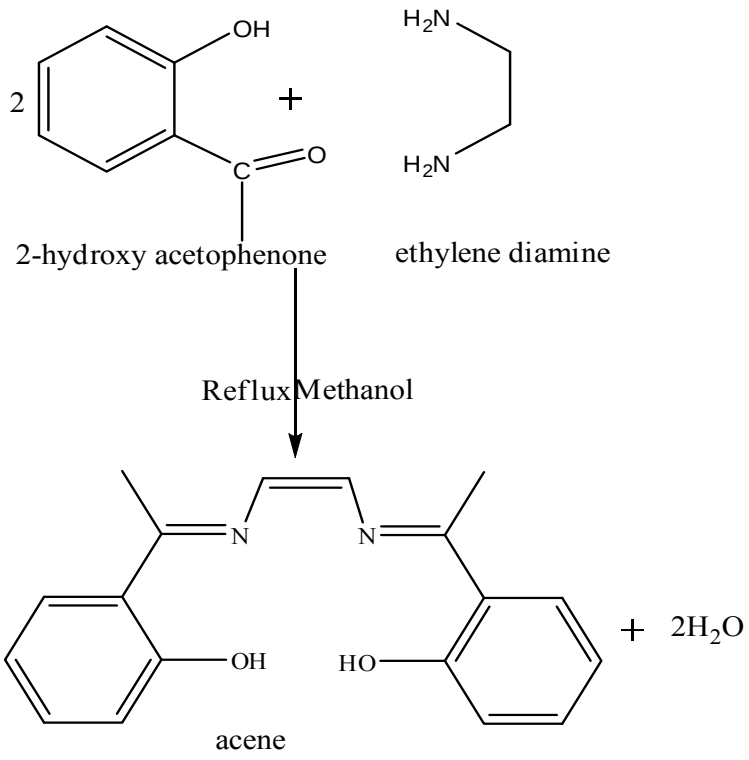

Scheme 2.3. Acene preparation

Color	:	Yellow
Melting point	:	423 K

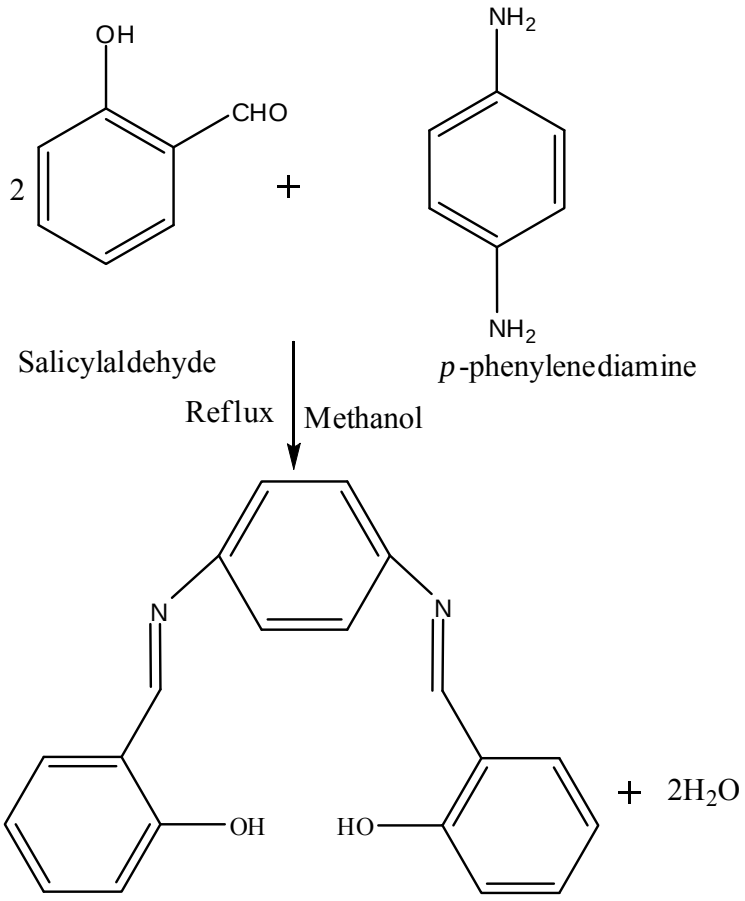

Scheme 2.4. Preparation of 1,4 Salophen

Color : Orange
Melting point : 493 K

2.2.1.2. Co and Mn Schiff base complexes

Cobalt and manganese salen complexes were prepared as per the literature method [2]. Methanol (50 mL) and water (20 mL) were first degassed by bubbling nitrogen gas through them. Salen (1.08 g, 0.004 moles) was then dissolved in the degassed methanol (50 mL) taking care that an inert nitrogen atmosphere was maintained throughout the reaction and the temperature was maintained at 333 K. Cobalt acetate

(1 g, 0.004 moles) was dissolved separately in 20 mL of degassed water and added dropwise into the solution of salen in methanol. The reaction mixture was refluxed for two hours. It was then cooled, filtered and washed with water. The reddish brown crystals of Co-salen were vacuum dried and the yield was recorded (89 %). Similar method was adopted for the preparation of other cobalt-Schiff base complexes.

2.2.1.3. Intercalation of the metal Schiff bases

A typical preparation of cobalt-Schiff base intercalated into the montmorillonite clay involved the addition of the solution of Co-salen (0.5.g, $1.53x10^{-3}$ moles) in chloroform (15 mL) under N_2 atmosphere to the slurry of montmorillonite clay (5 g) made in chloroform (150 mL). This mixture was kept 6 h for a stirring at room temperature and then for ageing 12 hours. After ageing, the catalyst was filtered, washed with chloroform and acetone and Soxhlet extracted with 250 mL chloroform to remove physically adsorbed metal complex. Catalyst thus prepared was designated as Co(salen)-mont. Other catalysts were also prepared by the same method.

Soxhlet extraction apparatus is shown in Figure 2.1

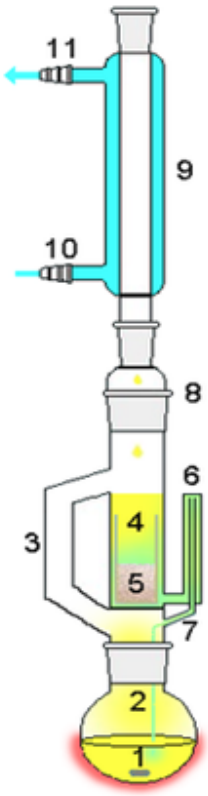

Figure 2.1. Soxhlet extraction

1: Stirrer bar/anti-bumping granules

2: Still pot (extraction pot)

3: Distillation path

4: Soxhlet Thimble

5: Extraction solid (residue solid)

6: Syphon arm inlet

7: Syphon arm outlet

8: Expansion adapter

9: Condenser

10: Cooling water in

11: Cooling water out

2.2.2. Solid cobalt saponite catalyst

A slurry of sodium silicate (17.97 g, 0.063 moles) was made in a solution of aluminum nitrate (3.13 g, 0.016 moles) and sodium hydroxide (0.391 g, 0.018 moles) in deionized water (120 mL) and was stirred for 0.5 h at 363 K. After obtaining the homogeneous mixture, cobalt acetate (3.0 g, 0.014 moles) and urea (15 g, 0.249 moles) were added to the above solution. This whole mixture was stirred for 12 h at 363 K . After cooling, Co-saponite cake was filtered, washed with distilled water, and then dried in a static air furnace at 383 K. Following this procedure, Co-saponite catalysts were prepared with Co content varying in the range of 5-30%.

2.2.3. Nano structured cobalt oxide

The nanostructured Co_3O_4 was prepared from $Co(NO_3)_2$ and K_2CO_3 by a simple protocol without using any template, involving a simultaneous coprecipitation/digestion technique followed by calcination at 573 K in air [3]. Experimental steps are shown schematically in Figure 2.2.

Initially, cobalt nitrate solution is made by dissolving 15.614 g (0.054 moles) in 400 mL of deionized water. Similarly solution of potassium carbonate is prepared by dissolving 7.95 g (0.057 moles) in 400 mL of deionized water. 200 mL of deionized water was taken in a 2 liter capacity round-bottom flask and stirred well using a magnetic stirrer. Then potassium carbonate and cobalt nitrate solutions were added to 200 mL of deionized water (from separate burettes) drop by drop to precipitate Co

cations in the form of their hydroxides. The temperature was maintained at 343 K during precipitation/digestion experiment. The pH after precipitation was found to be in the range of 7.0–8.0. The precipitates were further digested with different time intervals ranging from 0-16 h. The digested precipitates were filtered and re-dispersed again in 2 liter of hot deionized water, filtered and washed first with ethanol followed by acetone and air dried at room temperature. The as-dried precipitates were calcined in a programmable furnace at 573 K for 5 h in air with a heating rate of 2°C/min to produce nano-sized Co_3O_4 powder.

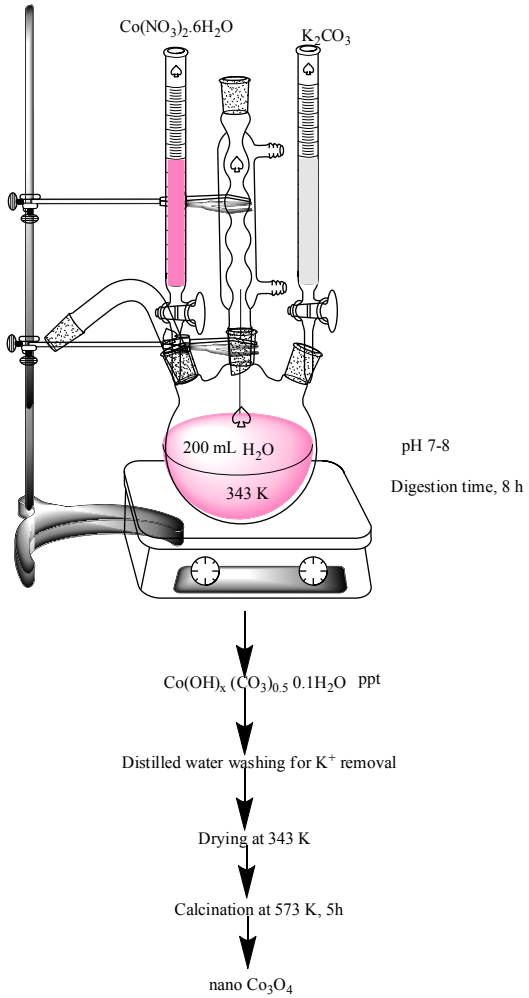

Figure 2.2. Nano catalyst preparation

2.3. Physicochemical characterization of catalyst

The prepared catalyst samples were characterized by various physico-chemical methods such as surface area and pore volume measurements, X-ray diffraction analysis, infrared spectroscopy, SEM, TG-DTA, XPS, XAFS, XANES, HRTEM and SEM. This section of chapter 2 gives a brief account of the theory and principle of various characterization techniques used for the current study. The procedure for each experimental technique is described. Characterization results are discussed in the relevant chapters.

2.3.1. Surface area measurement

Brunauer, Emmett and Teller (BET) method: This is based on the multilayer adsorption. The BET equation can be represented as

$$P/V(P_o-P) = 1/cV_m + [(c-1)/cV_m]\,(P/P_o), \qquad (2.1)$$

Where P is adsorption equilibrium pressure,

P_o is saturation vapor pressure of the adsorbate at the experimental temperature

V is volume of N_2 adsorbed at a pressure P

V_m is the volume of adsorbate required for monolayer coverage

c is a constant that is related to the heat of adsorption and liquefaction [4].

A linear relationship between $P/V(P_o-P)$ and P/P_o is required to be obtained for the quantity of nitrogen adsorbed.

The monolayer volume, V_m is given by

$$V_m = 1/(S+I) \quad (2.2)$$

where S is the slope and is equal to $(c-1)/cV_m$

I is the intercept equal to $1/cV_m$.

The surface area of the catalyst (S_{BET}) is related to V_m, by the equation

$$S_{BET} = (V_m/22414)N_a\sigma, \quad (2.3)$$

Where N_a is Avagadro number

σ is mean cross sectional area covered by one adsorbate molecule.

The value of σ generally accepted for N_2 is 0.162 nm^2. Adsorption of nitrogen measured by Brunauer-Emmett-Teller (BET) equation at low pressure (10^{-4} Torr) and liquification temperature of N_2 (77 K) is the standard method for determination of surface area, pore volumes and pore size distribution of molecular sieves.

N_2 adsorption-desorption isotherms of the catalysts were obtained at liquid N_2 temperature (77 K) using Quantachrome Nova-1200 adsorption unit. About 200 mg of sample was degassed at 473 K for about 4 hours till the residual pressure was $< 10^{-3}$ Torr. The isotherms were analyzed in a conventional manner, and the pore size distribution was calculated using the BJH method.

2.3.2. X-ray diffraction

The X-ray diffraction patterns are obtained by measurement of the angles at which an X-ray beam is diffracted by the sample. Bragg's equation relates the distance between two hkl planes (d) and the angle of diffraction (2θ) as:

$$n\lambda = 2d\sin\theta, \quad (2.4)$$

Where λ = wavelength of X-rays,

n = an integer known as the order of reflection (h, k and l represent Miller indices of the respective planes).

From the diffraction patterns, the uniqueness of mesoporous structure, phase purity, degree of crystallinity and unit cell parameters of the semicrystalline hybrid materials can be determined.

The identification of phase is based on the comparison of the set of reflections of the sample with that of pure reference phases distributed by International Center for Diffraction Data (ICDD). Unit cell parameter (a_0) of a cubic lattice can be determined by the following equation

$$a_0 = d_{hkl} \sqrt{(h^2 + k^2 + l^2)}, \quad (2.5)$$

Where d = distance between two consecutive parallel lattice planes having Miller indices h, k and l.

The average crystallites size of the nanoparticles can be estimated using the Debye-Scherrer [5] equation

$$D = k\lambda / \beta\cos\theta, \quad (2.6)$$

Where D = thickness of the nanocrystal,

k is a constant,

λ = wavelength of X-rays,

β = width at half maxima of (111) reflection at Bragg's angle 2θ [6-9].

XRD pattern of samples at wide-angle region was measured on Rigaku Model D/MAXIII VC, Japan, λ =1.5418 Å with Ni filtered Cu-Kα radiation.

2.3.3. X-ray photoelectron spectroscopy

The X-ray photoelectron spectroscopy [10-12] is based on the photoelectric effect, which involves the bombardment of a sample surface with X rays and the measurement of the concomitant photoemitted electrons. The photoemitted electrons have discrete kinetic energies that are characteristic of the emitting atoms and their bonding states. The kinetic energy, E_k, of these photoelectrons is determined by the energy of the X-ray radiation, hν, and the electron binding energy, E_b, as given by

$$E_k = h\nu - E_b \quad (2.7)$$

The experimentally measured energies of the photoelectrons are given by:

$$E_k = h\nu - E_b - E_w \quad (2.8)$$

Where E_w is the work function of the spectrometer.

The XPS technique is highly surface specific due to the short range of the photoelectrons that are excited from the solid. The binding energy of the peaks is characteristic of each element. The peak areas can be used (with appropriate sensitivity factors) to determine the composition of the surface materials. The shape of each peak and the binding energy can be slightly altered by the chemical state of the emitting atom. Hence XPS can provide chemical bonding information as well. XPS and the related Auger electron spectroscopy (AES) can provide elemental

analysis for essentially the entire periodic table. Because the electrons whose energies are analyzed arise from a depth of no greater than about 5 nm, the techniques are surface-sensitive.

X-ray Photoelectron spectra were acquired on a VG Microtech Multilab ESCA 3000 spectrometer using a non-monochromatized MgKα X-ray source (hν= 1253.6 eV) Base pressure in the analysis chamber was 4×10^{-10} Torr. Multichannel detection system with nine channels was employed to collect the data. The overall energy resolution of the instrument was better than 0.7 eV, determined from the full width at half maximum of the $4f_{7/2}$ core level of gold surface. The errors in all the B.E. values were within ±0.1 eV. The binding energy correction was performed using the C_{1S} peak of carbon at 284.6 eV as the reference.

2.3.4. XAFS and XANES

X-ray absorption fine structure spectroscopy uses the x-ray photoelectric effect and the wave nature of the electron to determine local structures around selected atomic species in materials. Unlike X-ray diffraction, it does not require long range translational order hence it works equally well in amorphous materials, liquids, (poly)crystalline solids, and molecular gases. XANES (near-edge structure) can be sensitive to charge transfer, orbital occupancy, and symmetry. Precise local structural information can be obtained (distances, numbers of atoms, types, disorder) for the crystalline or noncrystalline systems e.g. metalloprotein active sites, liquids,

amorphous materials. Additional information on charge state, orbital occupancy may also be available by studying XANES depending on the system and the edge.

X-ray absorption near edge structure (XANES) and extended X-ray absorption fine structure (EXAFS) measurements were performed using a synchrotron radiation ring at BL-9C, Photon Factory, KEK at Tsukuba (Japan) with a Si (111) double-crystal monochrometor in transmission mode at room temperature. The spectra were analyzed by the UWXAFS package [13]. The XANES spectra were normalized by their edge jumps to be unity. After background subtraction, k-weighted EXAFS functions in the k range of 20–110 nm-1 were Fourier transformed into an R-space. The spectrum was fitted in the corresponding k-space of the R range 0.10–0.20 nm. The backscattering amplitudes and phase shifts were calculated by the FEFF8 code [14].

2.3.5. Diffuse reflectance UV-visible spectroscopy

Diffuse reflectance spectroscopy (DRS) is a spectroscopic technique based on the reflection of light in the ultraviolet (UV), visible (VIS) and near-infrared (NIR) regions by a powdered sample. In a DRS spectrum, the ratio of the light scattered from an “infinitely thick” closely packed catalyst layer and the scattered light from an infinitely thick layer of an ideal non-absorbing (white) reference sample is measured as a function of the wavelength λ. The scattered radiation, emanating from the sample, is collected in an integration sphere and detected. UV-Vis spectroscopy generally deals with the study of electronic transitions between orbital or bands of

atoms, ions or molecules. One of the advantages of DRS is that the obtained information can be directly used for interpretation of chemical properties of the sample since outer shell electrons of the transition metal ions are probed. This further provides information about the oxidation state and coordination environment of transition metal ions in the solid matrices [15-18]. Also, the UV-Vis Spectroscopy is known to be very sensitive and useful technique for the identification of the electronic state of the metal atom as well as ligand geometry in heterogenized complexes. It gives information about the d-orbital splitting through the d-d transitions and the ligand-metal interaction through the ligand to metal charge-transfer transitions. The mechanism of reaction over "neat" complexes can be investigated by in situ UV-Vis spectroscopy.

The most popular continuum theory describing diffuse reflectance effect is Schuster-Kubelka-Munk (SKM) theory. If the sample is infinitely thick, the diffuse reflection of the sample ($R\infty$) is related to an apparent absorption (K) and apparent scattering coefficient (S) by the SKM equation [15-18]

$$F(R\infty) = (1-R\infty)^2 / 2R\infty = K/S \qquad (2.9)$$

At low concentrations of supported transition metal ions (TMI), this equation is a good representation of the absorbing spectrum and allows a quantitative determination of the TMI.

$$F(R\infty) = (1-R\infty)^2 / 2R\infty = K/S = \alpha C_{TMI} / S = k\, C_{TMI} \qquad (2.10)$$

At a given wavelength λ, S is constant, the above equation gives a linear relation between $F(R\infty)$ and the TMI concentration, C_{TMI}. The coefficients α and k are proportionality constants.

Diffuse reflectance UV-vis (DRUV–vis) spectra of catalyst samples were obtained using a Shimadzu UV-2101 PC spectrometer equipped with a diffuse reflectance attachment, with $BaSO_4$ as the reference. The reflectance spectra were converted into the Kubelka-Munk function, F(R), which is proportional to the absorption coefficient for low values of F(R). The spectra were measured in the range of 200-800 nm in air at room temperature.

2.3.6. Thermal analysis (TG-DTG)

The thermoanalytical technique has been widely used to get information on the thermal stability of the catalyst material. It can provide information about amount of intraclay complex and the thermal stability of the intercalated complex. Further, it provides information about the desorption of physisorbed water, oxidative decomposition of organic materials and dehydroxylation of Si-OH groups in the molecular sieves. From diferential thermal analysis (DTA), phase transformations can also be known of the materials.

Thermogravimetric analyses (TGAs) were performed on Perkin-Elmer TGA-7 analyzer at 10 °C/min scan rate in nitrogen atmosphere.

2.3.7. Fourier-transform infrared (FTIR) spectroscopy

The FTIR spectroscopy provides information on a) whether ligand molecules have coordinated to the transition metal cations; b) if different patterns appear in the free or

in the chelated state; c) if characteristic bands exhibit defined shift upon chelation. FTIR spectroscopy in the framework region (400-4000 cm^{-1}) provides additional information about the structural details of the support. In addition to the above, ligand features can be seen when the metal complex is encapsulated/immobilized in the cavities or channels of microporous and mesoporous materials.

Fourier transform infrared (FTIR) spectra were obtained from KBr pressed pellets using a Bio-Rad 17JC infrared spectrometer.

2.3.8. Scanning electron microscopy (SEM)

Scanning electron microscopy is a straightforward technique to probe the morphological features of catalyst materials. SEM scans over a sample surface with a probe of electrons (5-50 eV) and detects the yield of either secondary or back-scattered electrons as a function of the position of the primary beam. Contrast is generally caused by the orientation such that the part of the surface facing the detector appears brighter than the part of the surface with its surface normal pointing away from the detector. The interaction between the electron beam and the sample produces different types of signals providing detailed information about the surface structure and morphology of the sample [19]. When an electron from the beam encounters a nucleus in the sample, the resultant Coulombic attraction leads to a deflection in the electron's path, known as Rutherford elastic scattering. A fraction of these electrons will be completely backscattered, re-emerging from the incident

surface of the sample. Since the scattering angle depends on the atomic number of the nucleus, the primary electrons arriving at a given detector position can be used to produce images containing topological and compositional information [20]. A major advantage of SEM is that bulk samples can also be directly studied by this technique

The chemical composition of the sample was determined by energy-dispersive X-ray (EDX) attached to a scanning electron microscope (SEM; JEOL JSM 500).

2.3.9. Transmission electron microscopy

Transmission electron microscopy (TEM) is used for high resolution imaging of thin films of a solid sample for microstructural and compositional analysis. The technique involves: (i) irradiation of a very thin sample by a high-energy electron beam, which is diffracted by the lattices of crystalline or semicrystalline material and propagated along different directions, (ii) imaging and angular distribution analysis of the forward scattered electrons (unlike SEM where backscattered electrons are detected) and (iii) energy analysis of the emitted X-rays [21]. The topographic information obtained by TEM in the vicinity of atomic resolution can be utilized for structural characterization and identification of various phases of mesoporous materials, viz., hexagonal, cubic or lamellar [22, 23]. TEM also provides real space image on the atomic distribution in the bulk and surface of a nano crystal [24].

2.4. Catalyst activity measurement

2.4.1. High pressure reactor set up for liquid phase oxidation reactions

All the oxidation reactions at elevated pressure were carried out in a 300 mL capacity high pressure stirred autoclave supplied by Parr Instrument Company, USA.

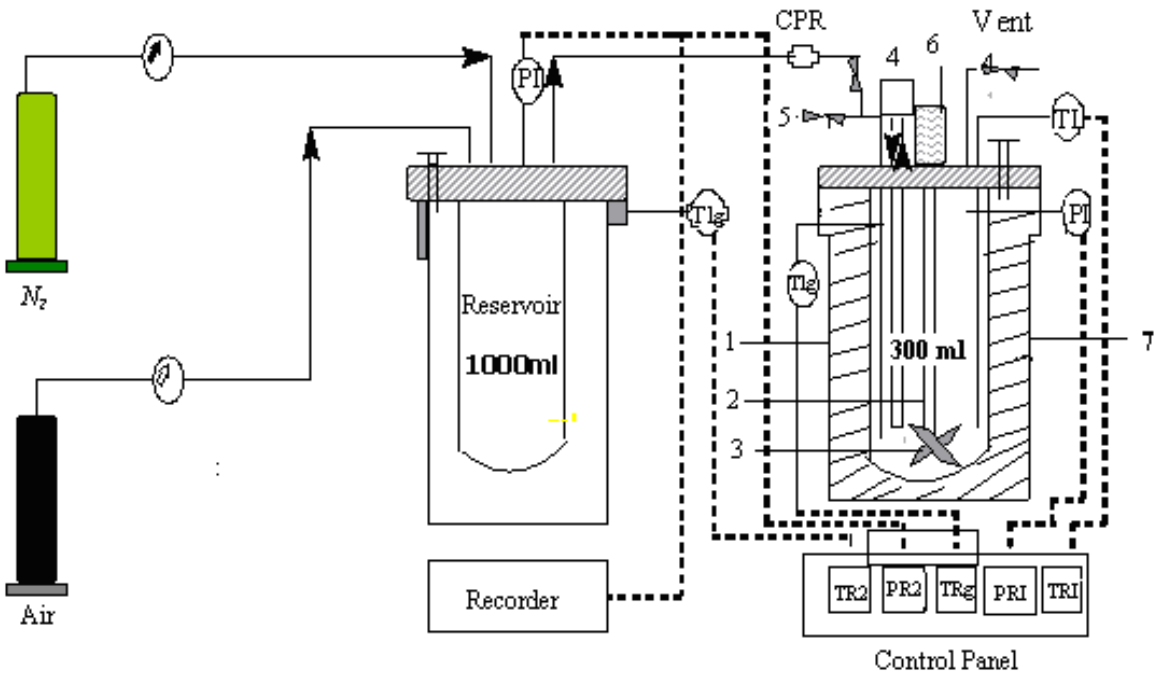

Figure 2.3. Parr reactor setup
(1) Reactor (2) stirrer shaft (3) impeller (4) cooling water (5) sampling valve (6) magnetic stirrer (7) electric furnace
TI: Thermocouple PI: Pressure transducer TIg: Thermocouple for gas N: Nitrogen cylinder CO: Carbon monoxide cylinder PR: Pressure regulator CPR: Content pressure regulatorTR1: Reactor temperature indicator PR1: Reactor pressure indicator TR2: Reservoir temperature Indicator TRg: Gas temperature indicator PR2: Reservoir pressure indicator

The autoclave was equipped with a heating arrangement, overhead stirrer, thermo well, internal cooling loop, pressure gauge as well as transducer, gas inlet, gas outlet, sampling valve and a rupture disc. There was a separate controller for agitation speed and temperature. Water circulation through the internal cooling loop equipped with automatic cut-off arrangement controlled the temperature inside the reactor with an accuracy of ±1° C. A schematic of the slurry reactor set-up is shown in Figure 2.3 [25].

In a typical oxidation experiment, 70 mL of methanol, 3.36 g (0.084 moles) of NaOH were heated in a flask with a reflux condenser until most of the NaOH was dissolved; then 3.0 gm, (0.027 moles) of *p*-cresol was added. This reaction mixture was charged to a 300 mL Parr autoclave (Figure 2.3). A weighed amount of the catalyst was added, and the reaction mixture was heated to desired temperature. When the desired temperature was attained, the reactor was pressurized with air/oxygen and then the reaction was started by agitating it at 900 rpm. When the pressure dropped to an extent of 20 % corresponding to the O_2 content in air, the reaction mixture was cooled to 283 K, and the rest of the gas (i.e., unabsorbed nitrogen) was vented out. Again the reactor was heated to the reaction temperature, and the reactor was pressurized with air. The same procedure was repeated until the stoichiometric amount of oxygen was absorbed. The progress of the reaction was monitored by the observed pressure drop in the reservoir vessel as a function of time. Liquid samples were also withdrawn from time to time and analyzed by HPLC for the reactant and product concentrations. After the reaction was over, the contents were cooled to room temperature and discharged

2.4.2. Atmospheric reactor set up

Catalytic oxidation experiments at atmospheric conditions were conducted in a 100 mL capacity three-necked glass reactor fitted with a cooling condenser as shown in Figure.2.4.

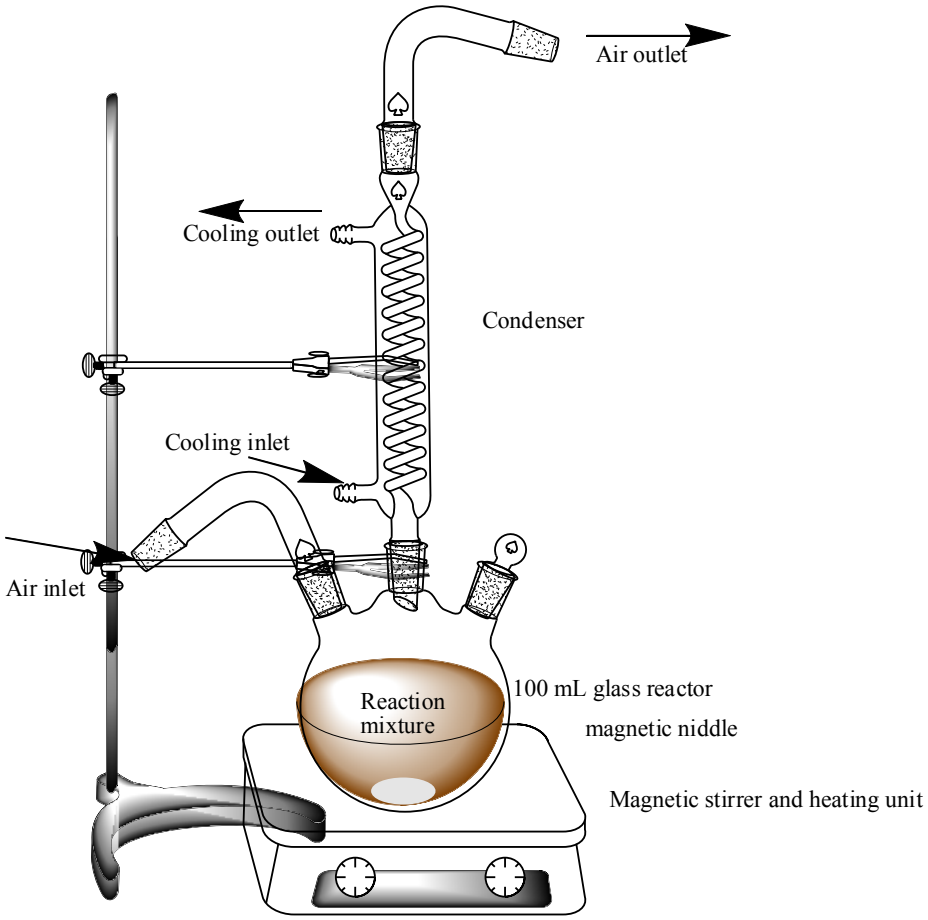

Figure 2.4. Atmospheric reactor setup

In a typical experiment, *p*-cresol (3 g, 0.027 moles), NaOH (3.36 g, 0.084 moles), and methanol (50 mL) were charged to the reactor and the contents were stirred

magnetically for 1 h at reflux temperature. To this, 0.2 g of catalyst was added and the oxidation was started by bubbling air at a desired flow rate through the reaction mixture. Timely samples were taken and analyzed on an HPLC.

2.5. Analytical method

A Hewlett-Packard model 1050 liquid chromatograph equipped with an ultraviolet detector was employed for the analysis of liquid samples. HPLC analysis was performed on a 25 cm RP-18 column supplied by Hewlett-Packard. The products and reactants were detected using a UV detector at λ_{max}, 223 nm using 30% methanol-water as mobile phase at a column temperature of 313 K and flow rate of 1 mL/min. Samples of 10 μL were injected into the column using an auto sampler.

2.6. References

1. J. J. Bozell, B. R. Hames, D. R. Dimmel, *J. Org. Chem*. **1995**, *60*, 2398.
2. R. H. Bailes, M. J. Calvin, *J. Am. Chem. Soc*. **1947**, *69*, 1886.
3. V. S. Kshirsagar, S. Vijayanand, H. S. Potdar, P. A. Joy, K. R. Patil, C. V. Rode, *Chem. Lett*. **2008**, 37, 310.
4. S. Brunauer, P. H. Emmett, E. Teller, *J. Am. Chem. Soc*. **1938**, *60*, 309.
5. N. F. M. Henry, J. Lipson and W. A. Wooster, "*The interpretation of X-ray diffraction photographs*" Macmillan and Co Ltd., L*ondon,* **1951.**

6. *W.H. Bragg, W.L. Bragg, The Crystalline State, Vol. 1*, McMillan, New York, **1949**.

7. S. Biz, M. Occelli, *Catal. Rev. Sci. Eng.*, **1998**, *40*, 329.

8. G. Bergeret, *Handbook of Heterogeneous Catalysis.* Vol. 2, Eds: G. Ertl, H. Knozinger, J. Weitkamp, Wiley-VCH, Weinheim, **1997**.

9. R.C. Rau *Advances in X-Ray Analysis*, Vol. 5, Ed: W.M. Mueller, Sir Isaac Pitman and Sons Ltd., London, **1962**.

10. T. A. Carlson, *X-ray Photoelectron Spectroscopy*, Dowden, Hutchinson & Ross: Stroudsburg, PA, **1978**.

11. D. Briggs, M. P. Seah, Eds, .*Practical Surface Analysis, Vol. 1*: *Auger and X-ray Photoelectron Spectroscopy*, 2nd ed., Wiley, New York, **1990**.

12. S. Hüfner, *Photoelectron Spectroscopy*, Springer-Verlag: Berlin, **1995**.

13. E. A. Stern, M. Newville, B. Ravel, Y. Yacoby, D. Haskel, *Physica B* **1995**, *208*, 117.

14. A. L. Ankudinov, B. Ravel, J. J. Rehr, S. D. Conradson, *Phys. Rev. B* **1998**, *58* 7565.

15. B.M. Weckhuysen, I.P. Vannijvel, R.A. Schoonheydt, *Zeolites* **1995**, *15,* 482.

16. X.T. Gao, I.E. Wachs, *J. Phys. Chem. B* **2000**, *104,* 1261

17. X.T. Gao, I.E. Wachs, *J. Catal*. **1999**, *188,* 325.

18. R.A. Schoonheydt, F. Delannay *Diffuse Reflectance Spectroscopy*, Chapter 4, in: *Characterization of Heterogeneous Catalysts*, (Ed.), Marcel Dekker, New York, **1984**

19. .J. I. Goldstein, H. Yakowitz (Eds.), *Practical Scanning Electron Microscopy*, Plenum Press, New York, **1975**.

20. G. Lawes, *Scanning Electron Microscopy and X-Ray Microanalysis*, John Wileyand Sons Ltd., Chichester, **1987**.

21. J. R. Fryer, *Chemical Applications of Transmission Electron Microscopy*, Academic Press, San Diego, **1979**

22. J. M. Thomas, O. Terasaki, P. L. Gai, W. Zhou, J. Gonzalez-Calbet, *Acc. Chem. Res*. **2001**, *34*, 583.

23. V. Alfredsson, M. Keung, A. Monnier, G. D. Stucky, K. K. Unger, F. Schuth, *J. Chem. Soc. Chem. Comm*. **1994**, 921.

24. Z. L. Wang, in: *Characterization of Nanomaterials*, Ed: Z. L. Wang, Wiley-VCH, Weinheim. **2000**, 37pp.

25. V.S. Kshirsagar, J.M. Nadgeri, P.R. Tayade, C.V. Rode, *Appl. Catal. A: Gen.* **2008**, *339*, 28.

3.1. Introduction

Soluble cobalt metal complexes due to their ability to bind reversibly molecular oxygen, catalyze a variety of oxidation reactions in solution which lead to dioxygenations [1, 2] monooxygenations, [3, 4] and dehydrogenations [5-7] that mimic biological oxidations. However, the major drawbacks of such oxidations are: (i) poor selectivity to the desired product since, a variety of oxygenated products are formed due to highly reactive nature of free radical intermediates; (ii) fast deactivation of homogeneous catalysts due to formation of μ-oxo dimmers; [8] (iii) carryover of trace metal impurities into the product stream during catalyst separation protocol. These drawbacks can be overcome using a heterogeneous catalyst that upon separation can be recycled easily [9-11]. Recently, several heterogeneous catalysts containing cobalt and/or some other metals such as copper or manganese supported on molecular sieves, carbon or resins have been reported [12-19]. Heterogenization of several other metal complexes has been also carried out using solids such as zeolite, clays, silicious materials and activated carbon [20-28]. Zeolite catalysts such as CoAPO-5 and CoAPO-11, these were found to dissolve in the reaction media while in other cases leaching of cobalt was found to be > 50% under reaction conditions [29]. In almost all these reports, large excess of catalyst (up to 8 mol %) was used. Apart from such drawbacks of these heterogeneous catalysts systems, there are no reports on immobilization of cobalt complexes into the interlamelar space of clay materials. Clays are also more advantageous than other supports, e.g. unlike zeolites clays can offer diffusion in only two-dimensional space instead of three-

dimensional volume. This increases the encounter frequencies between reactants, leading to enhancement in reaction rates at very mild conditions as well as reduction of the extent of undesired reactions [30]. Smectite clays are increasingly attracting interest as supports for metal and metal complex catalysts. These layered materials are having important physical and chemical properties such as laminar structure, transverse layer rigidity and intercalation ability which make them as a good catalyst material.

Direct oxyfunctionalization of side chain of anti-oxidizing cresols provides a clean route for many industrial and pharmaceutical chemicals [31, 32]. One such example is *p*-cresol oxidation which gives a mixture of oxidation products viz. *p*-hydroxy substituted benzyl alcohol, benzaldehyde and benzoic acid depending on the choice of catalysts and reaction conditions. Among these, both alcohol and aldehyde derivatives are important intermediates for the manufacture of vanillin, a widely used flavoring agent, trimethoxybenzaldehyde, various agrochemicals and pharmaceuticals such as semi synthetic penicillin, amoxicillin, antiemetic drug trimethobenzamide [33-35]. *p*-Hydroxybenzaldehyde is also used as an additive for metal plating brighteners, electroplating, in perfumes and in liquid crystals [36].

Therefore, the objectives of this work were (i) to prepare and characterize cobalt and manganese salen complexes intercalated into commercially available montmorillonite clay as well as the synthetically prepared saponite clays, and (ii) to measure the catalyst activity of these prepared catalysts for air oxidation of *p*-cresol under atmospheric conditions. The detailed characterizations were done so as to confirm the

intercalation of cobalt-salen complex into the montmorillonite clay by various techniques such as XRD, XPS, IR, DRUV, SEM, XANES, EXAFS and TGA. Most convincing evidence for intercalation has been provided by XPS, TGA, XANES and EXAFS [37]. A distinct shift in decomposition temperature for cobalt-salen intercalated into montmorillonite as well as the formation of an additional Co-O bond (bond length of 0.199 nm) as observed from EXAFS studies confirmed the host-guest relationship between cobalt-salen and montmorillonite clay.

It was found that cobalt salen intercalated into montmorillonite clay was an excellent catalyst for air oxidation of *p*-cresol under very mild reaction conditions (338 K and ambient pressure) and the selectivity ratio of PHB to PHBALc could be altered by varying the suitable process parameter e.g. air flow rate [38]. Effects of various reaction parameters such as temperature, substrate concentration, catalyst loading, air flow rate, NaOH concentration, solvents on the conversion of *p*-cresol and selectivity to *p*-hydroxybenzaldehyde were also investigated. The cobalt-salen intercalated into montmorillonite catalyst gave a TON as high as 150 with a selectivity of 90% to the oxyfunctionalized products for air oxidation of *p*-cresol under ambient pressure conditions [38].

3.2. Experimental

Details of preparation of various metal Schiff bases intercalated into the clay materials have been described in section 2.1.1. The prepared catalysts were evaluated for the liquid phase oxidation of *p*-cresol under atmospheric conditions with a

continuous flow of air. For this purpose, the experimental set up used and experimental procedure is described in section 2.4 while the catalyst characterization and analytical methods have been described in sections 2.3 and 2.5 respectively.

3.3. Results and discussion

3.3.1. Catalyst characterization

3.3.1.1. Diffused reflectance UV-visible spectroscopy

The DRUV-vis spectra of Co(salen)-mont showed two peaks at 380 and 288 nm due to d-d transition and ligand charge transfer respectively. These peaks showed a distinct blue shift from 482 and 337 nm of the parent Co-salen (Figure 3.1). The shifting of d-d transition band to the higher energy region clearly means that the in-plane ligand field around the metal ion is becoming stronger indicating the intercalation of the complex into the montmorillonite clay.

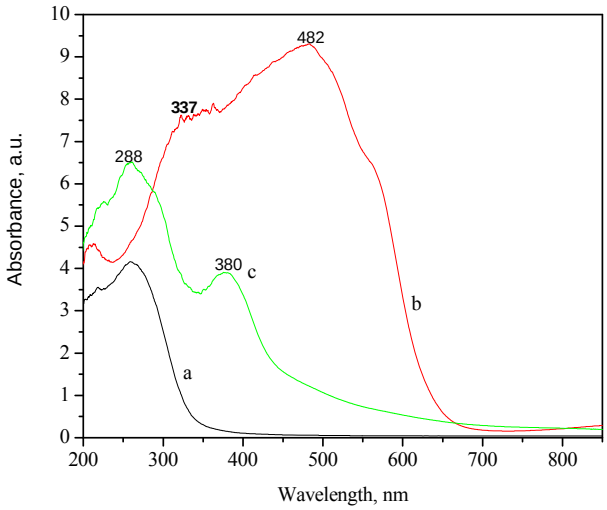

Figure 3.1. DRUV–vis spectra of (a) montmorillonite, (b) Co-salen, and (c) Co(salen)-mont.

3.3.1.2. FTIR spectroscopy

Figure 3.2 shows FTIR spectra in the region of 400-4000 cm^{-1} for the salen, Co-salen, parent montmorillonite and intercalated Co(salen)-montmorillonite samples. The –OH stretching vibrations in salen (d) at 3449 cm^{-1} has shifted to 3433 cm^{-1} in Co(salen) (c). A band at 3389 cm^{-1} in parent montmorillonite (a) is due to stretching vibrations of interlayer water molecules which has shifted to 3423 cm^{-1} after intercalation of Co-salen. Shift of this peak to higher frequency and its higher intensity as compared to parent clay is due to the intercalation of Co-salen. Figure 3.3 shows peaks in the region of 1500-2000 cm^{-1} in which characteristic C=N stretching frequency appears at 1635 cm^{-1} for salen ligand (d). In case of Co(salen)-mont (a), a peak at 1638 cm^{-1} with higher intensity shows the intercalation of Co-salen) into the clay. A broad and intense band at 1089 cm^{-1} in Co(salen)-mont (b) is due to asymmetric stretching vibrations of SiO_2 tetrahedra. A band at 798 cm^{-1} in parent clay (a) is due to the stretching vibration of Al^{IV} which has shifted to 807 cm^{-1} due to intercalation in (b). Peaks at 525-475 cm^{-1} correspond to the bending of Si-O vibrations [39]. Thus, IR results clearly indicate the intercalation of Co-salen into the montmorillonite clay.

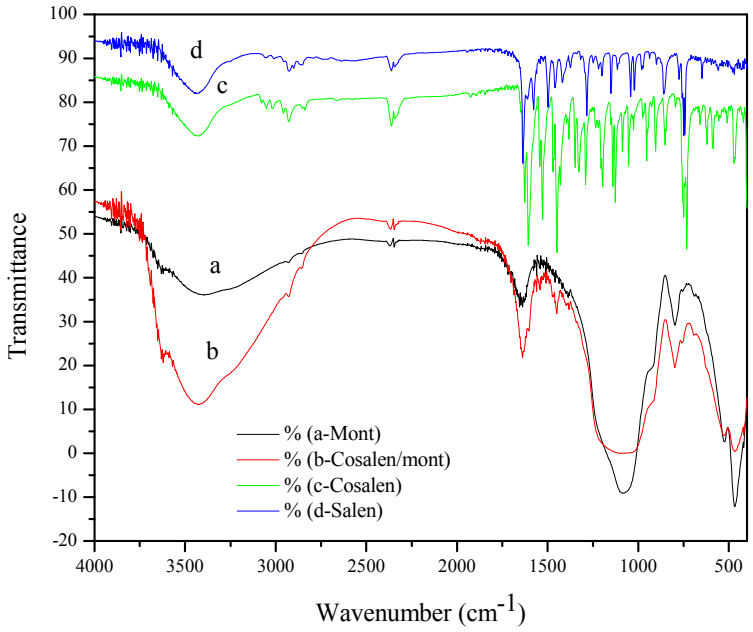

Figure 3.2. FTIR of (a) parent clay, (b) Co(salen)-mont, (c) Co-salen (d) salen ligand.

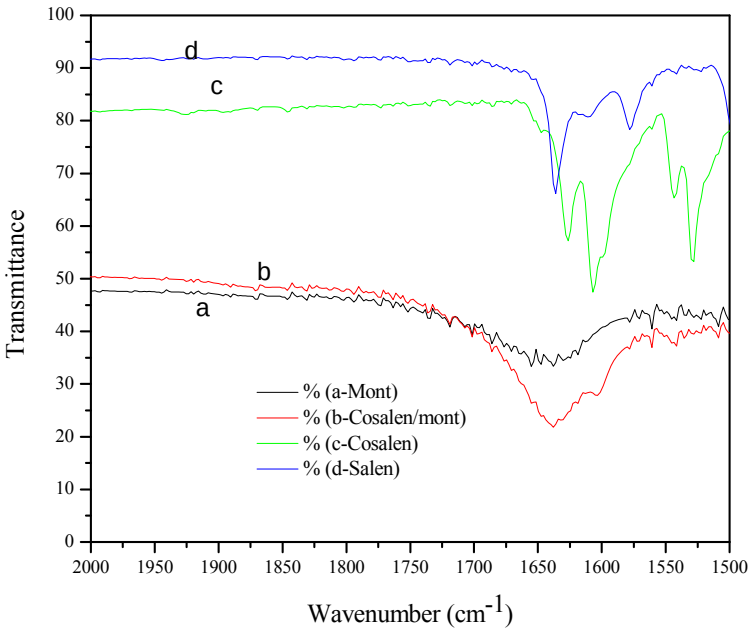

B

Figure 3.3 FTIR of (a) parent clay, (b) Co(salen)-mont, (c) Co-salen (d) salen ligand.

3.3.1.3. X-ray diffraction

XRD pattern (Figure 3.4) of the sample after intercalation of Co-salen into the clay was of the same intensity as that of the parent clay indicating the retention of the crystallinity as well as no delamination occurred during the preparation protocol. After intercalation, Co(salen)-mont sample displayed a small expansion of the basal spacings of 1 A^0 in XRD that are possibly due to the orientation of the square planar Co-salen parallel to the clay sheets, as shown schematically in Figure 3.5

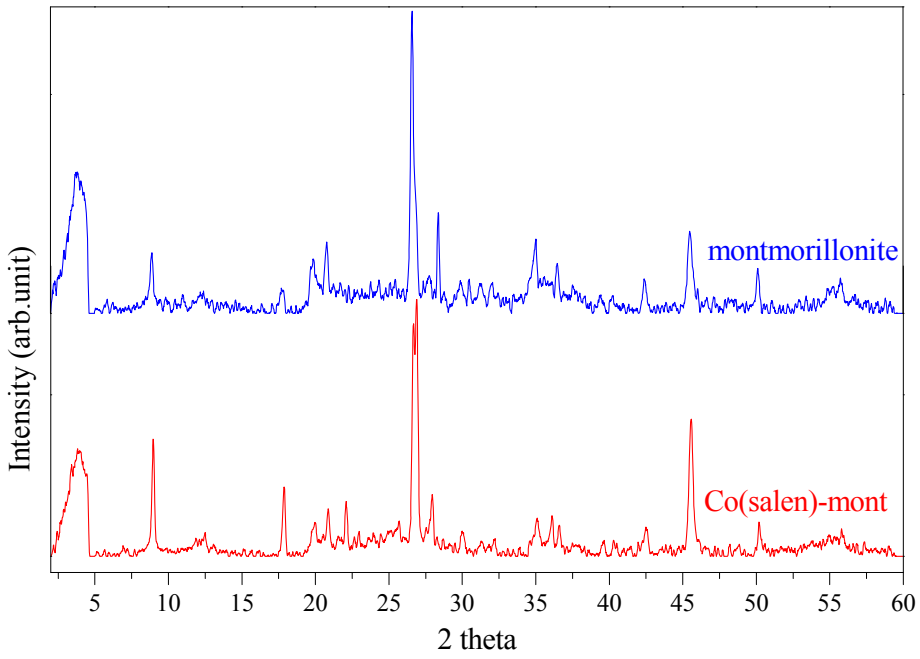

Figure 3.4. XRD pattern for montmorillonite and Co(salen)-mont catalyst**.**

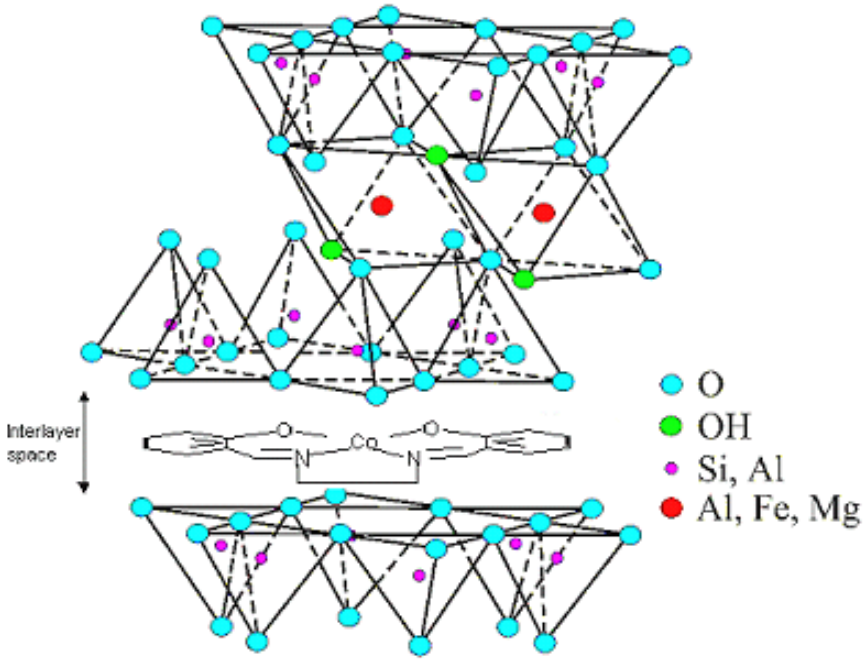

Figure 3.5. Schematic representation of intercalation of Co-salen into montmorillonite clay

3.3.1.4. Thermo gravimetric analysis (TGA)

TGA was also used to characterize the Co-salen intercalated into the montmorillonite clay. The extent of metal complex loading can also be estimated from the weight loss. TGA data of various samples are presented in Figure 3.6. The "neat" cobalt salen complex showed a weight loss at (642 K). However, for the corresponding intercalated complex weight loss occurred in two stages: in the first stage up to 403 K due to desorption of water and in the second stage, weight loss was observed at a higher temperature of 775 K due to decomposition of the complex. Thermal stabilization observed was due to the host-guest interaction of clay and metal complex and thus confirming the intercalation [40, 41].

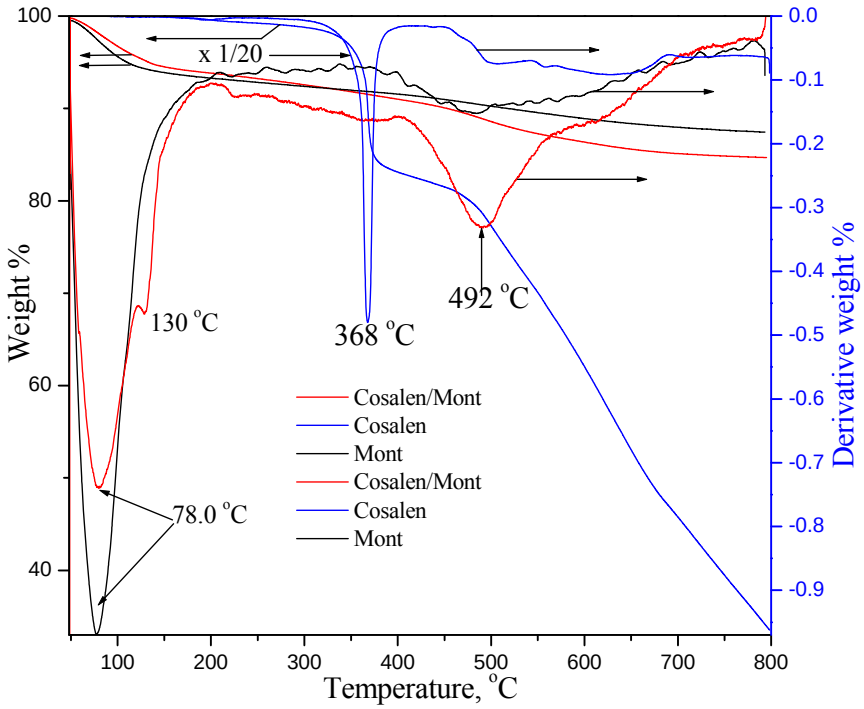

Figure 3.6. TG-DTG curves of Co-salen, montmorillonite, and Co(salen)-mont.

Figure 3.7 shows the TG-DTG curves for Co(salen)-mont, Co(salophen)-mont, Co(acene)-mont catalyst samples. Decomposition temperatures of intercalated Co-salophen, and Co-acene complexes were observed at 831 K and 842 K respectively which were higher than that of intercalated Co-salen complex indicating their greater stability at higher temperatures as compared to that of Co(salen)-mont catalyst.

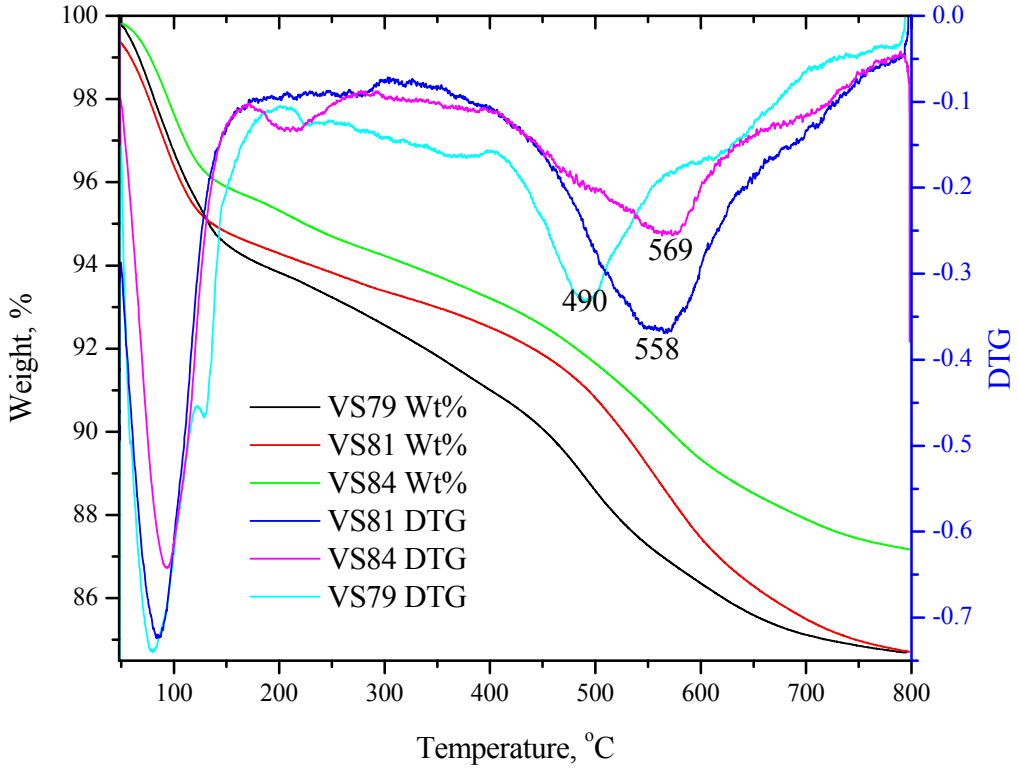

Figure 3.7. TG-DTG curves of Co(salen)-mont Co(salophen)-mont Co(acen)-mont VS79 Cosalen-mont VS81 Cosalophene-mont VS84 Coacen-mont

3.3.1.5. Scanning electron microscopy (SEM)

Figure 3.8 shows the comparison of SEM pictures of parent montmorillonite and Co(salen)-mont indicating that the intercalated samples have similar morphologies consisting mainly flake like particles corresponding to a layered structure. The flake like form of the parent clay was maintained after the intercalation procedure. The elemental composition of montmorillonite obtained using EDS (coupled with SEM) showed the atomic percentages as 63.12 (O), 28.0 (Si), 6.98 (Al), in addition to minimal amounts of Na and Mg.

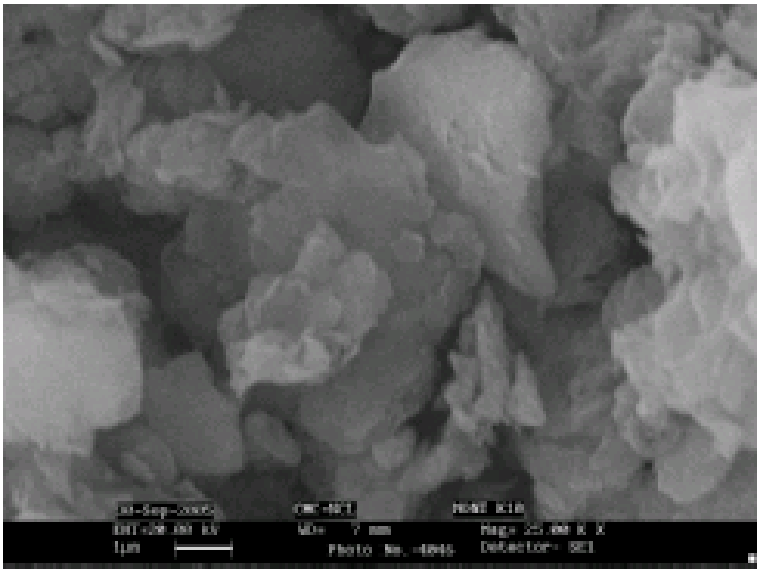

(a)

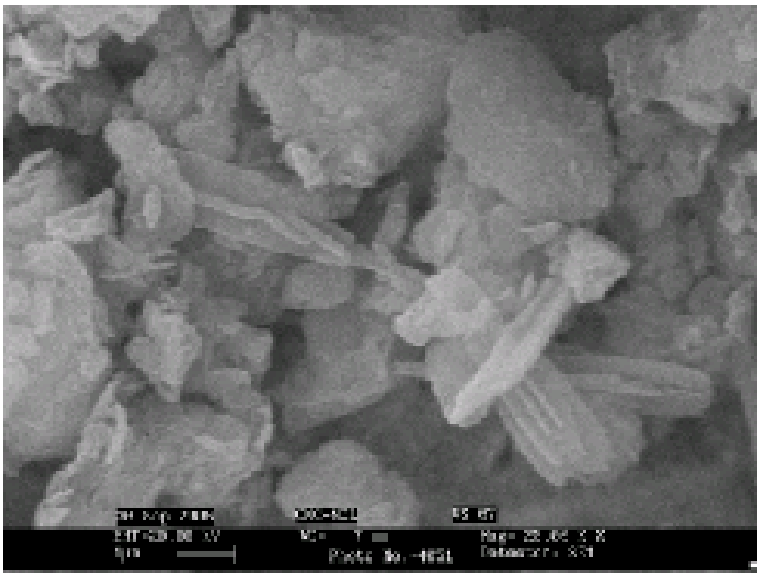

(b)

Figure 3.8. SEM photographs of (a) montomorilloniteK10, and (b) Co(salen)-mont**.**

Upon intercalation, the EDS analysis clearly showed the presence of carbon (13.56%) nitrogen (14.64 %) and cobalt (0.45%) indicating the incorporation Co-salen into the montmorillonite. However EDS is indicative of mainly the surface species; and more convincing evidence of intercalation was provided by DR-UV, IR, XRD, XPS, XAFS and XANES as discussed in the respective sections.

3.3.1.6. X-ray photoelectron spectroscopy

The oxidation state of cobalt was investigated by XPS. Figure 3.9a shows a general scan for Co(salen)-mont catalyst and Figure 3.9b shows the Co 2p XPS spectra for other Co-containing samples.

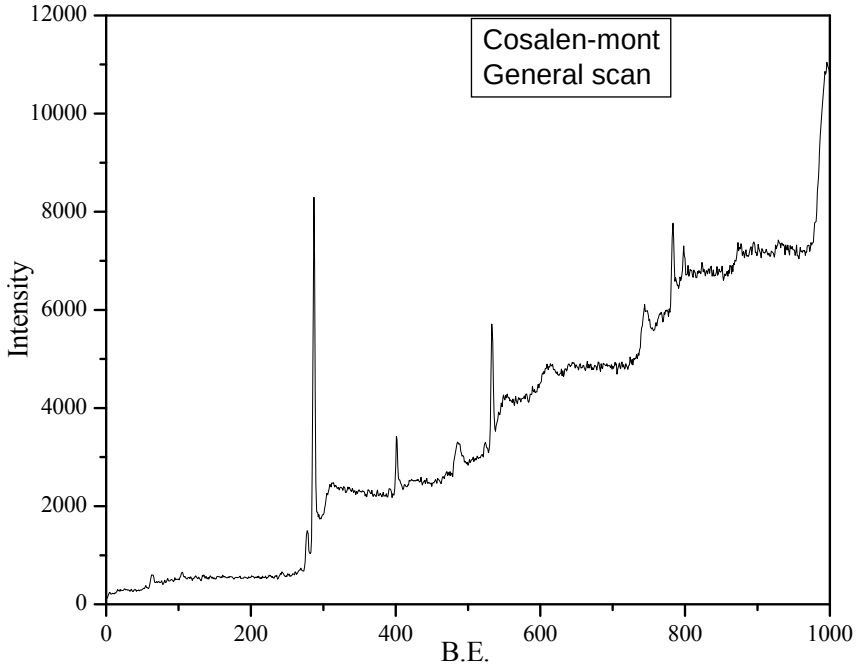

Figure 3.9a. XPS general scan for Co(salen)-mont catalyst

As can be seen from Figure 3.9b, Co-salen exhibits Co $2p_{3/2}$ core level peak at a binding energy of 780.4 eV, while the intercalated Co(salen)-mont complex shows a binding energy at higher value of 781.2 eV and are in accordance with the earlier literature [42]. The observed increased chemical shift of ~ 1 eV for the Co(salen)-mont sample can be attributed to the differences in the coordination environment of metal inside the interlayer spaces of montmorillonite and confirms the intercalation [43]. The comparison of the cobalt content of the catalyst by XPS before and after *p*-cresol oxidation reaction indicated that there was a marginal decrease in this value after catalytic reaction. The positive increase in binding energy of Co $2p_{3/2}$ in the catalyst sample after the catalytic reaction could be due to formation of superoxo cobalt species responsible for the oxidation [44]. Also a satellite was seen at about 787.7 eV for intercalated montmorillonite complex and this was due to charge transfer from ligand to metal as observed in transition metal complexes.

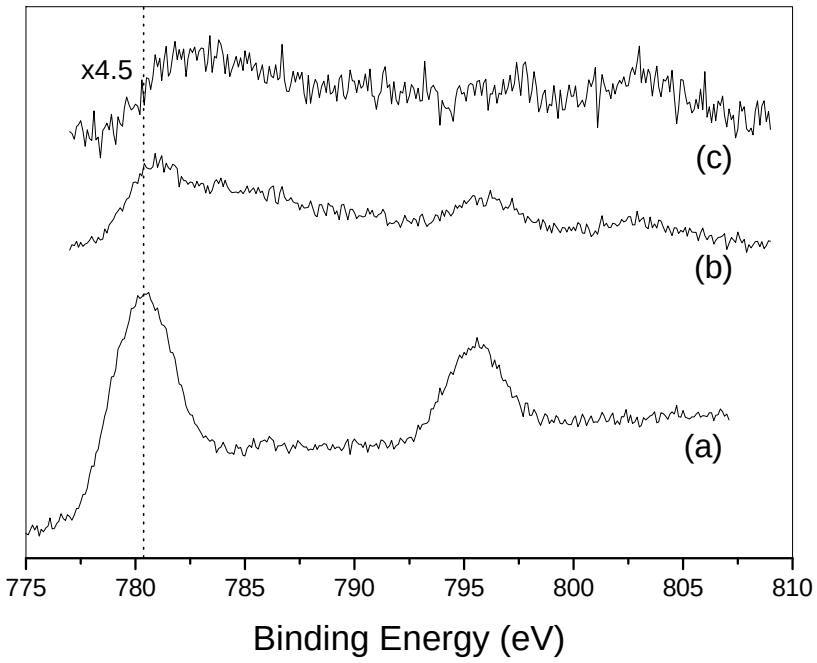

Figure 3.9b. Co 2p XPS spectra of Co-containing complexes (a) Co-salen (b) Co(salen)-mont (c) used catalyst.

Table 3.1 summarizes the binding energies of cobalt, nitrogen and oxygen in various samples. The positive shift in binding energy for nitrogen in Co(salen)-mont sample is consistent with a decrease in electron density on nitrogen upon donation of electron to cobalt. Also upon complexation, the electron density on oxygen is reduced and binding energy increases.

Table 3.1. Core-electron binding energies (eV) for cobalt, nitrogen and oxygen.

Complex	Co $2p_{3/2}$	N 1s	O 1s
Salen	_	398.4	532.1
Co(salen)	780.4	399.0	530.9
Co(salen)-mont	781,2	399.4	532.6
Used catalyst	781.9	399.9	532.1

Core-electron binding energies for different cobalt Schiff bases intercalated into montmorillonite complex are presented in Table 3.2. For all the three samples increased chemical shift of 0.4 to ~1 eV in the binding energy of Co can be attributed to the differences in the coordination environment of metal inside the interlayer spaces of montmorillonite, thus confirming the intercalation. Change in binding energies of nitrogen and oxygen are also consistent with this observation similar that made in case of Co(salen)-mont sample discussed above.

Table 3.2. Binding Energies values for different catalysts

Catalyst	Cobalt			Nitrogen	Oxygen
	$2p_{3/2}$	$2p_{1/2}$	δeV	1s	1s
Co(salen)-mont	781.0	795.9	14.9	399.4	532.6
Co(salophen)-mont	780.8	795.4	14.6	399.7	533.2
Co(acene)-mont	781.3	795.5	14.2	399.1	532.5

Figure 3.10 shows the binding energy of nitrogen for salen, Co-salen and Co(salen)-mont samples. The positive shift for nitrogen from 398.4 to 399 eV was consistent with a decrease in electron density on the nitrogen upon donation of its lone pair of electrons to the metal confirming the bonding between salen and cobalt.

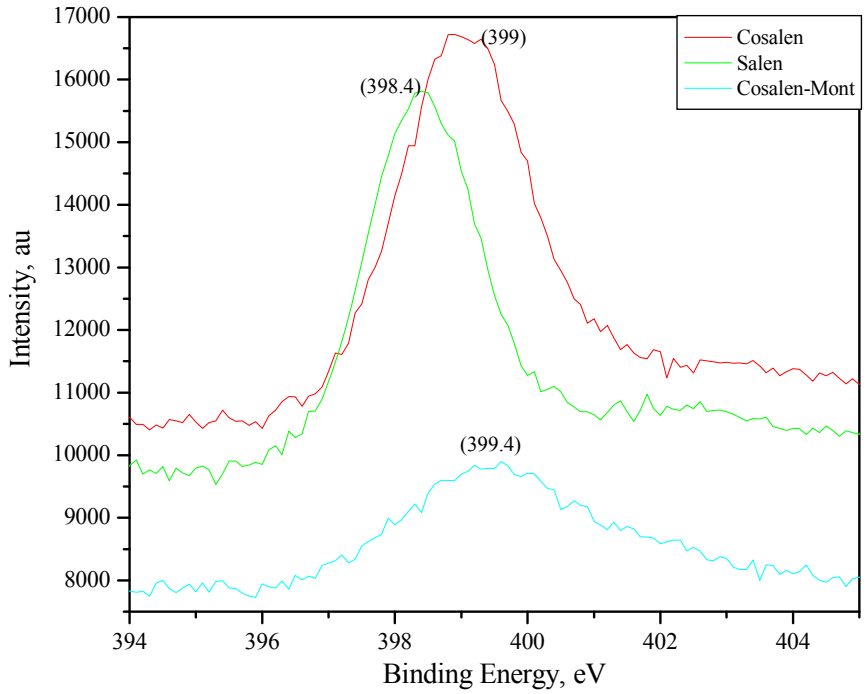

Figure 3.10. XPS spectra for nitrogen 1s core levels of salen, Co-salen, and Co(salen)-mont.

In Figure 3.11, Co $2p_{3/2}$ spectra of montmorillonite intercalated with various cobalt Schiff bases are presented. The relative intensity of satellite peak which appears to be about 6 eV higher than the main peak of Co $2p_{3/2}$ (about 781 eV) increased from Co-salen to Co-acene intercalated montmorillonite complexes. These observations suggest that the proportion of Co^{2+} tetrahedral increased on the surface with variation of the ligands. This could be due to more strong interaction between the respective Co-complexes and montmorillonite [45].

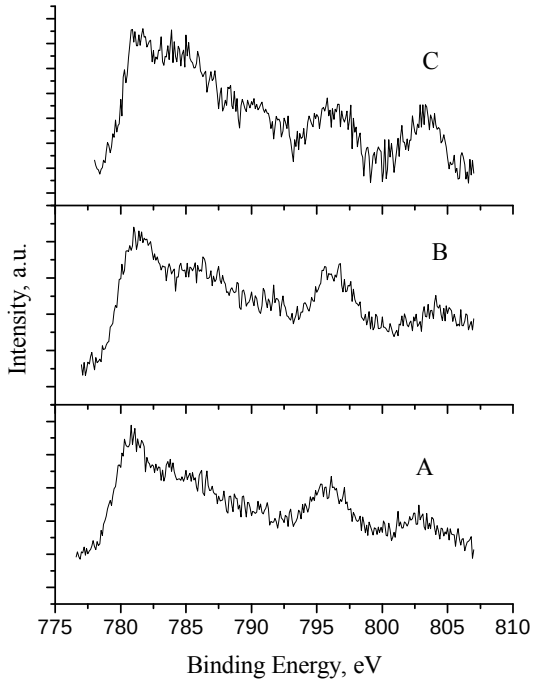

Figure 3.11. Co $2p_{3/2}$ and Co $2p_{1/2}$ spectra of A) Co(salen)-mont, B) Co(salophen)-mont, and C) Co(acene)-mont.

3.3.1.7. X-ray absorption near edge structure (XANES)

Figure 3.12 shows XANES spectra of Co-salen and Co(salen)-mont. The shoulder at 7715 eV (shown in red) was observed only in the case of Co-salen which has a tetrahedral geometry in plane. The spectrum of Co(salen)-mont sample showed (shown in blue, Figure 3.12) disappearance of the shoulder peak that was attributed to the change of symmetry from the tetetrahedral in plane to the octahedral structure having an axial bonding of oxygen to the cobalt [45], indicating that cobalt atoms in Co(salen)-mont were coordinated axially with lattice oxygen of montmorillonite. The lattice oxygen might play a significant role in directing the liquid phase oxidation via

Mars-van Krevelene pathway [46, 47]. However, more detailed work involving the evaluation of the solid state diffusion parameters for lattice oxygen under these conditions is necessary.

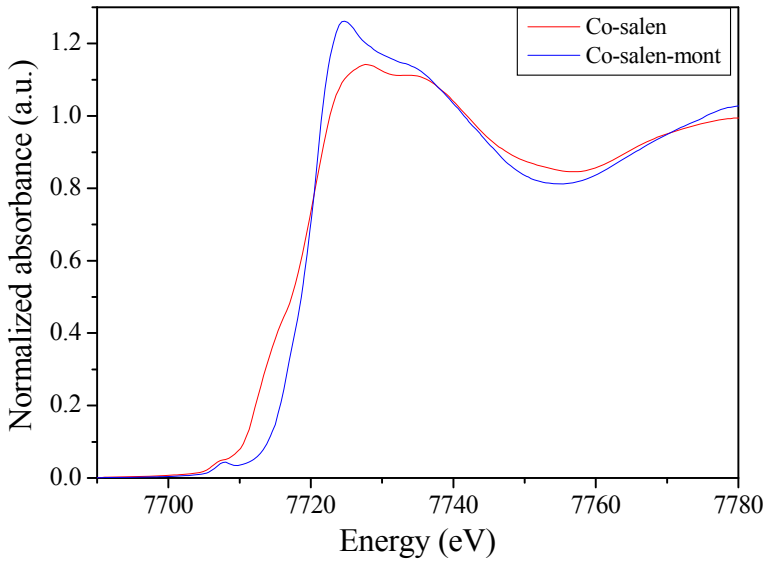

Figure 3.12. Co K-edge XANES spectra for Co-salen (red line and Co(salen)-mont (blue line).

Figure 3.13 shows Fourier transforms (FT) of *k*-weighted EXAFS spectra at Co K-edge of Co-salen and Co(salen)-mont. The first peak of FT for Co(salen)-mont was larger than that for Co-salen. Curve fitting analysis were carried out for the first peak, as shown in Figure 3.14, and structural parameters for Co-salen and Co(salen)-mont are summarized in Table 3.3.

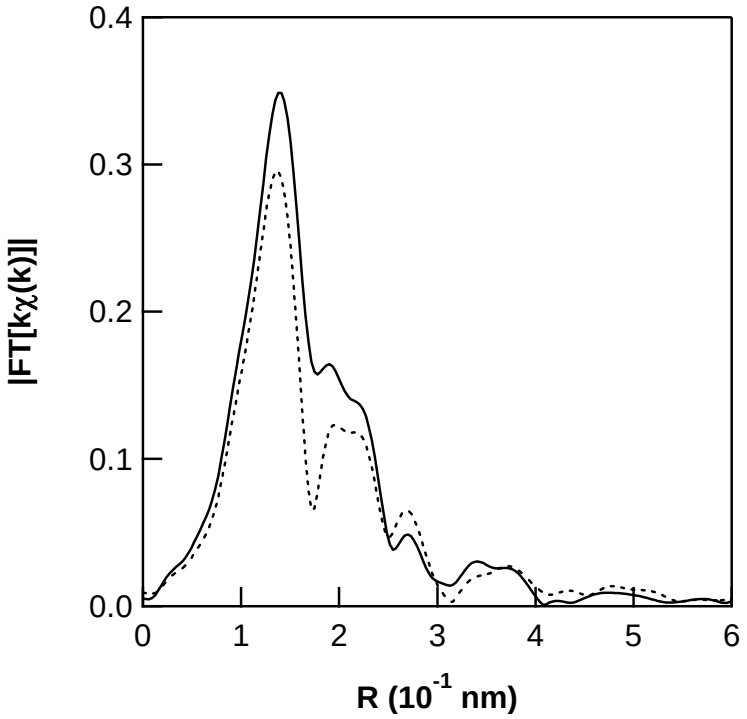

Figure 3.13. Fourier transforms of *k*-weighted EXAFS spectra at Co K-edge for Co-salen (---) and Co(salen)-mont (—).

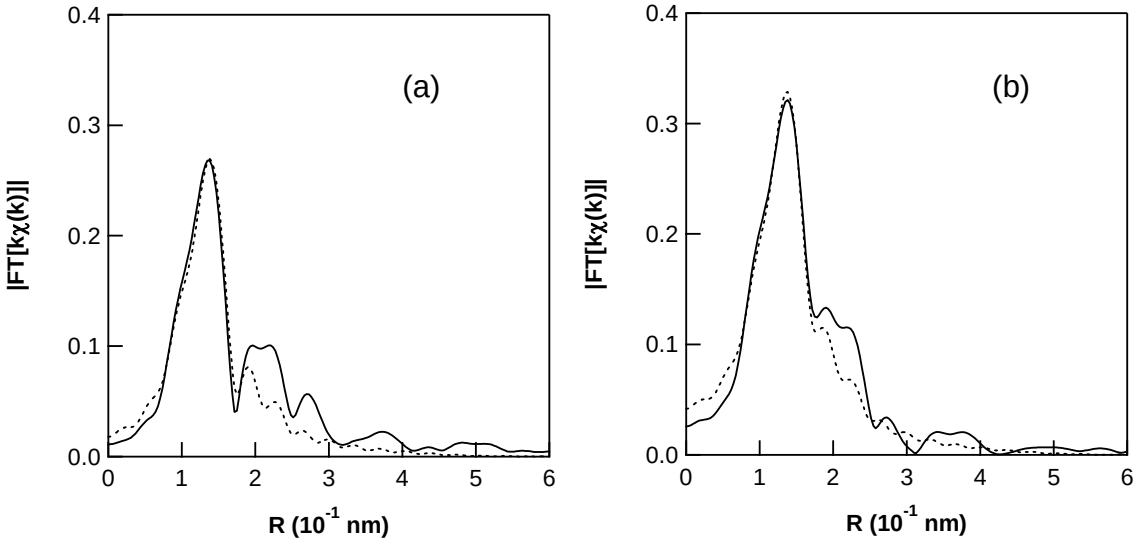

Figure 3.14. Fourier transformed Co K-edge *k*-weighted EXAFS functions of (a) Co-salen and (b) Co(salen)-mont. Solid line and broken line represent observed and fitted Fourier transforms, respectively.

Both XANES and EXAFS results indicate that cobalt atoms in Co(salen)-mont form additional two Co-O bonds with a bond length of 0.199 nm by the intercalation while retaining Co-salen structure as shown schematically in Figure 3.15

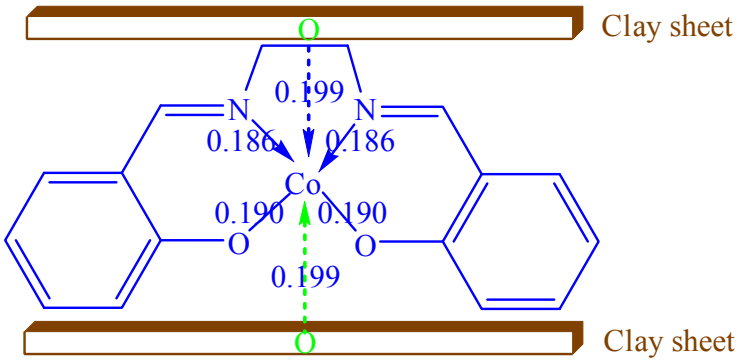

Figure 3.15. Schematic representation of Cosalen-mont catalyst

Table 3.3. Structural parameters for Co-salen and Co(salen)-mont determined by a curve fitting analysis of the EXAFS Fourier transforms.

Sample	Bond	coordination number	R (nm)	σ^2 (10^{-5} nm^2)	ΔE_0 (eV)	R_f (%)
Co-salen	Co-N	2.0 [a]	0.190 [a]	2.7	-4.1	0.8
	Co-O	2.0 [a]	0.186 [a]	10.9	-18.8	
Co(salen)-mont	Co-N	2.0 [a]	0.190 [a]	2.7	-4.1	0.7
	Co-O	2.0 [a]	0.186 [a]	10.9	-18.8	
	Co-O	1.6	0.199	7.2	-6.1	

[a] The value was determined by the X-ray structure analysis of Co-salen [45] and fixed in fitting.

3.3.2. *Activity measurement*

Catalyst activity results of this work are discussed on the basis of conversion of *p*-cresol, selectivity and turnover frequency (TOF) which were calculated as follows.

$$\%\ Conversion\ = \frac{\text{initial conc. of } p\text{ - cresol - final conc of } p\text{ - cresol}}{\text{initial conc. of } p - \text{cresol}} \times 100$$

$$\%\ \text{Selectivity} = \frac{\text{conc. of product formed}}{\text{conc. of } p - \text{cresol consumed}} \times 100$$

$$\text{TOF} = \frac{\text{conc. of } p - \text{cresol consumed}}{\text{conc. of catalyst (active metal)} \times \text{time}} \times 100$$

3.3.2.1. Screening of catalysts and clays

Figure 3.16 shows the results of catalyst screening for the liquid phase air oxidation of *p*-cresol under atmospheric conditions. For this purpose, salen complexes of cobalt and manganese were chosen and these were intercalated into the montmorillonite and other synthetic clays which had varying Si/Al ratio (6 and 8). Cobalt salen was of particular interest since, it has long been known to reversibly bind and activate dioxygen forming mononuclear superoxo species responsible for catalyst activity in the oxidation of phenolic substrates [48-51]. It was observed that Co(salen)-mont catalyst showed the highest activity among all the catalysts. Cobalt catalyst showed higher activity than that of manganese catalyst because, redox system for cobalt (Co^{II} ↔ Co^{III}) responsible for the oxidation could be more efficient than the Mn redox

couple. When Co-salen was intercalated into other synthetic clays (clay I and clay II), the activity was found to be considerably lower than that of intercalated montmorillonite catalyst. It was interesting to note that Co-salen alone showed a very poor oxidation activity, due to the fact that in the homogeneous phase, cobalt complexes are known to form binuclear species which are inactive towards oxidation [48, 50].

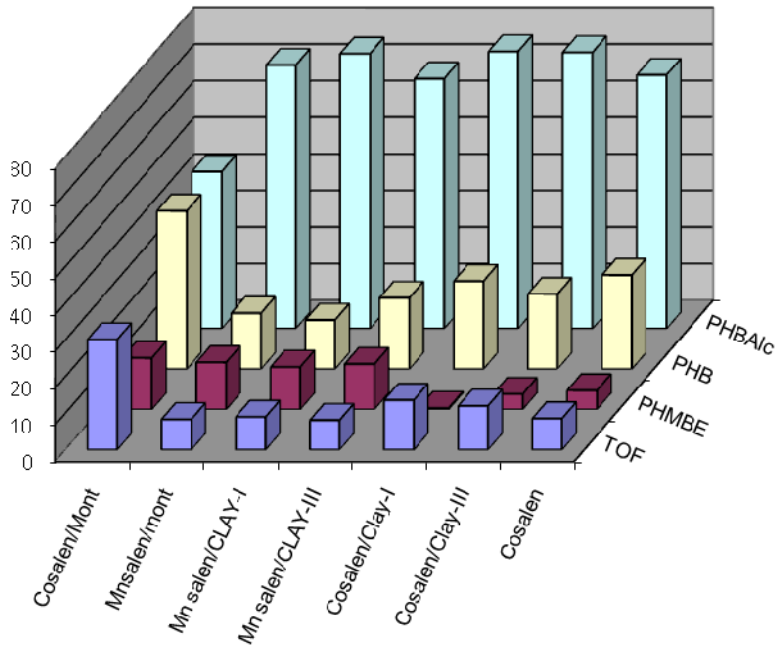

Figure 3.16. Catalyst screening for air oxidation of *p*-cresol
Reaction conditions: temperature, 338 K; NaOH : *p*-cresol, 2.9; catalyst loading, 3.7 kg/m^3; total reaction volume, 5.35 x 10^{-5} m^3; air flow rate, 50 mL/min; initial *p*-cresol concentration, 0.51 kmol/m^3.

Activity of our Co-salen intercalated into montmorillonite catalyst was about five times higher (TON 150) than that of homogeneous Co-salen reported (TON 29) for the air oxidation of phenolic derivatives which was carried out in an aqueous medium

under oxygen atmosphere in a batch mode [52]. The enhanced activity of our intercalated catalyst could be due to (i) the isolation of Co^{II} species, thus avoiding the formation of inactive binuclear cobalt complexes, and/or (ii) immobilization of cobalt complexes, which can offer diffusion in only two-dimensional space instead of three-dimensional volume. This increases the encounter frequencies between the reactants. In case of Co(salen)-mont catalyst, *p*-hydroxybenzyl alcohol and *p*-hydroxy benzaldehyde were obtained in almost equal proportions while selectivity to *p*-hydroxybenzyl methyl ether obtained was as high as 14%. Since, *p*-hydroxybenzyl methyl ether formation is due to nucleophilic attack of CH_3O^- on the benzyl carbon of *p*-hydroxy benzyl alcohol, it could be controlled with an appropriate optimization of reaction conditions, as discussed later.

3.3.2.2. Screening of Co-Schiff bases intercalated into montmorillonite clay

Figure 3.17 shows the results on catalyst activity of various Co Schiff bases intercalated into montmorillonite and homogeneous Co complex catalysts for the air oxidation of *p*-cresol under atmospheric conditions. Among all the catalysts, Co(salen)-mont catalyst showed the highest activity.

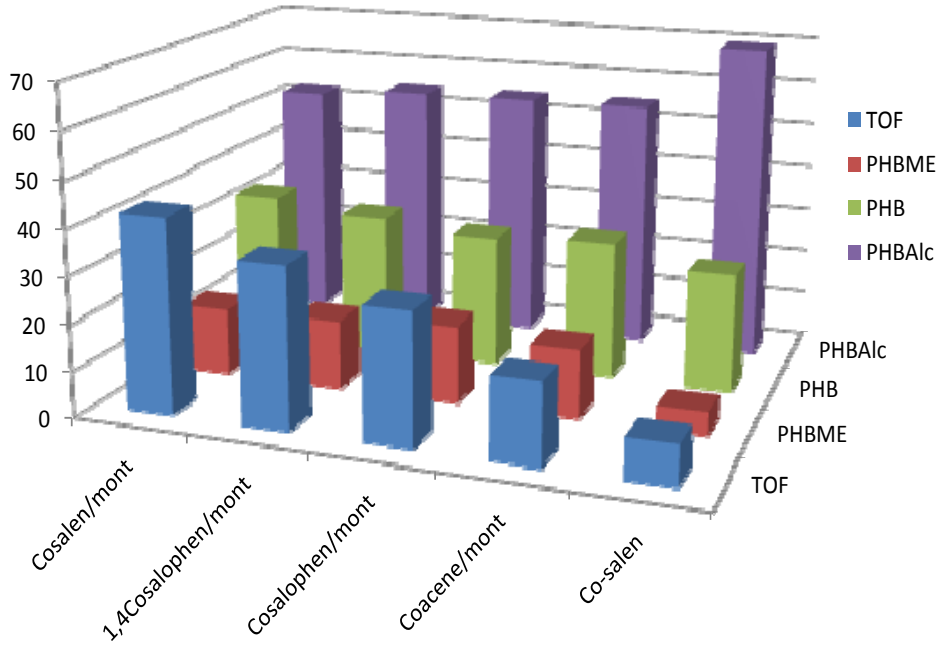

Figure 3.17. Catalyst screening for air oxidation of *p*-cresol
Reaction conditions: temperature, 338 K; NaOH : *p*-cresol, 2.9; total reaction volume, 5.35 x 10^{-5} m^3; air flow rate, 50 mL/min; initial *p*-cresol concentration, 0.51 kmol/m^3.

3.3.2.3. Product distribution and selectivity

In order to study the product distribution, a few preliminary experiments of *p*-cresol oxidation were carried out using Co(salen)-mont catalyst in methanol solvent under atmospheric conditions. In these experiments, the progress of the reaction was monitored by liquid-phase analysis as a function of time. Figure 3.18 shows the conversion and product selectivities vs time profile for *p*-cresol oxidation using Co(salen)-mont catalyst at 338 K. It was observed that as *p*-cresol was oxidized and

the initial oxidation product formed was *p*-hydroxybenzyl alcohol (PHBALc, 2) that undergoes further oxidation to give *p*-hydroxybenzaldehyde (PHB, 3).

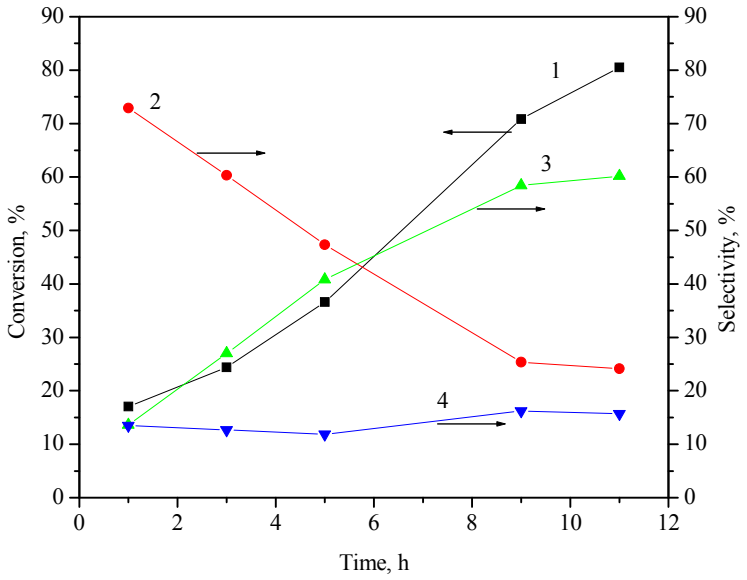

Figure 3.18. Conversion and product distribution with time for air oxidation of *p*-cresol over Co(salen)-mont catalyst
Reaction conditions: temperature 338 K; catalyst loading, 3.7 kg/m^3; total reaction volume, 5.35 x 10^{-5} m^3; air flow rate, 50 mL/min; initial *p*- cresol concentration, 0.51 kmol/m^3.

However, further oxidation of PHB to give *p*-hydroxybenzoic acid (PHBAcid, 5) was not observed under reaction conditions of the present work. Highest conversion of *p*-cresol achieved was 80% with increase in reaction time from 5 to 11 h. Since methanol was used as a solvent, formation of *p*-hydroxybenzyl methyl ether (PHBME, 4) was also observed due to a nucleophilic attack of CH_3O^- on the benzyl carbon of *p*-hydroxybenzyl alcohol. Based on these observations, the reaction pathway of *p*-cresol oxidation is as shown in Scheme 3.1.

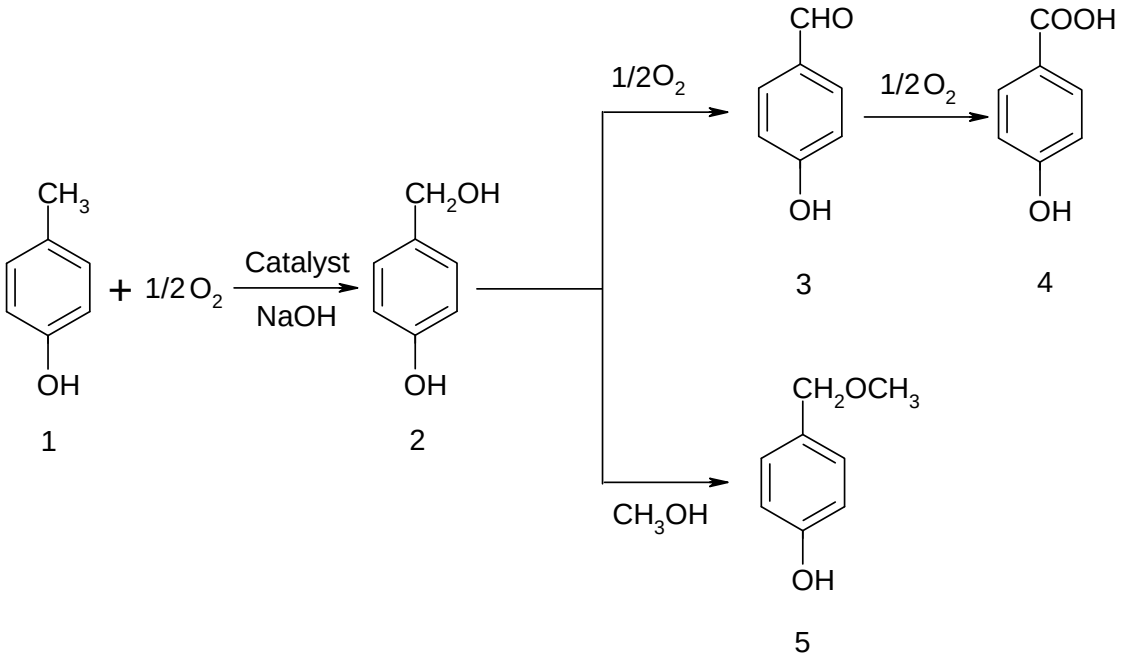

Scheme 3.1. Reaction pathway in oxidation of *p*-cresol.

3.3.2.4. Screening of solvent

The oxidation of *p*-cresol was also investigated in various solvents and the results are shown in Table 3.4. The activity was found to be in the following order, Methanol ~ ethanol > butanol > IPA > dioxane. This order of oxidation activity was consistent with the polarity of the solvents [54]. 1, 4-Dioxane showed the lowest activity (conversion, ~5%) possibly due to its lower polarity as well as lower oxygen solubility. Although, methanol and ethanol were found to give the same conversion of *p*-cresol, the selectivity to PHBALc was highest in ethanol due to no formation of any PHBME (Table 3.4). In case of butanol, selectivity to both alcohol and aldehyde was almost the same. Thus, the choice of solvent allowed achieving the desired selectivity of the oxidation products.

Table 3.4. Effect of solvent on air oxidation of *p*-cresol

Solvents	% Conversion	% Selectivity			
		PHBALc	PHB	PHBME	PHBAcid
Methanol	33	52	34	14	-
Ethanol	32	67	33	-	-
2-Propanol	8	78	21	-	< 0.5
1-Butanol	24	51	48	-	< 2
1,4 Dioxane	5	85	15	-	-

Reaction conditions: temperature 338 K; mole ratio, NaOH: *p*-cresol, 2.9; total reaction volume, 5.35 x 10^{-5} m^3; air flow rate, 50 mL/min; initial *p*-cresol concentration, 0.51 kmol/m^3.

3.3.2.5. Effect of NaOH concentration

It was necessary to study the effect of NaOH concentration on the *p*-cresol conversion and oxidation product selectivities, since the oxidation of alkyl group of phenol proceeds only after the conversion of –OH group to its sodium phenolate salt. As can be seen from Figure 3.19, conversion of *p*-cresol increased from 11 to 53% with increase in NaOH concentration from 0.56 to 3.42 kmol/m^3 while the selectivity to PHBALc decreased from 93 to 52 % and that for PHB increased from 7 to 33%. Formation of PHBME was almost negligible (<0.5%) at the lowest NaOH concentration (0.56 kmol/m^3) while its selectivity also increased substantially (18%) at higher NaOH concentration. Beyond 1.52 kmol/m^3 of NaOH concentration, both PHBALc and PHB were formed in equal amounts (1:1) while formation of PHBME,

a non-oxidation product was observed with a consistent selectivity of 18%. Higher concentration of NaOH would cause the stabilization of CH_3O^- in methanol solvent, favoring its nucleophilic attack on the the benzyl carbon of PHBAlc, thus reducing the selectivities of the oxidation products

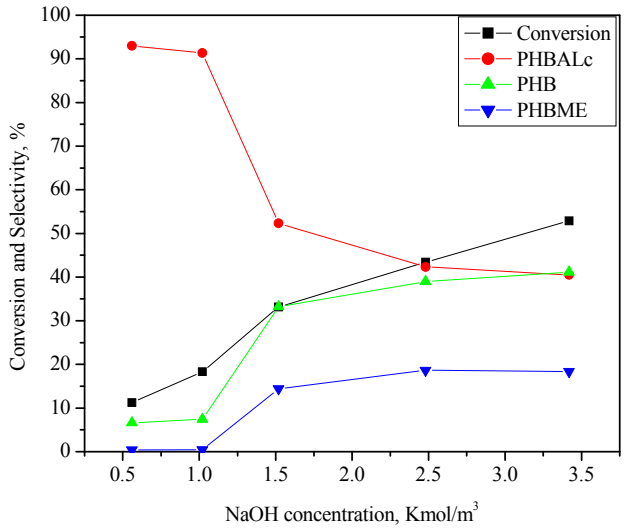

Figure 3.19. Effect of NaOH concentration on air oxidation of *p*-cresol over Co(salen)-mont catalyst
Reaction conditions: temperature 338 K; catalyst loading, 3.7 kg/m^3; total reaction volume, 5.35 x 10^{-5} m^3; air flow rate, 50 mL/min; initial *p*-cresol concentration, 0.51 kmol/m^3.

After establishing the product distribution in liquid phase oxidation of *p*-cresol, a systematic study on catalyst screening, and effect of various reaction parameters on conversion of *p*-cresol and product selectivities for a selected catalyst was carried out.

3.3.3. Effect of reaction variables

Further work on the effects of various reaction parameters on conversion of *p*-cresol and product selectivities were studied over Co(salen)-mont catalyst. In each experiment, a final sample was analyzed by HPLC to calculate conversion and selectivity Table 3.5 presents the range of various process parameters studied.

Table 3.5. Range of operating conditions

temperature, K	313-338
p-cresol concentration, kmol/m^3	0.271-1.06
catalyst loading, kg/m^3	3.73-9.25
air flow rate, mL/min	50-110
total reaction volume, m^3	5.35 x 10^{-5}
pressure	ambient

3.3.3.1. Effect of temperature

Figure 3.20 shows the effect of temperature on conversion of *p*-cresol and selectivity profile. The conversion of *p*-cresol increased from 10 to 34% with increase in temperature from 313 to 338 K. Since, methanol was used as a solvent and all the oxidation experiments were carried out at ambient pressure conditions, temperature could not be enhanced > 338K. The selectivity to *p*-hydroxybenzyl alcohol was high at lower temperature and decreased gradually to give *p*-hydroxybenzaldehyde with increase in temperature. This clearly indicates that *p*-hydroxybenzyl alcohol is the first intermediate formed in *p*-cresol oxidation (scheme 3.1). The selectivity to *p*-

hydroxybenzyl methyl ether also increased with increase in temperature. The rate of oxidation increased with increase in temperature, and the activation energy evaluated from the Arrhenius plot (Figure 3.21) was 43.7 kJ mol^{-1}.

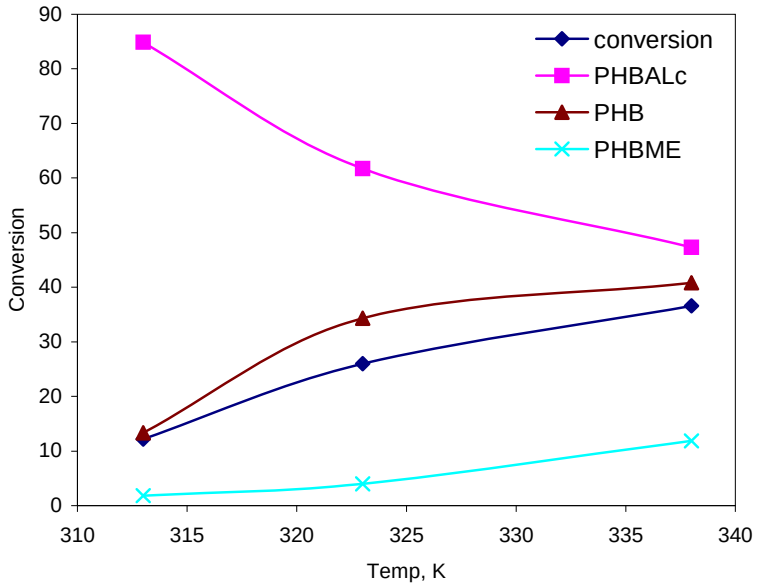

Figure 3.20. Effect of temperature on conversion and selectivity
Reaction conditions: NaOH : p-cresol, 2.9; catalyst loading, 3.7 kg/m^3; solvent, methanol; total reaction volume, 5.35 x 10^{-5} m^3; air flow rate 50 mL/min; initial *p*-cresol concentration, 0.51 kmol/m^3.

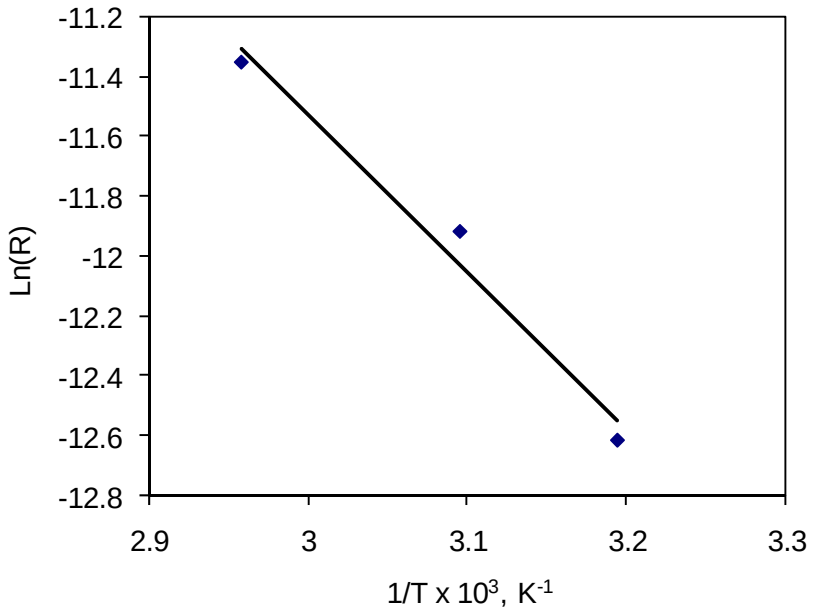

Figure 3.21 Arrhenius plot

3.3.3.2. Effect of substrate concentration

Effect of initial *p*-cresol concentration on conversion of *p*-cresol and selectivity of products was studied at 338 K. As can be seen from Figure 3.22, conversion of *p*-cresol increased from 15 to 36% with increase in substrate concentration up to 0.51 kmol/m^3 beyond which it almost remained constant. However, selectivity trends for *p*-hydroxybenzaldehyde and *p*-hydroxybenzyl alcohol were exactly opposite to each other. Formation of *p*-hydroxybenzyl methyl ether was almost negligible at lower substrate concentration (0.27 kmol/m^3) while its selectivity also increased substantially at higher substrate concentration. Beyond 0.51 kmol/m^3 concentration of *p*-cresol, formation of *p*-hydroxybenzyl methyl ether, a non-oxidation reaction was

found to compete with second step oxidation of *p*-hydroxybenzyl alcohol affecting adversely the selectivity to PHB.

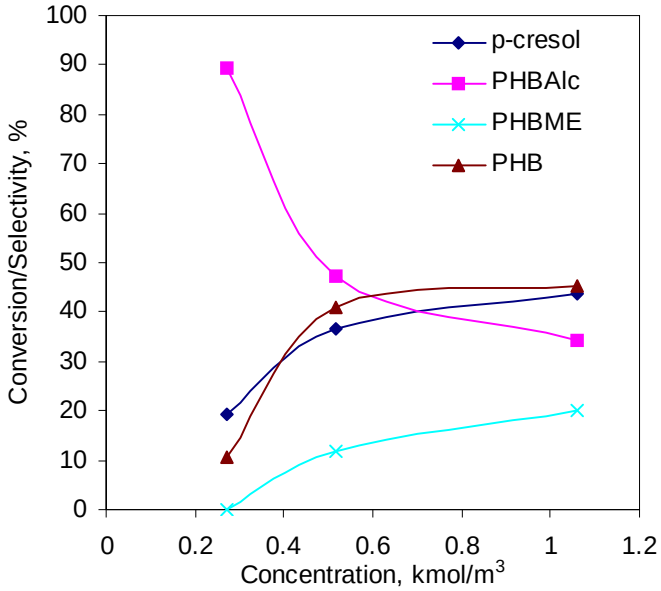

Figure 3.22. Effect of substrate concentration
Reaction conditions: temperature, 338 K; NaOH : *p*-cresol 2.9; catalyst loading, 3.7 kg/m^3; solvent, methanol; total reaction volume 5.35 x 10^{-5} m^3; air flow rate 50 mL/min.

3.3.3.3. Effect of air flow rate

Effect of volumetric air flow rate was studied at 338 K and the results are shown in Figure 3.23. The conversion of *p*-cresol decreased from 45 to 30% with increase in air flow rate from 50 to 108 mL/min. The selectivity pattern was almost similar for change in flow rates from 50 to 82 mL/min. However, there was a dramatic change in selectivity pattern for further increase in flow rate to 108 mL/min. At the highest flow rate (108 mL/min), studied in this work, selectivity to *p*-hydroxybenzyl alcohol sharply increased from 48 to 74% while that for *p*-hydroxybenzaldehyde decreased from 42 to 25 %.

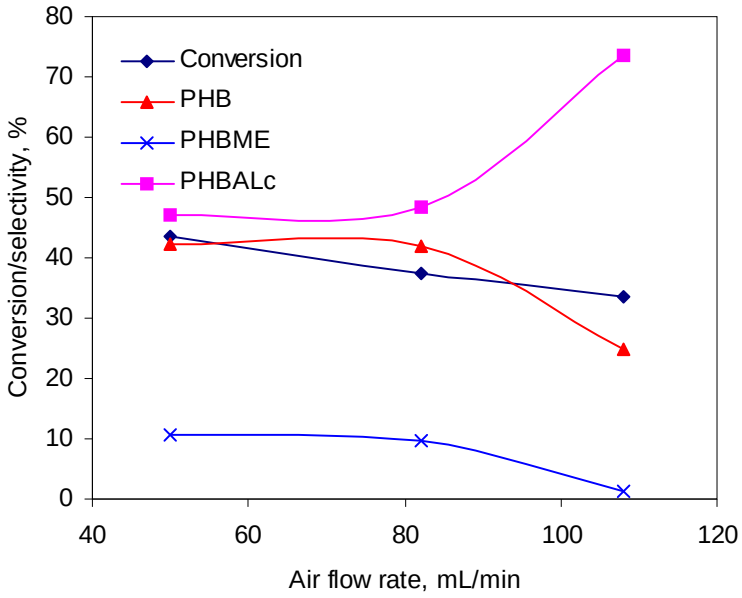

Figure 3.23. Effect of air flow
Reaction conditions: temperature, 338 K; NaOH: *p*-cresol 2.9; catalyst loading, 3.7 kg/m^3; solvent, methanol; total reaction volume 5.35 x 10^{-5} m^3; initial *p*-cresol concentration, 0.51 kmol/m^3.

These results indicate that at higher air flow rate the intermediate *p*-hydroxybenzyl alcohol gets desorbed faster and its readsorption for further oxidation to *p*-hydroxybenzaldehyde does not take place. Interestingly, selectivity to *p*-hydroxybenzyl methyl ether also decreased from 10 to 1.5 % (almost 7 fold decrease) which may be due to the fact that non-oxidation reaction of *p*-hydroxybenzyl alcohol and methanol could be inhibited by the higher concentration of substrate (i.e. *p*-hydroxybenzyl alcohol). This needs to be ascertained by conducting a separate reaction between *p*-hydroxybenzyl alcohol and methanol. This study clearly indicates that a continuous air oxidation of *p*-cresol under ambient pressure conditions over Co(salen)-mont catalyst would be feasible from process point view and the selectivity

ratio of PHB to PHBALc can be altered as per the demand while eliminating the undesired side product PHBME.

3.3.3.4. Effect of catalyst loading

The catalyst loading was varied in the range of 3.73 to 9.27 kg/m^3 at 338 K and the results are presented in Figure 3.24.

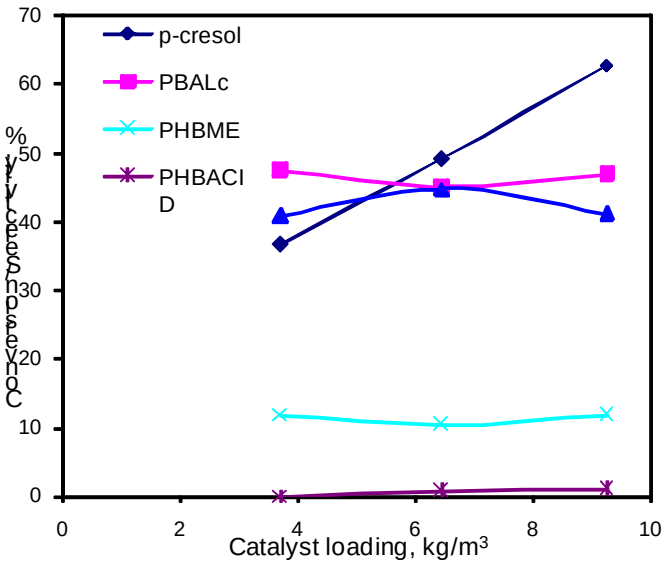

Figure 3.24. Effect of catalyst loading
Reaction conditions: temperature, 338 K; NaOH: *p*-cresol 2.9; solvent, methanol; total reaction volume 5.35 x 10^{-5} m^3; air flow rate, 50 mL/min; initial *p*-cresol concentration, 0.51 kmol/m^3.

The conversion of *p*-cresol increased linearly with increase in catalyst loading while the selectivity to *p*-hydroxybenzyl alcohol remained almost constant. However, selectivity to both *p*-hydroxybenzaldehyde and p-hydroxybenzyl methyl ether was affected marginally with increase in catalyst loading. Formation of *p*-hydroxybenzoic acid was almost negligible at all the catalyst loadings studied in this work.

The activity of Co(salen)mont catalyst was also tested for other cresol isomers viz. *o*- and *m*-cresol. Interestingly, both the isomers did not give any conversion. This clearly shows that the Co-salen has been located in the interlamellar spaces of montmorillonite with an orientation parallel to the clay sheets so that only a straight molecule like *p*-cresol could enter the two dimensional lamellar clay catalyst

3.4. Conclusion

Among various solid catalysts screened, clay intercalated cobalt salen showed an excellent activity for the liquid phase air oxidation of *p*-cresol under ambient pressure conditions. Hence, this catalyst was thoroughly characterized and the intercalation of the complex into the clay matrix was confirmed by the following evidences.

- The shifting of d-d transition band of the parent Co-salen to the higher energy region indicated the in-plane ligand field around the metal ion becoming stronger due to the intercalation of the complex into the montmorillonite clay.
- Thermal stabilization observed from TGA studies was due to the host-guest interaction of clay and metal complex.
- The binding energy (BE) of Co $2p_{3/2}$ level for Co-salen observed was 780.4 eV while, the intercalated montmorillonite complex showed a clear shift towards higher BE (781.1 eV).
- A shoulder at 7715 eV of XANES spectra of Co-salen which has a tetrahedral geometry in plane disappeared in case of Co(salen)-mont due to the change of symmetry from the tetrahedral in plane to the octahedral structure having an

axial bonding of oxygen to the cobalt indicating that cobalt atoms in Co(salen)-mont were coordinated axially with lattice oxygen of montmorillonite.

- The structural parameters obtained from a curve fitting analysis of the EXAFS Fourier transforms for Co-salen and Co(salen)-mont indicated that cobalt atoms in Co(salen)-mont form additional two Co-O bonds with a bond length of 0.199 nm by the intercalation while retaining Co-salen structure.
- Cobalt-salen intercalated into the montmorillonite catalyst showed the highest conversion with the selectivity as high as 88% to the oxidation products, in methanol under ambient pressure conditions.
- A heterogeneous catalyst was developed by intercalating cobalt-salen into the montmorillonite clay for the air oxidation of *p*-cresol. The oxidation was studied in a semi batch reactor under ambient pressure conditions. The oxidation of *p*-cresol involves a consecutive reaction scheme giving a mixture of products, *p*-hydroxybenzyl alcohol, *p*-hydroxybenzaldehyde and *p*-hydroxy benzoic acid. With increase in NaOH concentration, conversion of p-cresol increased linearly while the formation of non-oxidation product (PHBME) was predominant. Formation of benzoic acid and other side products due to non-oxidation reactions could be significantly minimized using our catalyst. In a semi batch mode, the ratio of *p*-hydroxybenzyl alcohol and *p*-hydroxybenzaldehyde could be manipulated by tailoring the operating conditions for the same catalyst. Effect of various process parameters were

also studied using this catalyst and the activation energy from the Arrhenius plot was found to be 43.7 kJ/mol.

3.5. References

1. D. T. Sawyer, Coord. *Chem. Rev*. **1997**, *165*, 297.
2. D. Ramprasad, A. G. Gilicinski, T. J. Markley, G. P. Pez, *Inorg. Chem*. **1994**, *33*, 2841.
3. I. G. Denisov, T. M. Makris, S. G. Sligar, I. Schlichting, *Chem. Rev*. **2005**, *105*, 2253.
4. A. K. Udit, F. H. Arnold, H. B. Gray, *J. Inorg. Biochem*. **2004**, *98* 1547.
5. T. Punniyamurthy, S. Velusamy, J. Iqbal, *Chem. Rev*. **2005**, *105*, 2329.
6. A. Nishinaga, S. Yamazaki, T. Matsuura *Tetrahedron Lett*. **1988,** *29*, 4115.
7. S. Fukuzumi, K. Okamoto, Y. Tokuda, C. P. Gros, R. Guilard, *J. Am. Chem. Soc*. **2004**, *126*, 17059.
8. R. A. Sheldon, in *Catalytic Oxidation: Principles and Applications*. Ed. R. A. Sheldon; R. A. van Santen, World Scientific, Singapore, **1995**, p. 177.
9. R. A. Sheldon, H. Bekkum, *Fine Chemicals Through Heterogeneous Catalysis*, Wiley-VCH, Weinheim, **2001**, p.4.
10. Z. Gao, Y. Shao, S. Wang, P. Yang, *Appl. Catal. A: Gen*. **2001**, *209*, 27.
11. J. H. Clark, D. J. Mcquarrie, *Chem. Soc. Rev.* **1996**, *25*, 303.
12. F. Wang, G. Yang, W. Zhang, W. Wu, J. Xu, *Chem. Commun*. **2003**, 1172.
13. M. P. Peeters, J. M.Busio, P.Leijten, *Appl. Catal. A: Gen*. **1994**, *118*, 51.

14. L.Yumin, L. Sheitian, X. Y. Kaizheng, W. Yue, *Appl. Catal. A: Gen*. **1998**, *169*, 127.

15. C. V. Rode, M. V. Sonar, J. M. Nadgeri, R. V. Chaudhari *Org. Proc. Res. Dev.* **2004**, *8*, 873.

16. V. S. Kshirsagar; S. Vijayanand; H. S. Potdar; P. A. Joy; K. R. Patil; C. V. Rode, *Chem. Lett*. **2008**, *37*, 310.

17. F. Wang, G. Yang, W. Zhang, W. Wu, *Chem. Commun*. **2003**, 1172.

18. M. P. Peeters, J. M. Busio, P. Leijten, *Appl. C atal. A: Gen.* **1994**, *118*, 51.

19. L. Yumin, L. Sheitian, X. Y. Kaizheng, W. Yue, *Appl. Catal. A: Gen.* **1998**, *169*, 127.

20. D. E. De Vos, M. Dams, B. F. Sels, P. A. Jacobs, *Chem. Rev.* **2002**, *102*, 3 615.

21. C. E. Song, S. Lee, *Chem. Rev*. **2002**, *102*, 3495.

22. Q. H. Fan, Y. M. Li, A. S. C. Chan, *Chem. Rev*. **2002**, *102,* 3385.

23. R. Ferreira, M. Silva, C. Freire, B. de Castro, J. L. Figueiredo, *Micro. Meso. Mater*. **2000**, *38*, 391.

24. R. Ferreira, C. Freire, B. de Castro, A. P. Carvalho, J. Pires, M. Brotas de Carvalho, *Eur. J. Inorg. Chem.* **2002**, *11*, 3032.

25. V. Ramaswamy, M. Sivarama Kirshnan, A. V. Ramaswamy, *J. Mol. Catal. A: Chem*. **2002**, *181*, 81.

26. A. R. Silva, C. Freire, B. de Castro, M. M. A. Freitas, J. L. Figueiredo, *Micro. Meso. Mater*. **2001**, *46*, 211.

27. A. R. Silva, C. Freire, B. de Castro, M. M. A. Freitas, J. L. Figueiredo, *Langmuir*, **2002**, *18*, 8017.

28. A. R. Silva, M. Martins, A. Valente, M. M. A. Freitas, C. Freire, B. de Castro, J. L. Figueiredo, *Micro. Meso. Mater*. **2002**, *55*, 275.

29. M. P. Peeters, J. M. Busio, P. Leijten, *Appl. Catal. A: Gen*. **1994**, *118*, 51.

30. S. Cheng, *Catal. Today* **1999**, *49*, 303.

31. J. A. Labinger, E. Bercaw, *Nature* **2002**, *417*, 507.

32. V. M. Akhmedov, S. H. Al-khowaiter, *Catal. Rev. Sci. Engg*. **2002**, *44*, 455.

33. A. J. Poss, R. K. Belter, *J. Org. Chem*. **1988**, *53*, 1535.

34. T. Sigeru, T. Hideo, S. Takasi, A. Mitstio, *J. Org. Chem.* **1979**, *44*, 3305.

35. D. V. Rao, F. A. Stuber, *Synthesis*, **1983**, *4*, 308.

36. S. Mitchell, *Kirk-Othmer Encyclopedia of Chemical Technology*, 4th ed.; Willy- Interscience: New York, **1998**; vol. 13, pp 1030.

37. V. S. Kshirsagar, A. C. Garade, K. R. Patil, A. Yamaguchi, M. Shirai, C. V. Rode *accepted* in *Appl. Catal. A: Gen*. **2009**

38. C. V. Rode, V. S. Kshirsagar, J. M. Nadgeri, K. R. Patil, *Ind. Eng. Chem. Res.* **2007**, *46*, 8413.

39. N. N. Binitha, S. Sugunana, *Micro. Meso. Mater*. **2006**, *93*, 82.

40. K. J. Balkus Jr., A.G. Gabrielov *J. Incl. Phenom. Mol. Recog. Chem*. **1995**, *21*, 159.

41. K. J. Balkus Jr. and J. P. Ferraris, *J. Phys. Chem*. **1990**, *94*, 8019.

42. L. Guczi, R. Sundararajan, Zs. Koppány, Z. Zsoldos, Z. Schay, F. Mizukami, S. J. Niwa, *J. Catal.* **1997**, *167*, 482.

43. B. V. Romanovsky, A. G. Gabrielov, *J. Mol. Catal*. *A:Chem*. **1992,** *74*, 293.

44. Zombeck, A.; Drago, R. S.; Corden, B. B.; Gaul, J. H. *J. Am. Chem. Soc*. **1981**, *103*, 7580.

45. K. Omata, T. Takada, S. Kasahara, M. Yamada *Appl. Catal. A: Gen.* **1996**, *146*, 255.

46. H. Nishide, H. Mizuma, E. Tsuchida, J. McBreen, *Bull. Chem. Soc. Jpn.* **1999**, *72*, 1123.

47. V. D. Makwana, Y. C. Son, A. R. Howell, S. L. Suib, *J. Catal*. **2002**, *210*, 46.

48. V. S. Kshirsagar, A. C. Garade, K. R. Patil, R. K. Jha, C. V. Rode, *Ind. Eng. Chem.Res.* **2009** (Doi: *10.102/ie801941e)*

49. R. A. Sheldon, J. Kochi, *Metal-catalyzed oxidations of organic compounds*, Academic Press, **1981** p.72.

50. Martell, in *Oxygen complexes and oxygen activation by transition metals*, (Eds. Martell, A.; Sawyer, D.), Plenum Press, **1987**.

51. J. Bozell, B. R. Hames, D. R. Dimmel, *J. Org. Chem*. **1995**, *60*, 2398.

52. D. E. Hamilton, R. S. Drago, A. Zombeck, *J. Am. Chem. Soc*. **1987**, *109*, 374.

53. K. Kervinen, H. Korpi, M. Leskela, T. Repo, *J. Mol. Catal. A: Chem.* **2003**, *203*, 9.

54. C. Reichardt, *Sovents and solvent effects in organic chemistry*, VCH Pub. 2nd ed., **1988.**

4.1. Introduction

In continuation of our efforts on developing new insoluble catalysts for oxidation, we report here for the first time synthetic saponite containing Co^{2+} in the octahedral layer as a highly efficient catalyst for liquid phase oxidation of *p*-cresol. Smectites are one of the most common phyllosilicate types of clays used as solid catalysts for several types of reactions due to their specific characteristics, such as a high specific surface area, cation exchange or hydration capacities etc. [1-4]. Saponite clay is an example of trioctahedral smectite in which the charge imbalance due to isomorphic substitutions in the structure layers is compensated by cations placed in interlamellar position. Therefore, Co-saponite obtained can be viewed as a nanocomposite (100nm) of Co phases over aluminosilicate support as a catalyst for oxidation reactions.

Co-saponites with varied cobalt compositions prepared by a simple protocol were characterized by DRUV, XPS, IR, TGA, SEM, DRUV-vis and BET surface area technique. Among various compositions, 13% Co-saponite showed an excellent activity and selectivity for the liquid phase oxidation of *p*-creol to *p*-hydroxybenzaldehyde [5]. For this catalyst, effects of various reaction parameters such as catalyst loading, temperature, oxygen partial pressure on the conversion and selectivity pattern were also investigated.

Many investigators have studied the mechanism of participation of lattice oxygen in alcohol oxidation systems involving metal oxide as catalysts [6, 7]. These studies were directed towards finding the nature of adsorbed oxygen species and their reactivity, and also that of lattice oxygen. In this chapter we have tried to explain the role of

lattice oxygen in liquid phase oxidation based on some key experiments and XPS studies. From XPS measurements, cobalt was found to be present as Co^{2+} indicating its coordination with lattice oxygen. XPS studies and the oxidation experiments with Co-saponite without oxygen, support that the liquid phase *p*-cresol oxidation proceeds probably through Mars-van Krevelen pathway involving the lattice oxygen and the subsequent reoxidation of the vacant sites by molecular oxygen [8].

4.2. Experimental

Various Co-saponite catalyst samples were prepared with 5, 13 and 30% Co content according to the procedure given in detail in section 2.2.2. Detailed catalyst characterization was also carried out by various techniques, details of which are given in section 2.3. Activity testing of these catalyst samples was carried out under partial pressure of oxygen in the range of 0.020-0.827 MPa in a high pressure reactor as per the description given in sections 2.4.

4.3. Results and discussion

4.3.1. Catalyst characterization

In this work, saponite clay was prepared with Si/Al ratio =8 and using Co as a divalent cation. The ratio of oxygen anion radius (1.4 Å) to that of Co^{2+} (0.65 - 0.74 Å depending on low spin, high spin state) was found to vary in the range of 0.46-0.53, giving the coordination number of cobalt as 4 or 6 [9]. Hence, Co ions are suggested to be in both the tetrahedral and octahedral positions of the saponite clay.

4.3.1.1. Nitrogen adsorption-desorption

BET surface area of Co-saponites prepared with 5, 13 and 30% Co content was found to be in a range of 397-417 m^2/g (Table 4.1).

Table 4.1. BET surface area of catalysts

Sr. No.	% Cobalt in Co-saponite	Surface Area m^2/g
2	05	418
4	13	405
5	30	397

The nitrogen adsorption-desorption isotherm for 13% Co-saponite sample is shown in Figure 4.1. It is of Type I isotherm based on the IUPAC classification, indicating the microporous nature of Co-saponite. The adsorption occurred at low pressure without any steps and the uptake of gas is governed by the accessible micropore volume rather than by the internal surface area [10]. A sharp increase at $p/p_o > 0.9$ is indicative of capillary condensation. BJH adsorption isotherm for 13% Co-saponite sample is shown in Figure 4.2, from which the pore size distribution of 17-19 Å was obtained which again confirms that this catalyst was essentially microporous in nature [11].

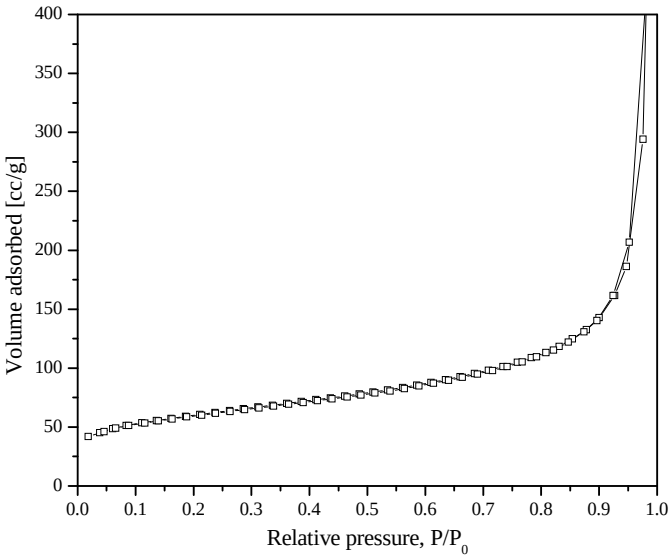

Figure 4.1. Adsorption isotherm of 13% Co-saponite

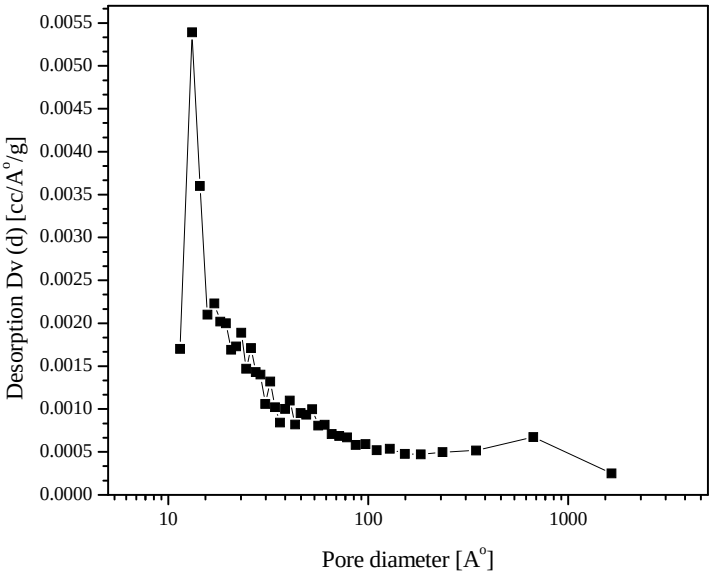

Figure 4.2. BJH adsorption

4.3.1.2. Diffused reflectance UV-visible spectroscopy

DRUV-visible spectrum of Co-saponite in Figure 4.3 shows a strong charge transfer band between O and the Co central atom in the range of 190-600 nm [12]. Bands at 495, 530, and 645 nm can be assigned to tetrahedral Co^{2+} species. The bands at 237, 351.6 and 387.5 nm are associated with oxygen-to-metal charge transfer (CT) transition while a broad and intense band at 530 nm suggests the presence of an extra-lattice Co(II) in octahedral symmetry [13].

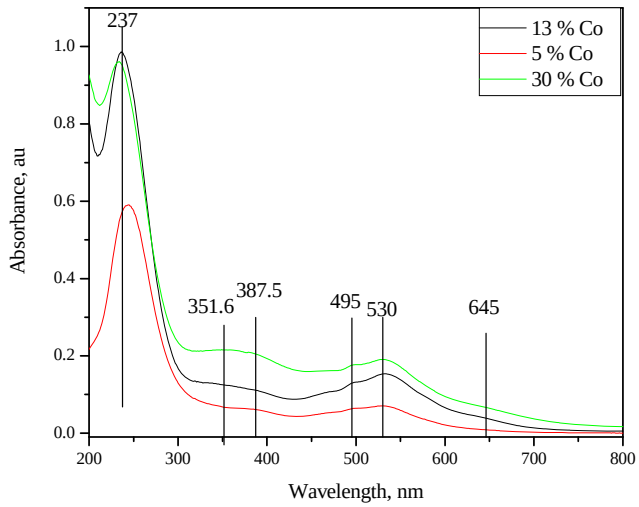

Figure 4.3. DRUV-Visible spectra of Co-saponite

4.3.1.3. Scanning electron microscopy

The elemental composition of 13% Co-saponite determined by EDS coupled with SEM (Figure 4.4) showed the atom weight percentages as Co (13.15%), Si (31.68), Al

(5.77%), Na (4.05%) and Oxygen (45.35) which was in excellent agreement with the theoretical percentages of elements.

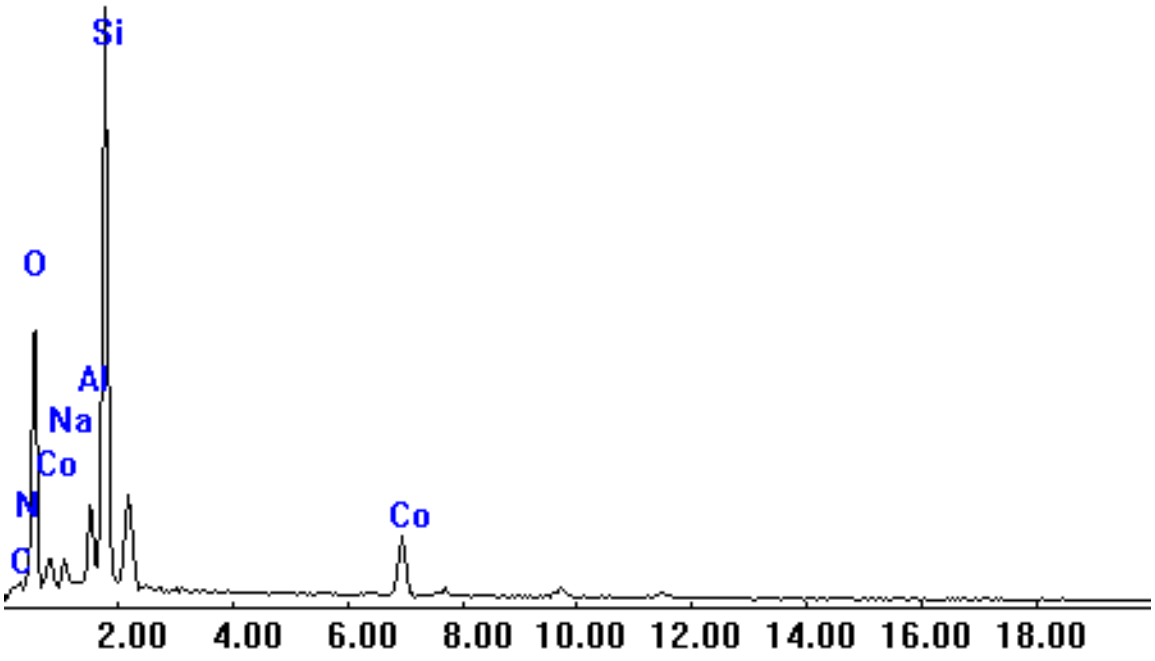

Figure 4.4. EDS of Co-saponite (13%)

SEM images of Co-saponite particles in Figure 4.5 shows the presence of aggregates formed by packing of sheets thus demonstrating that the synthetic procedure led to the production of materials with layered morphology. The solids obtained were of the size around 100 nm.

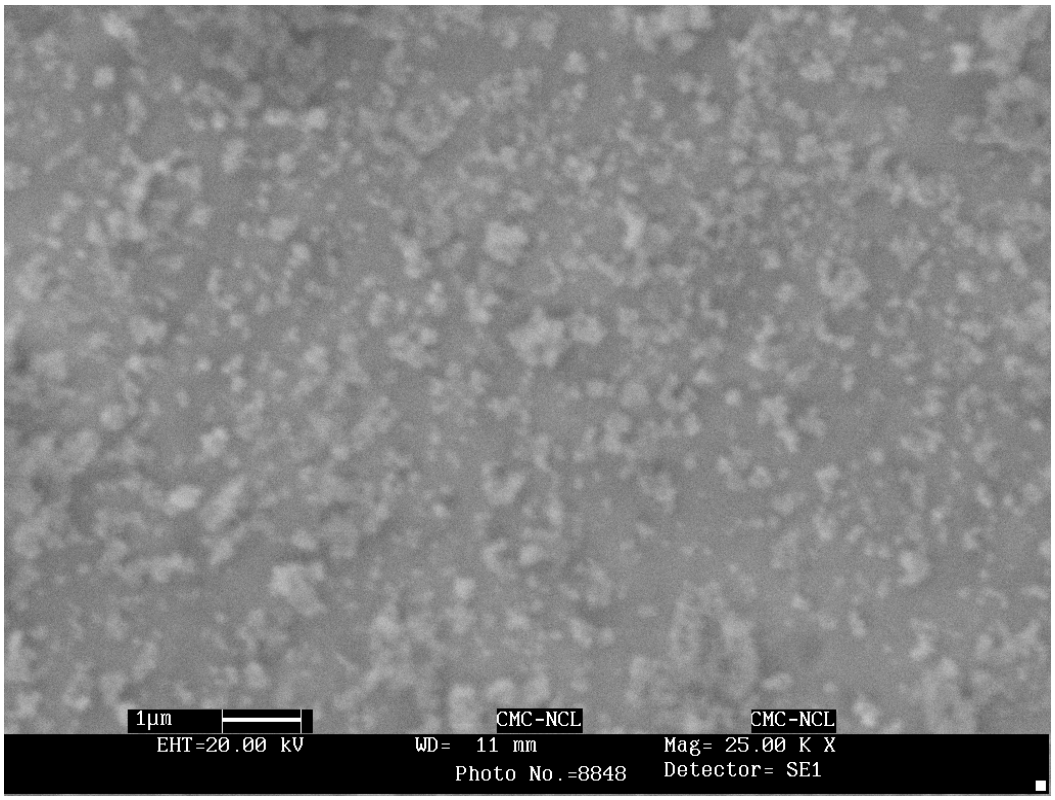

Figure 4.5. SEM image of Co-saponite

4.3.1.4. FTIR spectroscopy

Figure 4.6 shows the IR spectra for 13% Co-saponite clay. The band at 3435 cm^{-1} is assigned to O-H stretching vibrations. The band at 1031 cm^{-1} is assigned to Si-O stretching vibrations.

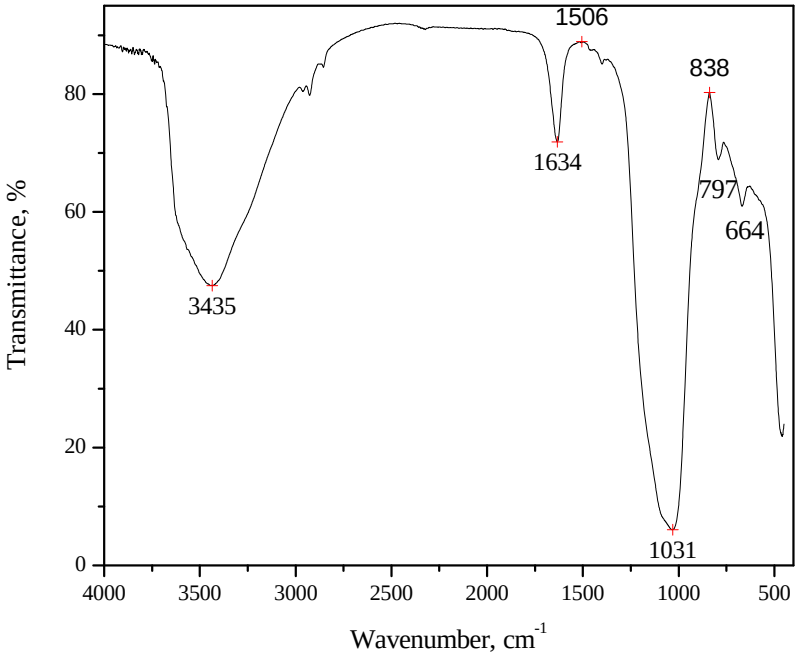

Figure 4.6. FTIR spectra of Co-saponite catalyst

4.3.1.5. X-ray photoelectron spectroscopy (XPS)

Figure 4.7 shows the Co 2p XPS spectra for Co-saponite catalyst. It can be clearly seen that the core level BE of $Co2p_{3/2}$ was at 781.9 eV. This value was very close to that reported for Co^{2+} as well as Co^{2+} exchanged NaY and for highly dispersed Co species in Co-ZSM-5 indicating that cobalt was coordinated to lattice oxygen and probably associated with silanol groups [14-16]. The core level BE of $Co2p_{1/2}$ was at 797.6 eV which was also close to that reported earlier for Co^{2+} [16]. In addition to these spin-orbital peaks, the satellites for $2p_{3/2}$ and $2p_{1/2}$ were also observed at 787.4

and 803.3 eV respectively, confirming that cobalt was mainly present in (II) oxidation state [17, 18]. The broad peak (FWHM=3.4 eV) of $Co2p_{3/2}$ (shown as inset in Figure 4.7) in Co-saponite suggests the presence of octahedrally and tetrahedrally coordinated divalent cobalt species.

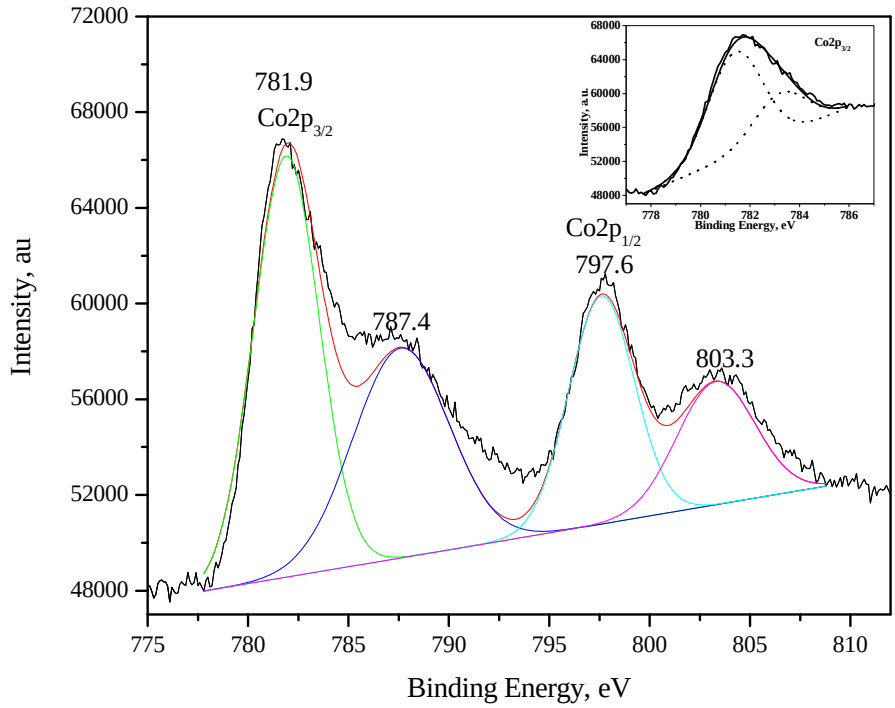

Figure 4.7. Co 2p XPS spectra of Co-saponite

4.3.2. Activity measurement

4.3.2.1. Product distribution

In order to study the product distribution, few preliminary experiments of *p*-cresol oxidation were carried out using 13% Co-saponite catalyst in n-propanol solvent under

atmospheric as well as high pressure reaction conditions. In these experiments, the progress of the reaction was monitored by liquid-phase analysis as a function of time and the conversion, selectivity versus time profile is shown in Figure 4.8. From this figure, it was observed that the initial oxidation product was *p*-hydroxybenzyl alcohol (PHBAlc) that undergoes further oxidation to give *p*-hydroxybenzaldehyde (PHB) and the *p*-hydroxybenzoic acid (PHBAcid). Based on these observations, the reaction pathway of *p*-cresol oxidation is shown in Scheme 4.1. Unlike in our previous work on *p*-cresol oxidation in methanol as solvent (scheme 3.1, chapter 3) [19-21], no formation of a non-oxidation product or alkylated product of *p*-HBALc was observed in this work.

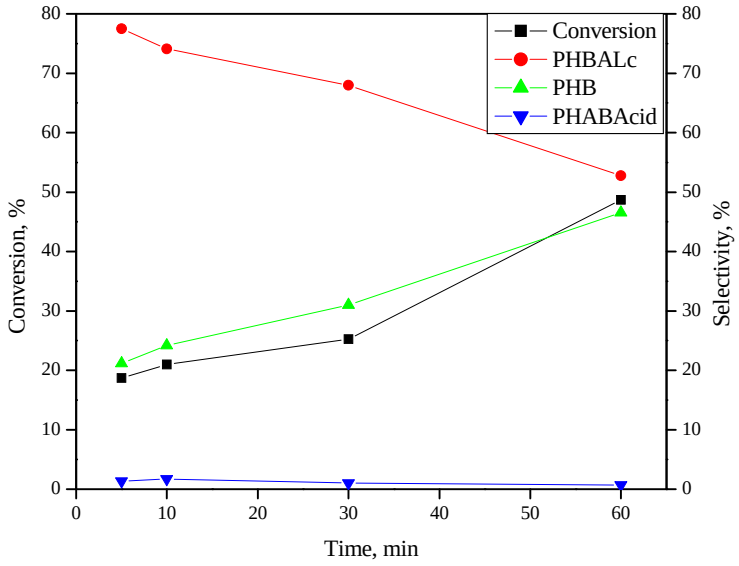

Figure 4.8. Conversion vs. time profile for oxidation of *p*-cresol
Reaction conditions: temperature, 343 K; NaOH : *p*-cresol, 4; catalyst loading, 2.67 kg/m^3; total reaction volume, 7.5 x 10^{-5} m^3; $p_{O2,}$ 0.414 MPa, reaction time, 1h.

Figure 4.9 shows a concentration-time profile for oxidation of *p*-cresol using 13% Co-saponite catalyst in n-propanol solvent in which the progress of the reaction was monitored by liquid-phase analysis as a function of time.

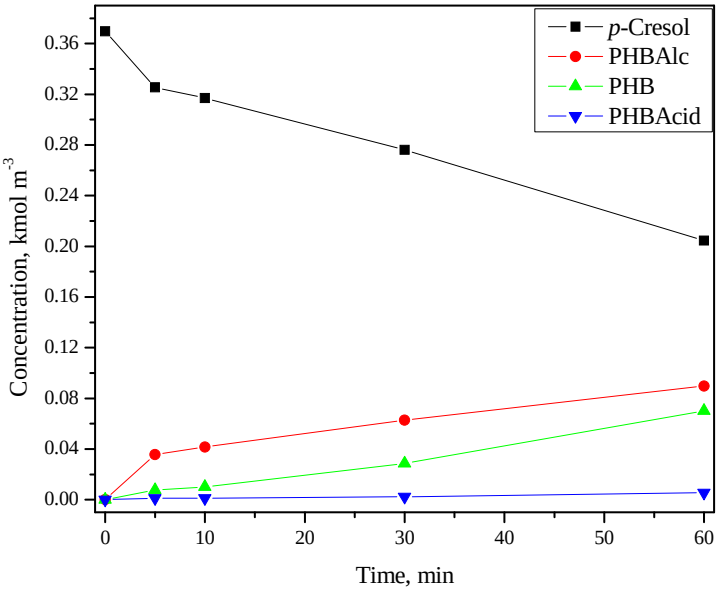

Figure 4.9. Concentration-time profile for oxidation of *p*-cresol with 13% cobalt saponite catalyst
Reaction conditions: temperature, 343 K; NaOH : *p*-cresol, 4.2; catalyst loading, 2.667 kg/m^3; total reaction volume, 7.5 x 10^{-5} m^3;oxygen pressure, 0.344MPa, solvent, n-propanol

It was observed that the initial oxidation product was PHBALc that undergoes further oxidation to give PHB and the PHBAcid**.** Based on these observations, the reaction pathway of *p*-cresol oxidation is shown in Scheme 4.1.

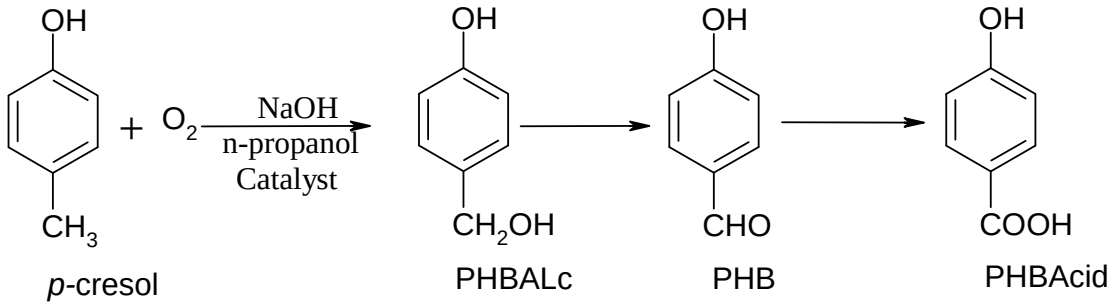

Scheme 4.1. Reaction scheme for oxidation of *p*-cresol

4.3.2.2..Effect of cobalt loading

Figure 4.10 shows the effect of cobalt concentration in Co-saponite catalyst on the rate of oxidation of *p*-cresol. For this purpose, Co-saponite catalyst samples prepared with varying cobalt content from 5% to 30% were evaluated for the oxidationof *p*-cresol at 343 K and 0.344 MPa pressure conditions. It was observed that the rate of reaction increased with increase in Co loading from 5 to 13% and then remained constant up to 30 % of Co loading. Hence, further work on the effects of various reaction parameters on conversion of *p*-cresol and product selectivities were studied over 13% Co-saponite catalyst. In each experiment, initial rate of reaction was also calculated from the oxygen consumption vs. time data.

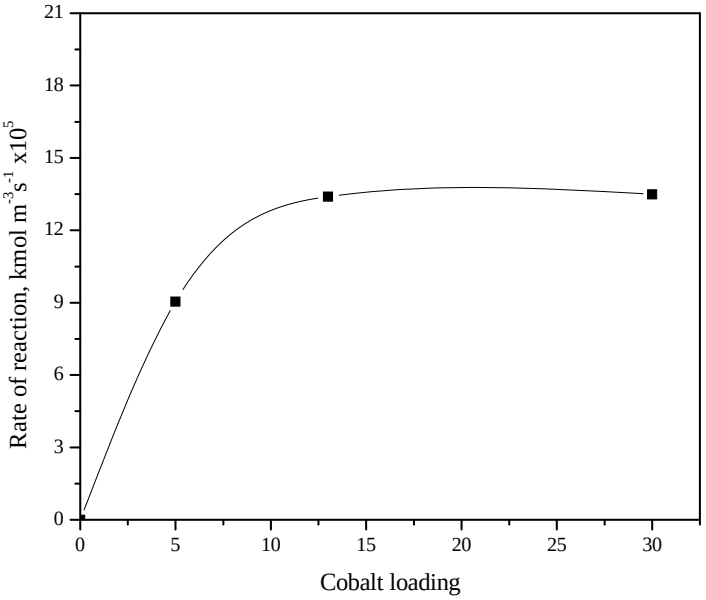

Figure 4.10. Effect of catalyst (Co content) on rate of reaction
Reaction conditions: temperature, 343 K; NaOH : *p*-cresol, 4.2; catalyst loading, 2.667 kg/m^3; total reaction volume, 7.5 x 10^{-5} m^3;oxygen pressure, 0.344 MPa; solvent, n-propanol; reaction time, 1 h.

Figure 4.11 shows the results of effect of Co content for the liquid phase air oxidation of *p*-cresol under high pressure reaction in the range of 5 to 30% on the conversion of *p*-cresol and the selectivity pattern. It was found that 13% Co-saponite catalyst showed the highest activity among all the catalysts. With increase on Co loading from 5 to 13 %, selectivity to PHB increased from 42.4 to 46.5 % as the further oxidation of PHBAlc proceeded.

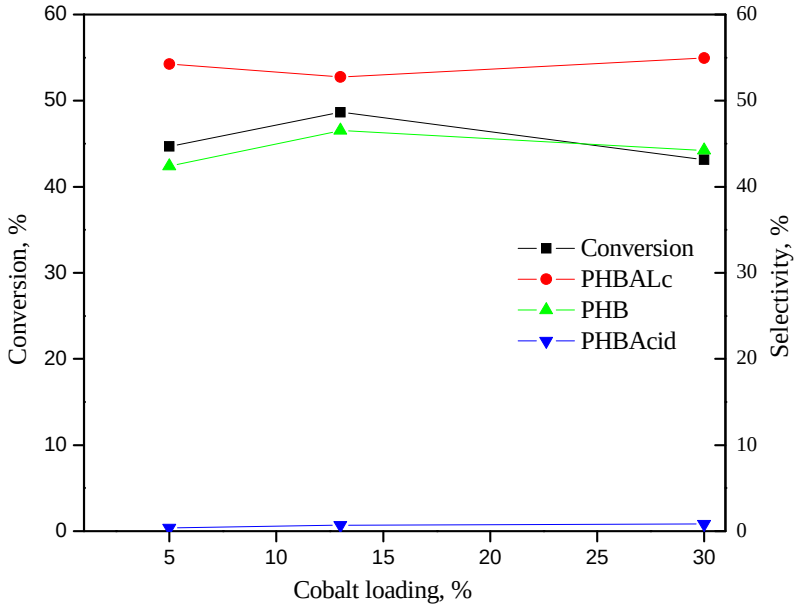

Figure 4.11. Effect of metal content on oxidation of *p*-cresol.
Reaction conditions: temperature, 343 K; NaOH : *p*-cresol, 4; catalyst loading, 2.67 kg/m^3; total reaction volume, 7.5 x 10^{-5} m^3; p_{O2}, 0.414 Mpa, reaction time, 1h.

4.3.2.3. *Effect of pressure*

Oxidation experiments were carried out by varying the oxygen pressure to study the effect of oxygen partial pressure on the rate of oxidation of *p*-cresol. For this purpose, the partial pressure of oxygen was varied in the range of 0.020 -0.827 MPa at 373 K and the results are shown in Figure 4.12.

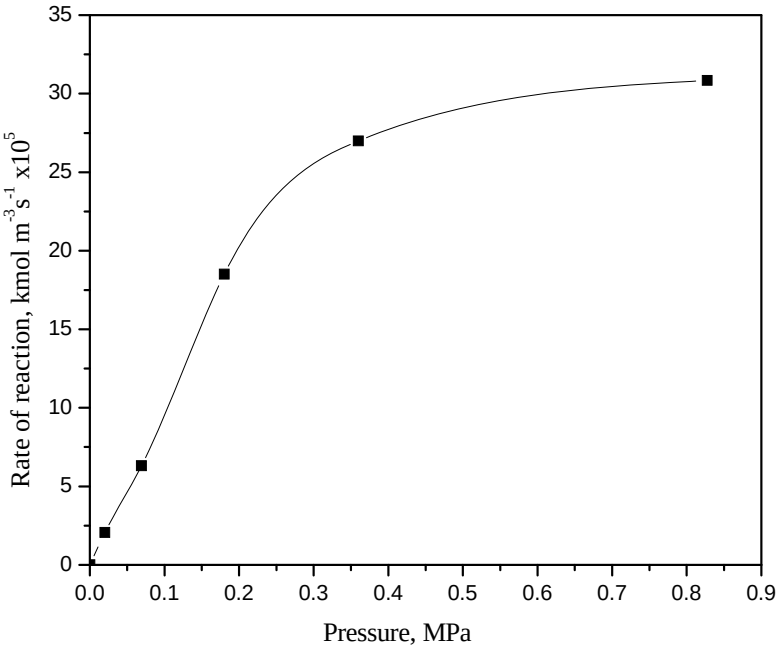

Figure 4.12. Effect of partial pressure of oxygen on rate of reaction
Reaction conditions: temperature, 373 K; NaOH : *p*-cresol, 4.2; catalyst loading, 2.667 kg/m^3; total reaction volume, 7.5 x 10^{-5} m^3; solvent, n-propanol.

Initially, the rate of *p*-cresol oxidation showed a first order dependence on the partial pressure of O_2 up to 0.30 MPa beyond which it showed a zero order dependence with respect to oxygen. It was also found that the conversion of *p*-cresol and selectivity to PHB increased substantially with increase in partial pressure of oxygen.

The effect of oxygen partial pressure on conversion of *p*-cresol as well as on the selectivity of *p*-hydroxybenzaldehyde is shown as % conversion versus ln P, in Figure

4.13. The conversion of *p*-cresol increased substantially from 35 to 92% with increase in partial pressure of oxygen from 0.020 to 0.827 MPa while selectivity to PHBAlc decreased dramatically from 50 to 10% indicating higher oxygen partial pressure was required for the second step oxidation to form PHB.

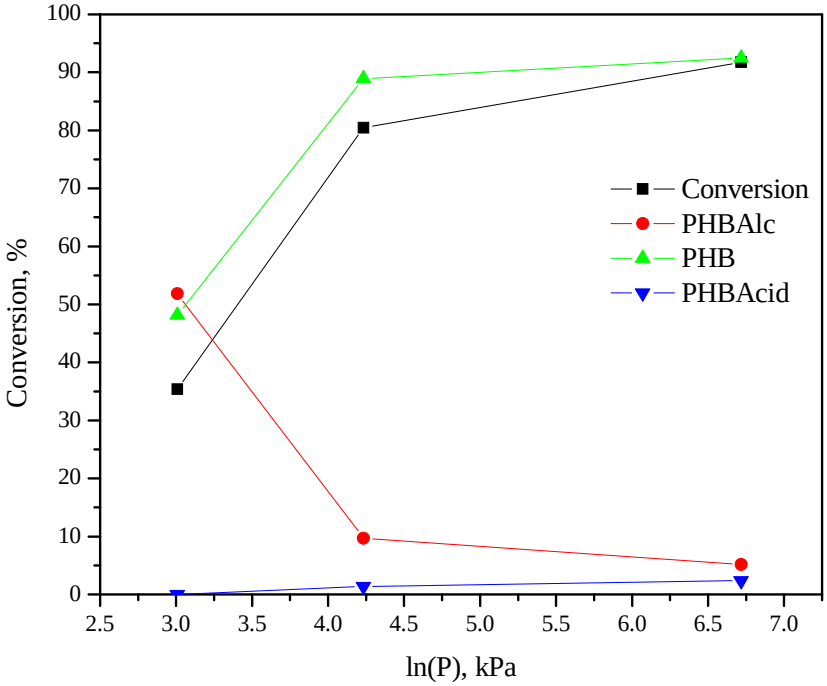

Figure 4.13. Effect of oxygen partial pressure on conversion and product selectivity
Reaction conditions: *p*-cresol concentration 0.37 kmole/m^3; NaOH to *p*-cresol 4; catalyst loading, 2.67 kg/m^3; temperature 373 K; total reaction volume 7.5 x 10^{-5} m^3; reaction time 3 h.

4.3.2.4. Effect of temperature

Figure 4.14 shows the effect of temperature on conversion of *p*-cresol. The conversion of *p*-cresol increased linearly from 15 to 70% with increase in temperature from 333 to

373 K. The highest selectivity of 68% to PHBALc was obtained at 333 K which decreased gradually due to its further oxidation to PHB with increase in temperature (scheme 4.1). The selectivity to PHBAcid was < 1% up to 343 K which also increased to 7% with increase in temperature to 393K.

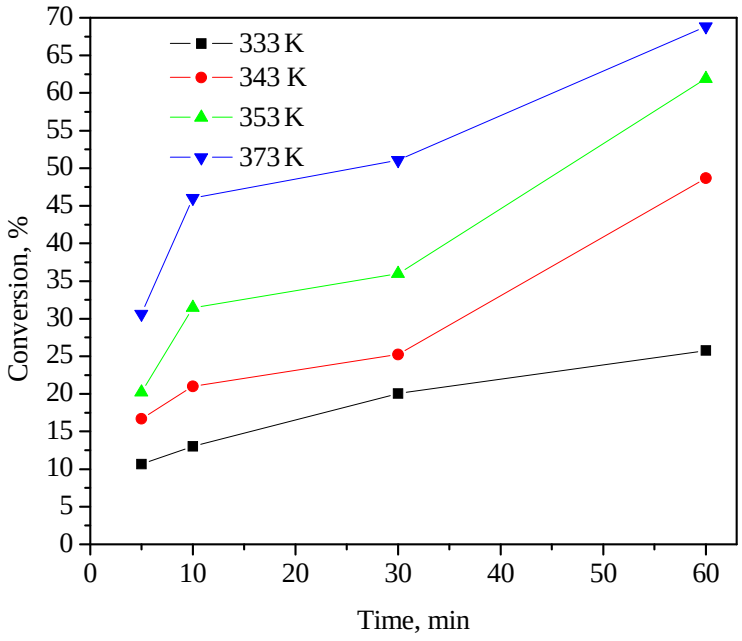

Figure 4.14. Effect of temperature on oxidation of *p*-cresol
Reaction conditions: temperature, 343 K; NaOH : *p*-cresol, 4.2; catalyst loading, 2.667 kg/m^3; total reaction volume, 7.5 x 10^{-5} m^3; p_{O2}, 0.344MPa; solvent, n-propanol reaction time, 1 h.

Effect of temperature on the initial rate of reaction was also studied in a temperature range of 333 to 373 K and the results are presented as lnR vs 1/T in Figure 4.15. Activation energy evaluated from this Arrhenius plot was found to be 42 kJ mol^{-1}

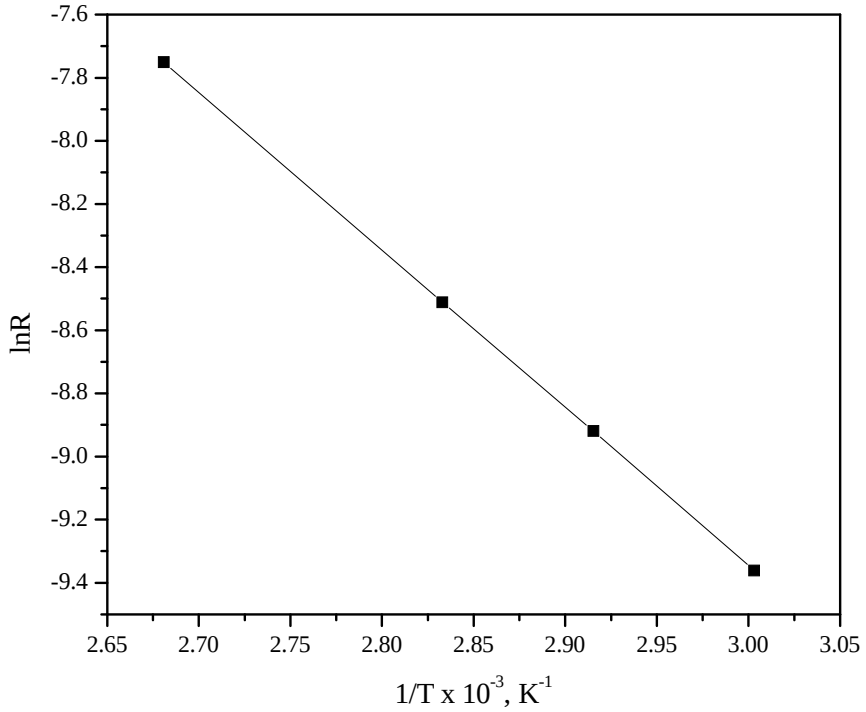

Figure 4.15. Arrhenius plot

The stability of the Co-saponite catalyst under the reaction conditions was confirmed by conducting the leaching test. For this purpose, the oxidation experiment was interrupted after a partial conversion of ~ 27% and the catalyst was removed by filtration and the reaction was further continued without the catalyst. As can be seen from Figure 4.16, the conversion of *p*-cresol remained constant at ~ 27% after continuing the reaction without the catalyst.

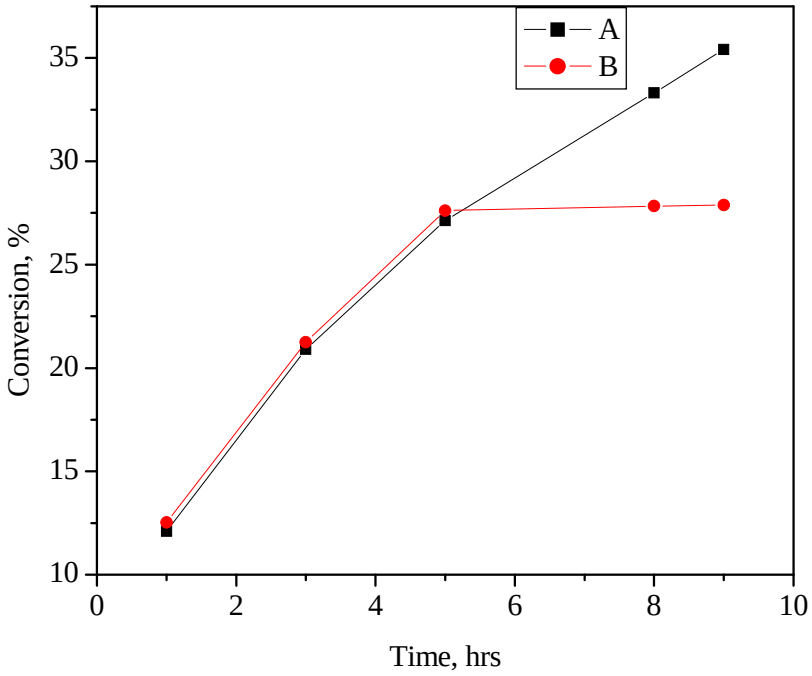

Figure 4.16. Leaching test for catalyst 13% cobalt saponite during oxidation of *p*-cresol
Reaction conditions: temperature, 338 K; NaOH : *p*-cresol, 4.2; catalyst loading, 3.7 kg/m^3; total reaction volume, 5.35 x 10^{-5} m^3; air flow rate, 35 mL/min; solvent, n-propanol; A: with catalyst; B: catalyst removed after partial conversion.

4.3.3. Mars van Krevelen mechanism for liquid phase oxidation

A set of very interesting results were obtained for oxidation of *p*-cresol using Co-saponite catalyst under inert (N_2) atmosphere and these results are shown in Table 4.2.

Table 4.2. Oxidation of *p*-cresol over 13%Co-saponite catalyst in an inert atmosphere

Sr. No.	Catalyst used	Conversion (%)	Selectivity (%)	
			PHBALc	PHB
1	5% Cosaponite	< 0.1	98	1
2	13% Cosaponite	1	89	11
3	30% Cosaponite	1	91	9

Reaction condition: temperature, 373 K; reaction under nitrogen blanket; solvent, n-propanol; *p*-cresol, 0.37 kmol/m^3; NaOH, 4.5gm; reaction time, 1 h.

For 5% Co-saponite sample, conversion of *p*-cresol was < 0.1% while for 13% and 30% Co-saponite sample, the conversion of *p*-cresol was almost the same ~ 1% with a major product formed was PHBAlc. The significance of these results is that under inert atmosphere, the oxidation of *p*-cresol was possible only by utilizing the lattice oxygen of the Co-saponite catalyst. This strongly supports the fact that Mars van Krevelen pathway is operating for the liquid phase oxidation of *p*-cresol over Co-saponite catalyst [22, 23]. As can be seen from Figure 4.18, the intensity of the O 1s peak of the Co-saponite sample used for the oxidation under inert conditions was lower than that of the fresh catalyst.

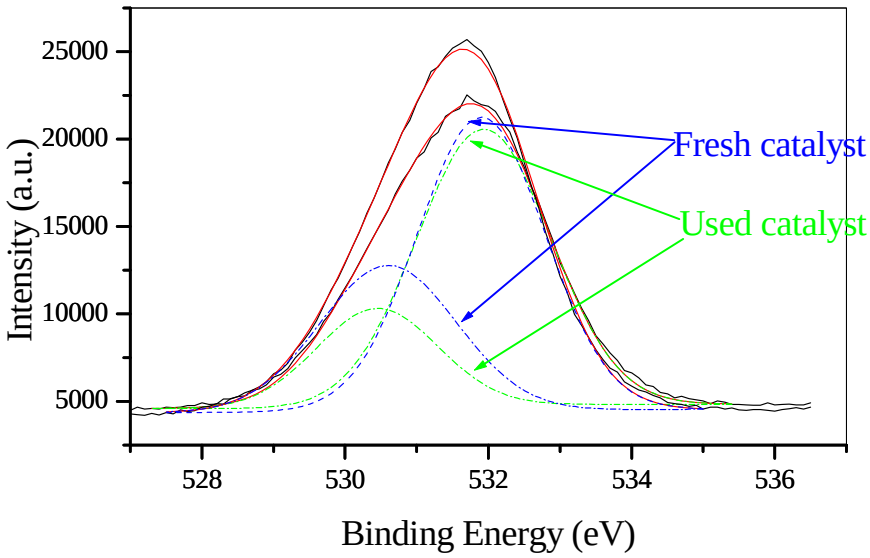

Figure 4.17. XPS of O 1s

From the above results the role of lattice oxygen in the liquid phase oxidation of *p*-cresol can be depicted as shown in Figure 4.17. According to this Figure, lattice oxygen is first used in the oxidation of the substrate followed by filling up the vacancy by molecular oxygen.

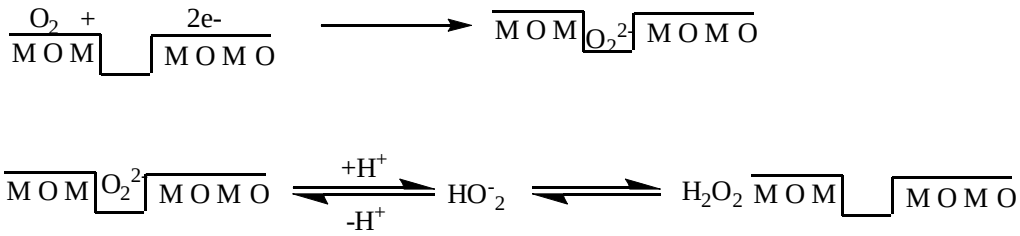

Figure 4.18. Mars–van Krevelen-type mechanisms [23]

Mars van Krevelen pathway for this type of oxidation can be further proven experimentally as well as by deriving the kinetic expressions and evaluation of solid state diffusion parameters for lattice oxygen which is in progress.

4.4. Conclusion

Co-saponite catalysts were prepared with cobalt concentration varying in the range of 5-30%. A detailed characterization showed that divalent cobalt species was octahedrally and tetrahedrally coordinated in Co-saponite. Among various Co-saponite samples, 13% Co-saponite showed the highest conversion of 92% with >90% selectivity to PHB for liquid phase oxidation of *p*-cresol under very mild conditions. Type I isotherm was observed indicating the microporous nature of Co-saponite with a pore size distribution of 17-20 Å. The rate of *p*-cresol oxidation showed a first order dependence on the partial pressure of O_2 up to 0.30 MPa beyond which it showed a zero order dependence with respect to oxygen.

4.5. References

1. F. Figueras, *Catal. Rev. Sci. Eng*. **1988,** *30*, 457.
2. H. Ming-Yuan, L. Zhongui and M. Enze, *Catal. Today,* **1988**, *2*, 321.
3. R. Burch, and C. I. Warburton, *J. Catal*. **1986**, *97*, 511.
4. R. Mokaya, and W. Jones, *J. Catal*. **1995**, *153*, 76.
5. V. S. Kshirsagar, K. R. Patil, M. Shirai, C. V. Rode, *Top. Catal*. **2009**, *52*, 784.

6. H. H. Kung, *Studies in Surface Science and Catalysis 45, Transition Metal Oxides*: *Surface Chemistry and Catalysis,* Elsevier, Amsterdam, **1989.**
7. M. Che, G.C. Bond, *Studies in Surface Science and Catalysis 21, Adsorption and Catalysis on Oxide Surfaces,* Elsevier, Amsterdam, **1985**.
8. V. S. Kshirsagar, A. C. Garade, K. R. Patil, R. K. Jha, C. V. Rode, *Ind. Eng. Chem. Res.* **2009**.(doi *10.1021/ie801941e*).
9. S. Kawai, Y. Z. Yao, *Micro. Meso. Mat*. **1999**, *33*, 49.
10. K. S. W. Sing, D. H. Everett, R. A. W. Haul, L. Moscou, R. A. Pioretti, J. Rouquerol, T. Siemieniewska, *Pure & Appl. Chem*. **1985**, *57*, 603.
11. T. J. Barton, L. M. Bull, W. G. Klemperer, D. A. Loy, B. McEnaney, M. Misono, P. A. Monson, G. Pez, G. W. Scherer, J. C. Vartuli, O. M. Yaghi, *Chem. Mater*. **1999**, 2633.
12. B. M. Weckhuysen, A. A. Verberckmoes, M. G. Uytterhoeven, F. E. Mabbs, D. Collison, E. De Boer, R. A. Schoonheydt, *J. Phys. Chem. B.* **2000,** *104*, 37.
13. J. Jamas, T. Machej, J. Gurgul, R. P. Socha, M. Che, S. Dzwigaj, *Appl. Catal. B: Envi.* **2007,** *75*, 239.
14. J.F. Moulder, W.F. Syicle, P.E. Sobol and K.D. Bomben, in: J. Chastain (Ed.) *Handbook of X-Ray Photoelectron Spectroscopy:* A Reference Book of Standard Spectra for Identification and Interpretation of XPS Data, Perkin-Elmer, Eden Prairie, MN, **1992**, p. 82.

15. R.S. Da Cruz, A.J.S. Mascarenhas and H.M.C. Andrade, *Appl. Catal. B: Env.* **1998**, *18*, 223.

16. J.M. Stencel, V.U.S. Rao, J.R. Diehl, K.H. Rhee, A.G. Dhere and R.J. De Angelis, *J. Catal*. **1983**, *84*, 109.

17. G. Fierro, M.A. Eberhardt, M. Houalla, D.M. Hercules and W.K. Hall, *J. Phys.Chem.* **1996**, *100*, 8468.

18. X.-Y. Chen, S.-C. Shen, H.H. Chen and S. Kawi, *J. Catal*. **2004**, *221*, 137.

19. C. V. Rode, M. V. Sonar, J. M. Nadgeri, R. V. Chaudhari, *Org. Proc. Res. Dev*. **2004**, *8*, 873.

20. C. V. Rode, V. S. Kshirsagar, J. M. Nadgeri, K. R. Patil, *Ind. Eng. Chem. Res*. **2007**, *46*, 8413.

21. V. S. Kshirsagar, J. M. Nadgeri, P. R. Tayade, C. V. Rode, *Appl. Catal. A: Gen*. **2008**, *339*, 28.

22. C. Doornkamp, V. Ponec, *J. Mol. Catal. A: Chem*. **2000**, *162*, 19.

23. V. D. Makwana, Y. C. Son, A. R. Howell, S. L. Suib, *J. Catal*. **2002**, *210*, 46.

5.1. Introduction

Use of metal nanoparticles as catalysts for a variety of reactions is a rapidly growing field of research [1-3]. Nanoparticles are near mono dispersed particles generally < 100 nm in size having some unique characteristics such as i) very high surface area ii) short range ordering iii) enhanced interactions with environment iv) great variety of valence band electron structure and v) self-structuring for optimum performance in chemisorption and catalysis [4]. Nano-structured metal particles have been exploited as novel catalysts for various reactions such as hydrogenation, hydroformylation, hydration etc. Particularly, three-dimensional organization of catalytic components is highly important for solid-state catalysts, which is often necessary for various multi product catalytic reactions like oxidation in which selectivity to the desired product can be tailored suitably.

The spinels (AB_2X_4) are one of the most interesting materials having significant applications in diverse areas including catalysis [5]. The nano-structured spinels can become still more interesting as novel catalytic materials. Designing and synthesizing a highly selective catalyst has been a challenging goal in catalysis research and efforts have been already made to achieve control of properties by which selectivity can be altered. Further step in this direction involves correct ensemble of metal atoms, metal ions or other active components e.g. oxides etc. and a cavity around the active site that can change configuration to bind a specific functional group to the active site and thereby tailoring the selectivity to the desired product. Solid-state materials with nano structures are expected to be potential catalysts for chemical reactions due to their unique reaction field around catalytic active sites.

A variety of compounds exist as spinels e.g. oxides, sulphides, tellurides, selenides etc. which are represented by AB_2X_4, having A as a divalent cation, B a trivalent cation, and X a divalent anion [6, 7]. A and B can occupy two different sites in the spinel structure, octahedral and tetrahedral and studies of such compounds are very important in solid-state chemistry for better understanding of structure and properties. Among spinels, Co_3O_4 is a versatile oxide used in advanced applications such as solar selective absorbers, field emitters, gas sensors as well as in catalytic applications e.g. low temperature CO oxidation, Fischer-Tropsch synthesis and hydrocarbon oxidations [8-10]. Turkevich and Kim first reported the preparation of dispersed gold nano particles as early as in 1970 [11]. Thereafter, most of researchers focused their work on colloidal nano particles of various transition metals. Hirai et al. reported the preparation of colloidal transition metals in polymers by chemical reduction with alcohols or ethers [12]. However, the synthesis of the nanostructures without the use of templates or surfactants is more preferred. Spinel oxides in nano forms with different morphologies become very interesting materials from catalysis point of view since, their structure due to non stoichiometric composition become very much different from that of the bulk samples. This leads to the stabilization of high-spin configuration of the divalent cation which can result in higher catalytic activity for oxidation reactions. Synthesis of oxides in nano forms have been accomplished using various chemical methods such as micro emulsion, spray pyrolysis, hydrothermal, reduction/oxidation, precipitation of precursor particles followed by their calcination in air etc [13, 14]. It is clear from the literature that though, nano particle materials have been synthesized and characterized by various methods however, a systematic

investigation with the aim of their application as tailor made catalysts for activity and selectivity enhancement is lacking. Such materials have a very high number of low coordination number atoms at edge and corner sites which can provide a large number of catalytically active sites unlike bulk materials.

Control of size and morphology of nanostructures is a great challenge in catalysis because nature and number of active sites of the material are size and shape dependent. The selectivity of nano structured catalyst can also be altered by the surrounding environment of an active site [15]. It is also important that the selected preparation method yields catalyst which is reproducible with respect to physico-chemical characteristics and these nano materials or surface structures remain stable after exposure to the reaction conditions. Also, synthesis of nanostructures without the use of templates or surfactants is highly desirable in order to minimize the cost, pollution hazards, tedious process operation and carryover of impurities in the final product. With these perspectives in mind, we have synthesized spinel type nano-structured cobalt oxides with very high surface area, their characterization and performance evaluation in model liquid phase air oxidation of *p*-cresol reaction. It is worth noting that there have been only a few studies reported in the literature on the study of the nanoparticles during and after catalysis and recycling.

In this chapter, we describe the synthesis of Co_3O_4 porous nanorods by controlling aggregation behavior of cobalt-hydroxy carbonate precursor particles by novel simultaneous precipitation /digestion route by optimizing digestion time. The nanostructured Co_3O_4 was prepared from $Co(NO_3)_2$ and K_2CO_3 by a simple protocol without using any template, involving a simultaneous co-precipitation/digestion

technique followed by calcination at 573 K in air [16]. These nanoparticles were characterized by XRD, HRTEM and XPS and were found to exhibit higher catalyst activity for the liquid phase oxidation of *p*-cresol than that shown by its bulk counterpart [17].

5.2. Experimental

Catalyst preparation by simultaneous co-precipitation/digestion method, catalyst characterizations such as powder XRD, TEM, BET surface area and catalyst activity measurement have been discussed in details under section 2.2.3 in chapter 2.

5.3. Results and discussion

5.3.1. X-ray diffraction

Figure 5.1 shows the XRD patterns of the Co_3O_4 catalyst prepared in this work and XRD peaks were indexed on the basis of spinel structure with the space group of *Fd*3*m*. The lattice parameter obtained, a = 8.072 Å, is in good agreement with the reported value for Co_3O_4 powder (a = 8.072 Å; JCPDS No. 76-1802). The relatively broader peaks of A0, A2, A4, A8, and A16 samples indicate nanocrystalline nature of the prepared catalyst samples.

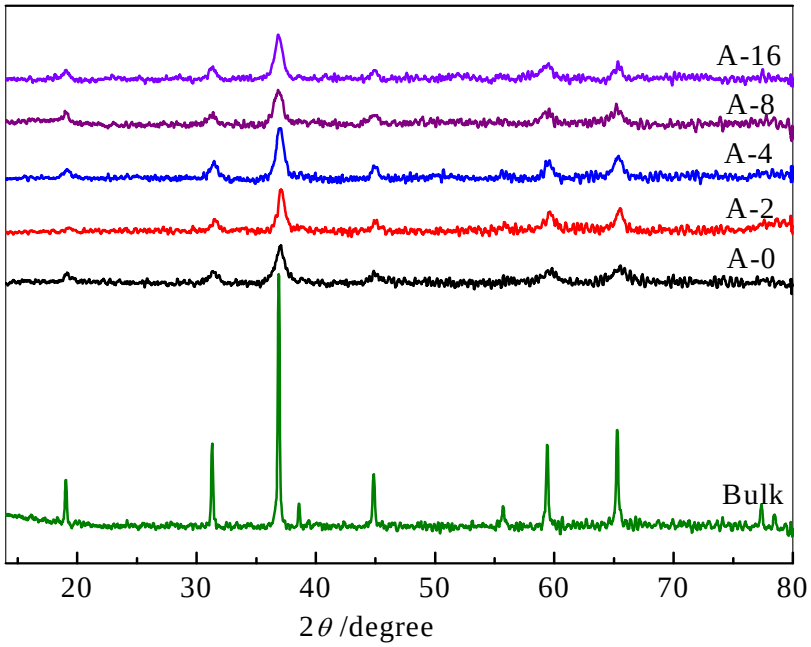

Figure 5.1. XRD patterns of Co_3O_4 nanoparticles prepared with different digestion times of 0 h (A0), 2 h (A2), 4 h (A4), 8 h (A8) and 16 h (A16).

5.3.2. High resolution transmission electron microscopy

The HRTEM image of Co_3O_4 particles (Figure 5.2a) indicates rod type aggregates (diameter, 4–5 nm; length, 20–30 nm) that are formed from 2–3 nm primary particles. The parallel lattice fringes across almost all the primary particles are clearly visible (Figure 5.2b) which confirm the perfectly oriented aggregation of nanoparticles of Co_3O_4. It is clearly seen that the aggregated Co_3O_4 rod like particles are composed of many small Co_3O_4 nanoparticles. These interconnected nanoparticles of Co_3O_4 form pores having an average diameter of 15 nm.

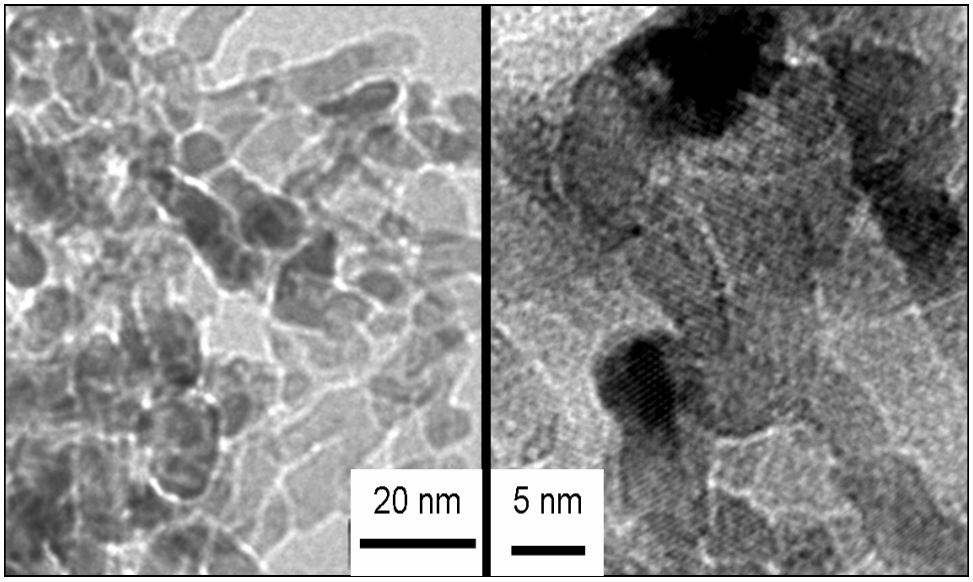

Figure 5.2. HRTEM images of (a) nanorod aggregates of Co_3O_4; (b) primary nanoparticles of Co_3O_4.

5.3.3. X-ray photoelectron spectroscopy

Figure 5.3 shows the Co 2p XPS spectrum exhibiting Co $2p_{3/2}$ and Co $2p_{1/2}$ doublet core level peaks at binding energies (BE) of 780.2 and 795.3 eV with a difference of 15.1 eV between the $2p_{3/2}$ and $2p_{1/2}$ binding energies. These binding energies are comparable to that reported for Co_3O_4 indicating the presence of both Co^{2+} and Co^{3+} species in the catalyst [18]. This redox couple of cobalt is responsible for catalyzing the oxidation reaction.

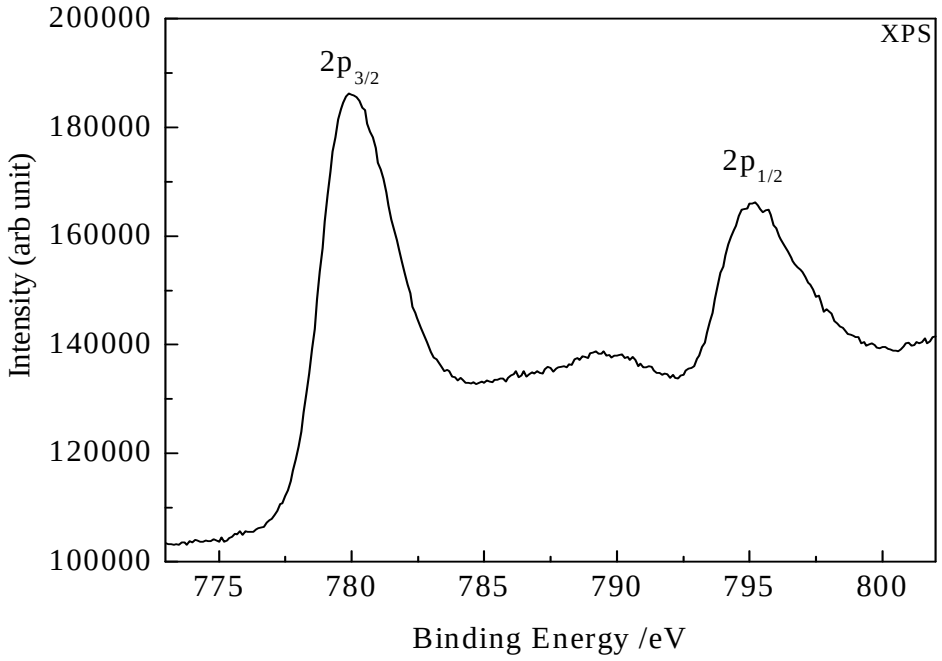

Figure 5.3. Co 2p XPS spectrum of Co_3O_4.

5.3.4. Product distribution and selectivity

In order to study the product distribution, oxidation of *p*-cresol was studied using nanostructured Co_3O_4 catalyst in n-propanol at 0.137 MPa pressure of oxygen. The progress of the reaction was monitored by liquid-phase analysis as a function of time. Figure 5.4 shows the conversion and product selectivities vs time profile for *p*-cresol oxidation using Co_3O_4 catalyst at 368 K. Similar to the previous studies *p*-cresol was oxidized to give first step oxidation product as *p*-hydroxybenzyl alcohol (PHBALc) that undergoes further oxidation to give *p*-hydroxybenzaldehyde (PHB). After 1.5 h,

the conversion of *p*-cresol obtained was 69 % with 88 % selectivity to *p*-hydroxy benzaldehyde.

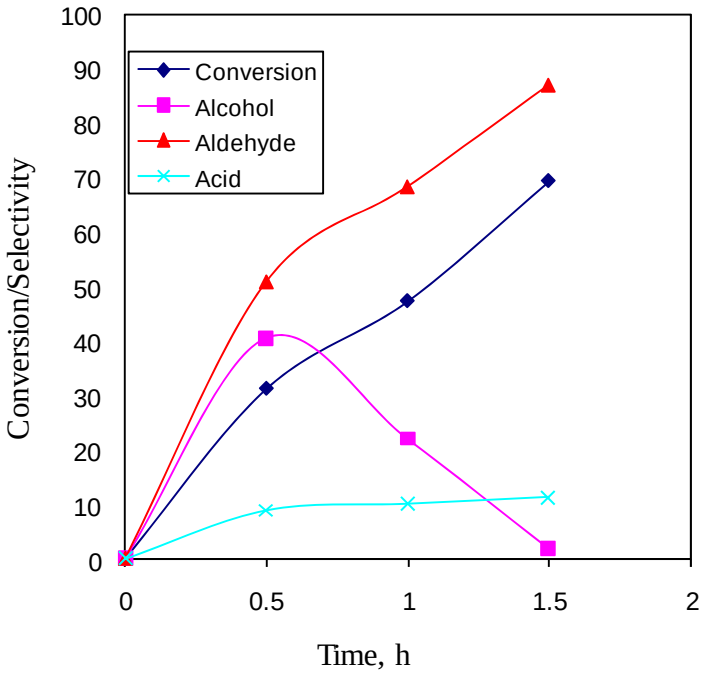

Figure 5.4. Conversion, selectivity versus time profile for *p*-cresol oxidation
Reaction conditions: temperature, 368 K; partial pressure of O_2, 0.137 MPa; *p*-cresol, 0.38 kmol/m^3; catalyst loading, 0.27 kg/m^3; solvent, n-propanol; NaOH : *p*-cresol, 4; total reaction volume, 7.3 x 10^{-3} m^3.

5.3.5. Effect of digestion time

Table 5.1 shows the comparison of the activity (expressed as TOF, h^{-1}) and selectivity of nanostructured Co_3O_4 catalyst prepared at different digestion times with those of bulk Co_3O_4 catalyst, for liquid phase air oxidation of *p*-cresol. The nanostructured Co_3O_4 catalyst (Entry 2, Table 5.1) showed more than twice activity than that of the

bulk catalyst (Entry 1). This can be attributed to the lower particle size (6–8 nm) and very high specific BET surface area (95 m^2/g as against 9 m^2/g of the bulk Co_3O_4) of the nanostructured Co_3O_4 catalyst.

Table 5.1. Comparison of catalyst activities and selectivities for *p*-cresol oxidation

Sr. No	Co_3O_4 catalyst	Digestion time, h.	TOF, h^{-1}	% Selectivity		
				PHBAlc	PHB	PHBacid
1	Bulk	----	8	67	33	--
2	A0	0	18	59	41	--
3	A2	2	21	50	49	01
4	A4	4	20	42	58	--
5	A8	8	31	33	66	01
6	A16	16	9	56	44	--
7	A8	8	174	16	83	01

Reaction conditions: *p*-cresol, 0.51 $kmol/m^3$; catalyst loading, 0.37 kg/m^3; solvent, n-propanol; total reaction volume, 5.35 x 10^{-5} m^3; NaOH : *p*-cresol, 4; reaction time, 5 h; reaction temperature, 368 K; air flow rate, 35 mL/min; partial pressure of O_2, 0.0202 MPa (except entry 7).

Effect of digestion time was also studied on the activity and selectivity pattern of Co_3O_4 nanocatalysts as shown in Figure 5.5 and Table 5.1(Entries 2–6). The highest activity (TOF, 31 h^{-1}) was obtained for the digestion time of 8 h (Entry 5) while

further increase in digestion time lowered the activity substantially (TOF, 9 h^{-1}). It is interesting to note that the highest selectivity to PHBAlc was obtained for Co_3O_4 bulk catalyst with the lowest TOF while the selectivity trend exactly reversed as the TOF was increased for Co_3O_4 nanocatalysts.

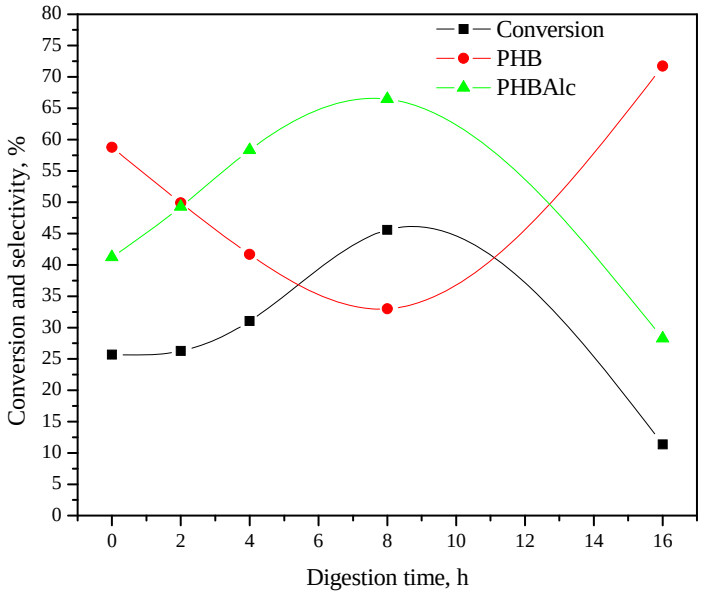

Figure 5.5. Effect of digestion time on conversion of *p*-cresol and product selectivity Reaction conditions: *p*-cresol, 0.51 kmol/m^3; catalyst loading, 0.37 kg/m^3; solvent, n-propanol; total reaction volume, 5.35 x 10^{-5} m^3; NaOH : *p*-cresol, 4; reaction time, 5 h; reaction temperature, 368 K; air flow rate, 35 mL/min.

The highest selectivity (83%) to PHB was achieved for Co_3O_4 nanocatalyst which showed the highest TOF of 174 h^{-1} (Entry 7, Table 1) under slightly higher partial pressure of oxygen of 0.068 MPa. It should also be noted that for all catalysts, only the major oxidation products formed were PHBAlc and PHB without the formation of any other non-oxidation side products [19, 20]. It is well known that the two

oxidation states of Co^{2+} and Co^{+3} co-exist in the spinel type Co_3O_4 and a dynamic equilibrium is set up involving Co^{2+}, Co^{3+} and the lattice oxygen (O_2^-) species under liquid phase oxidation conditions [21]. Oxidation proceeds through activation of C–H bond, its dissociation and formation of C–O bond on an active site of the catalyst [22]. If one C–H bond is activated and dissociates, PHBAlc is formed; while activation and dissociation of another C–H bond gives PHB. In case of nanostrutured Co_3O_4 catalyst, the dynamic equilibrium of Co^{2+}, Co^{3+} and O_2^- gets modified even at mild conditions in such a way that the tuning of selectivity to alcohol and aldehyde could be achieved as shown in Table 5.1.

5.3.6. Catalyst recycle study

To study the stability and reusability of the catalyst, two recycle experiments were performed and the results are shown in Figure 5.6. The catalyst recycle experiment showed the same activity as that for the fresh catalyst. A leaching test was also carried out by hot filtration to remove the catalyst after an intermittent *p*-cresol conversion of 17%. No further conversion of *p*-cresol was observed for the hot filtrate without catalyst, confirming no leaching of Co occurred under the reaction conditions.

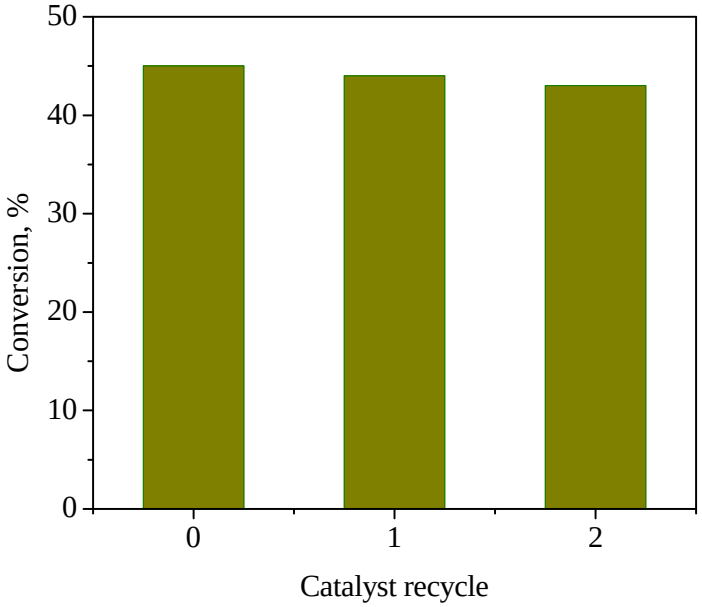

Figure 5.6. Recycle study

Reaction conditions: *p*-cresol, 0.51 kmol/m^3; catalyst loading, 0.37 kg/m^3; solvent, n-propanol; total reaction volume, 5.35 x 10^{-5} m^3; NaOH : *p*-cresol, 4; reaction time, 5 h; reaction temperature, 368 K; air flow rate, 35 mL/min; partial pressure of O_2, 0.0202 MPa.

5.4. Conclusion

In summary, Co_3O_4 nanoparticles which aggregated to form stable nanorods were prepared by a simple co-precipitation-digestion method without using a template or a capping agent. These nanoparticles were found to be highly active for air oxidation of *p*-cresol under mild conditions while the selectivity to the oxidation products could be altered by changing the digestion time during the preparation of the catalyst. The catalyst recycle experiment showed the same activity as that for the fresh catalyst. Reproducibility of the catalyst preparation with respect to its physico-chemical

characterization as well as the activity measurement for oxidation was found to be excellent. This approach allows the preparation of nanosize metal oxides with controlled morphology having potential applications in catalysis and other electronic devices.

5.5. References

1. G. Schmid, M. Baumle, M. Geerkens, I. Heim, C. Osemann, T. Sawitowski, *Chem. Soc. Rev*. **1999**, *28*, 179.
2. C. N. R. Rao, G. U. Kulkarni, P. J. Thomas, P. P. Edwards, *Chem. Soc. Rev*. **2000**, *29*, 27.
3. T. Trindade, P. O'Prien, N. L. Pickett, *Chem. Mater*. **2001**, *13*, 3843.
4. J. D. Aiken III, Y. Lin, R. G. Finke, *J. Mol. Catal. A: Chem*. **1996,** *114*, 29.
5. P. A. Cox, *Transition Metal Oxides*, Oxford University, Oxford, **1992**.
6. R. J. Hill, J. R. Craig, G. V. Gibbs, *Phys. Chem. Mineral*. **1979**, *4*, 317.
7. S. H. Sun, H. Zeng, D. B. Robinson, S. Raoux, P. M. Rice, S. X. Wang, G. X. Li, *J. Am. Chem,. Soc.* **2004,** *126*, 273
8. Y. Z. Wang, Y. X. Zhao, C. G. Gao, D. S. Liu, *Catal. Lett*. **2007**, *116*, 136.
9. E. V. Steen,H. Schlz, *Appl. Catal. A Gen.* **1999**, *186*, 309.
10. Y. Yu, F. Yung, *J. Catal*. **1974**, *33*, 108.
11. J. Turkrevich, G. Kim, *Science* **1970**, *169*, 873.
12. H. Hirai, Y. Nako, N. Toshima, *J. Macromol. Sci.-Chem A*, **1978**, *12* 1117.
13. R. M. Wang, C. M. Liu, H. Z. Zhang, C. P. *Chen, Appl. Phys. Lett.* **2004**, *85* 2080.

14. B. Li, Y. Xie, C. Wu, Z. Li, J. Zhang, *Mater. Chem. Phys*. **2006**, *99*, 479

15. J. M. Thomas, R. Raja, G. Sankar, R. G. Bell, *Nature*, **2000**, *398*, 227.

16. H. S. Potdar, K. W. Jun, J. W. Bae, S. M. Kim and Y. Lee, *Appl Catal A: Gen*. **2007**, *321*, 109.

17. V. S. Kshirsagar, S. Vijayanand, H. S. Potdar, P. A. Joy, K. R. Patil, C. V. Rode, *Chem. Lett*. **2008**, *37*, 310

18. B. J. Tan, K. J. Klabunde, P. M. A. Sherwood, *J. Am. Chem. Soc*. **1991**, *113*, 855.

19. C. V. Rode, V. S. Kshirsagar, J. M. Nadgeri, K. R. Patil, *Ind. Eng. Chem. Res*. **2007**, *46*, 8413.

20. C. V. Rode, M. V. Sonar, J. M. Nadgeri, R. V. Chaudhari *Org.Proc. Res. Dev*. **2004**, *8*, 873.

21. A. Bielanski, J. Haber, *Catal. Rev.-Sci. Eng*., **1979**, *19*, 1.

22. F. Wang, J. Xu, S. Liao, *Chem. Commun*. **2002**, *6*, 626.

6.1. Introduction

Previous chapters and our studies dealt with the synthesis of different types of catalysts, their, characterization and activity evaluation for *p*-cresol oxidation [1-5]. Thus, in the literature published so far, studies have been mainly aimed at the product distribution and selectivity issues for the liquid phase oxidation of *p*-cresol. Therefore, a major objective of this work was to develop an intrinsic kinetic rate equation for this industrially important reaction, using the experimental initial rate data obtained from a batch slurry reactor and commercially available Co_3O_4 catalyst. Effects of oxygen partial pressure, concentration of *p*-cresol and catalyst loading on the rate of oxidation were studied at various temperatures. Developing a batch slurry reactor model provided a validation of the proposed rate equation and the predicted concentration-time profiles were compared with those observed experimentally over a wide range of reaction conditions. This study also demonstrates the approach of kinetic modelling that can be followed for similar multiphase catalytic reactions.

6.2. Experimental

Details of materials, catalyst characterization and experimental set up along with the procedure and analytical methods have been described in chapter 2.

6.3. Results and discussion

6.3.1. Catalyst characterization

***6.3.1.1. Surface area*:** The surface area of the Co_3O_4 catalyst as determined by the BET method was found to be 14 m^2/g.

6.3.1.2. X-ray photoelectron spectroscopy

The oxidation state of cobalt was investigated by XPS. Figure 6.1 shows Co 2p XPS spectrum. It exhibits Co $2p_{3/2}$ and Co $2p_{1/2}$ doublet core level peaks at binding energies (BE) of 780.2 and 795.3 eV with a difference of 15.1 eV between the $2p_{3/2}$ and $2p_{1/2}$ binding energies indicating the presence of both Co^{2+} and Co^{3+} species in the catalyst [6]. It is reported that a dynamic equilibrium is setup involving Co^{2+}, Co^{3+}, and the lattice oxygen (O_2^-) species under liquid phase oxidation conditions for *p*-cresol oxidation (Scheme 6.1) [7]. In subsequent steps, nucleophilic lattice oxygen species (O_2^-) attack the activated hydrocarbon substrate to form the oxygenated product, which is desorbed from the catalyst surface. Dissolved molecular oxygen is then filled into oxygen vacancies of the catalyst surface [8].

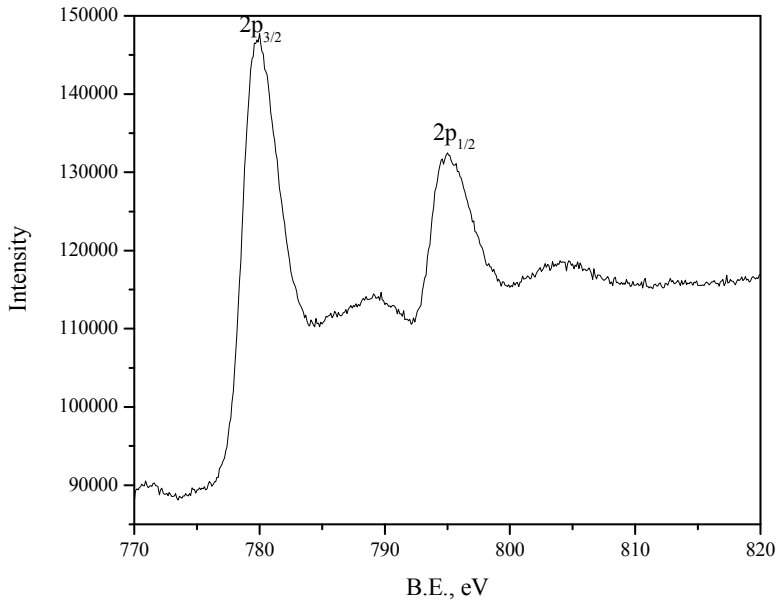

Figure 6.1. Co 2p XPS spectra of Co_3O_4

6.3.1.3. X-ray diffraction

The powder X-ray diffraction pattern of Co_3O_4 is shown in Figure 6.2, that shows the peaks corresponding to the Co_3O_4 spinel phase. The peaks at 2θ 19.38^o, 31.68^o, and 37.28 ^{o} correspond to (1 1 1), (2 2 0) and (3 1 1) reflections of Co_3O_4 [9]. There were no peaks observed corresponding to CoO or Co phases in the sample. The most intense reflection (3 1 1) appearing at 2θ = 37.28^o was used to determine the crystallite size of about 174 nm, using the Scherrer equation. The intense and sharp nature of peaks and the shift of the diffraction angle towards slightly higher values indicate bigger particle size [10].

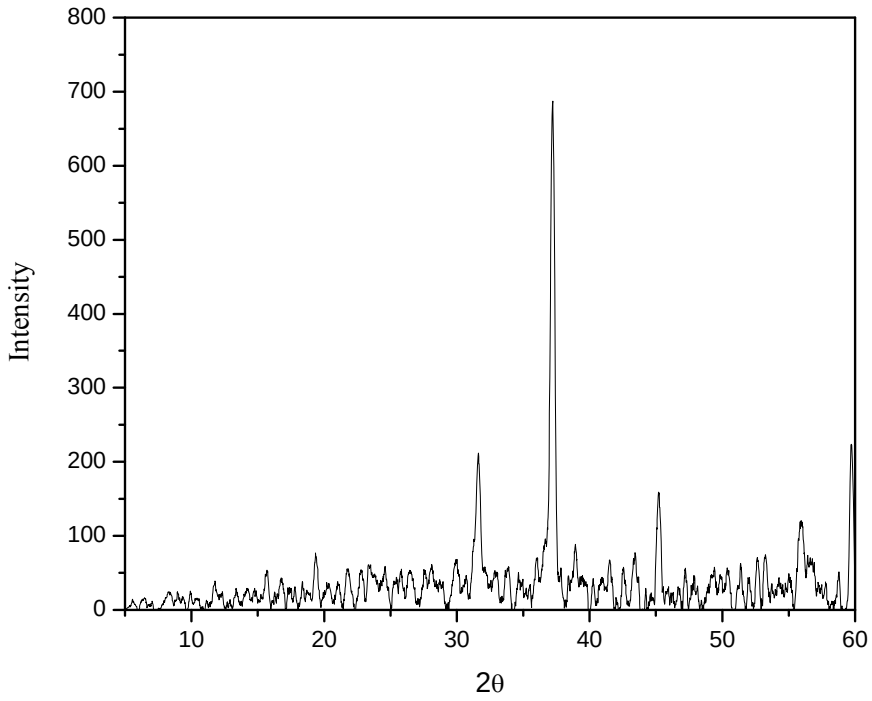

Figure 6.2. XRD pattern for Co_3O_4

6.3.2. Reaction kinetics

The main objectives of this work were: i) to study the effect of various reaction parameters on the conversion and rate of *p*-cresol oxidation reaction; ii) to study the intrinsic kinetics of liquid phase oxidation of *p*-cresol over cobalt oxide (Co_3O_4) catalyst in a batch slurry reactor; and iii) to develop a reactor model for predicting the concentration time profiles and to validate the predicted values with the experimental results under various inlet conditions. For this purpose, the experimental data were obtained at different reaction conditions (see Table 6.1) to observe both initial rates of oxidation and integral concentration-time profiles.

Table 6.1. Range of operating conditions

1	Partial pressure of O_2	0.1-1.5 MPa
2	Temperature	333-393 K
3	*p*-cresol concentration	0.49-1.53 kmol/m^3
4	Mole ratio of NaOH to *p*-cresol	1-5
5	Catalyst loading	0.38-3.03 kg/m^3
6	Substrate to solvent ratio	0.13-0.24
7	Total reaction volume	7.2 x 10^{-5} m^3
8	Agitation speed	900 rpm

Initial experiments on catalytic oxidation of *p*-cresol were carried out to establish that the material balance of reactants consumed (O_2 and *p*-cresol) and products (PHB-alcohol, PHB-aldehyde, PHBME, PHB-acid) formed agreed to the extent of 95% as per the reaction scheme 6.1.

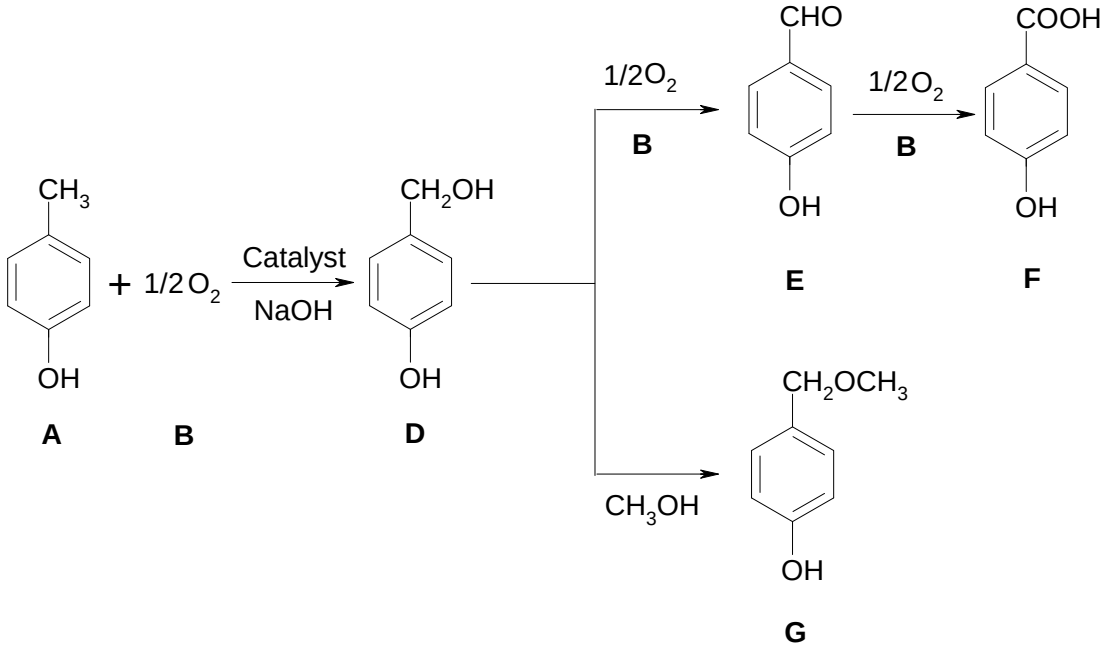

Scheme 6.1. Reaction products of *p*-cresol oxidation

The presence of homogeneous reaction was not observed while running a few experiments without catalyst [11]. The reproducibility of the rate measurement was found to be within 5-8% error as indicated by the few repeated experiments. In order to ensure that the activity of heterogeneous cobalt oxide (Co_3O_4) catalyst was constant during the run, we carried out catalyst recycle experiments, in which the catalyst was found to retain its activity even after the third recycle without affecting the conversion of *p*-cresol. The catalyst recycle studies also showed the absence of leaching of cobalt in the solution under reaction conditions.

6.3.2.1. Analysis of mass transfer effects

In a three-phase slurry reactor, gas-liquid, liquid-solid and intraparticle diffusional resistances are likely to be present; hence, the contribution of various mass transfer steps in the present system were quantitatively assessed by the well-known criteria [12]. In this approach the significances of gas-liquid, liquid-solid and intraparticle mass transfer effects, represented by factors $\alpha_{1,}$ α_2 and Φ_{exp} respectively, were calculated [13]. These factors are defined as the ratios of the observed rate of reaction to the maximum rates of gas-liquid, liquid-solid and intraparticle mass transfer rate respectively. The calculations of these factors are described below.

(a) Absence of gas-liquid mass transfer if

$$\alpha_1 = \frac{R_{Ai}}{k_L a\, A^*} \langle 0.1 \qquad (6.1)$$

(b) Absence of liquid –solid mass transfer if

$$\alpha_2 = \frac{R_{Ai}\, \rho_P\, d_P}{6 k_s w\, A^*} \langle 0.1 \qquad (6.2)$$

(c) Absence of pore diffusion if

$$\phi_{exp} = \frac{d_P}{6}\left[\frac{R_{Ai}\, \rho_P}{w D_e\, A^*}\right]^{0.5} \langle 0.2 \qquad (6.3)$$

This analysis showed that the values of α_1, α_2 and Φ_{exp} at different temperature were well below 0.1, 0.1 and 0.2 (Table 6.2) respectively, confirming that the rate data obtained were in the kinetic regime.

Table 6.2. Values of α_1, α_2 and ϕ_{exp} at various temperatures

Temperature (K)	α_1	α_2	ϕ_{exp}
343	0.00051	0.032	0.0370
363	0.00076	0.048	0.0456
373	0.00125	0.079	0.0581

For the calculation of α_1, α_2 and Φ_{exp} , knowledge of the mass transfer parameters and of the solubility of O_2 in methanol and *p*-cresol is required. The gas-liquid mass transfer coefficients ($k_L a$) were calculated from the correlation proposed by Chaudhari et al. for a stirred high pressure reactor similar to that used in the present work [14]. Liquid-solid mass transfer coefficients (ks) and effective diffusivity (De) were calculated using the correlations of Sano et al. and Wilke and Chang, respectively [15, 16]. For evluavating the values of A* the solubility of O_2 in the reaction medium (mixture of *p*-cresol and methanol) was determined experimentally using the reported procedure in the temperature range of 298-263 K and the pressure range of 2.75-6.20 MPa respectively [17]. These results are shown in Table 6.3.

Table 6.3. Experimental solubility of oxygen

Temperature (K)	Pressure (MPa)	Solubility in methanol x 10^{-1} kmol/m^3atm
333	5.86	3.968
348	5.86	3.975
363	5.86	4.182

6.3.2.2. Initial rate Data

The analysis of initial rates are useful in understanding the dependency of the reaction rate on individual reaction parameters and also in assessing the importance of mass transfer effects [18]. Effects of various reaction parameters such as catalyst loading, oxygen partial pressure, *p*-cresol concentration and temperature on the initial rate of reaction are discussed below.

6.3.2.2.1. Effect of catalyst loading

The effect of catalyst loading on the initial rate of *p*-cresol oxidation was studied in the range of 0.38-3.03 kg/m^3 in a temperature range of 343 - 373 K and at 0.83 MPa of oxygen partial pressure and their results are presented in Figure 6.3.

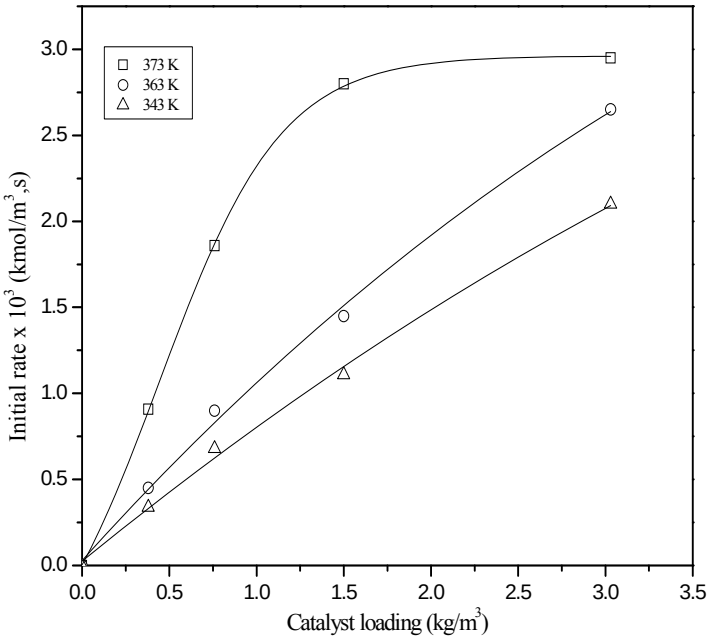

Figure 6.3. Effect of catalyst loading on rate of oxidation of *p*-cresol.
Reaction conditions: *p*-creosl, 1.5 kmol/m^3, NaOH : *p*-cresol, 4; p_{O2}, 0.83 MPa; total reaction volume, 7.2 x 10^{-5} m^3.

The initial oxidation rate showed linear dependence on the catalyst loading at 343 and 363 K, suggesting that gas-liquid mass transfer resistance may not be important under these conditions. In the case of a higher temperature of 373 K, the initial rate was found to increase by about 3 times when the catalyst loading was increased from 0.38 to 1.5 kg/m^3, beyond which the rate of reaction was independent of catalyst loading, indicating that external gas-liquid mass transfer resistance may be significant under these experimental conditions.

6.3.2.2.2. Effect of partial pressure of oxygen

p-Cresol oxidation experiments were carried out by varying the air pressure that allowed the partial pressure of oxygen variation in the range of 0.1-1.5 MPa at 343, 363, and 373 K.

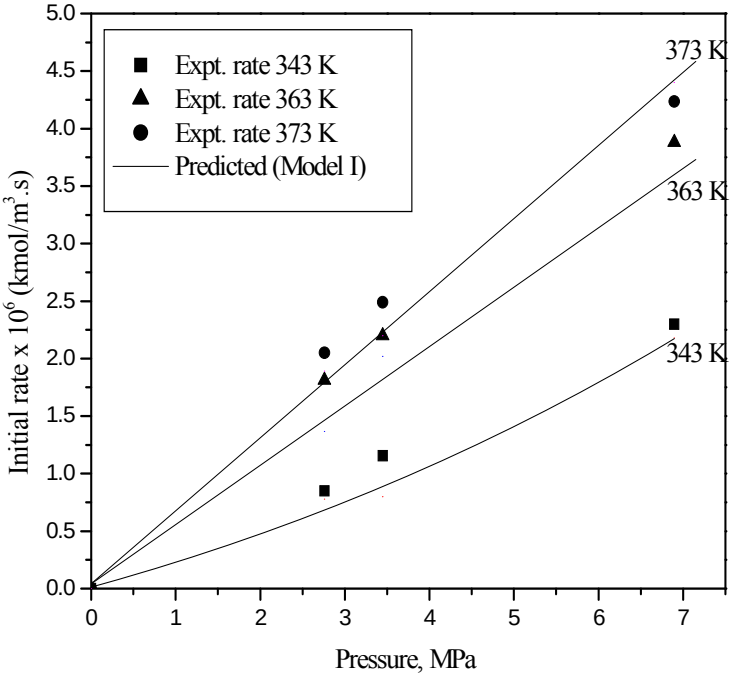

Figure 6.4. Effect of partial pressure of oxygen on initial rate of *p*-cresol oxidation. Reaction conditions: *p*-cresol, 1.5 kmol/m^3; NaOH: *p*-cresol, 4; catalyst loading, 1.5 kg/m^3; total reaction volume, 7.2 x 10^{-5} m^3.

The initial rate increased linearly with increase in partial pressure of oxygen, as shown in Figure 6.4, indicating a first-order dependence with respect to the oxygen partial pressure.

6.3.2.2.3. Effect of substrate concentration

The effect of initial concentration of substrate in the range from 0.4-1.73 kmol/m^3 at 343, 363 and 373 K on the initial rate of oxidation is shown in Figure 6.5.

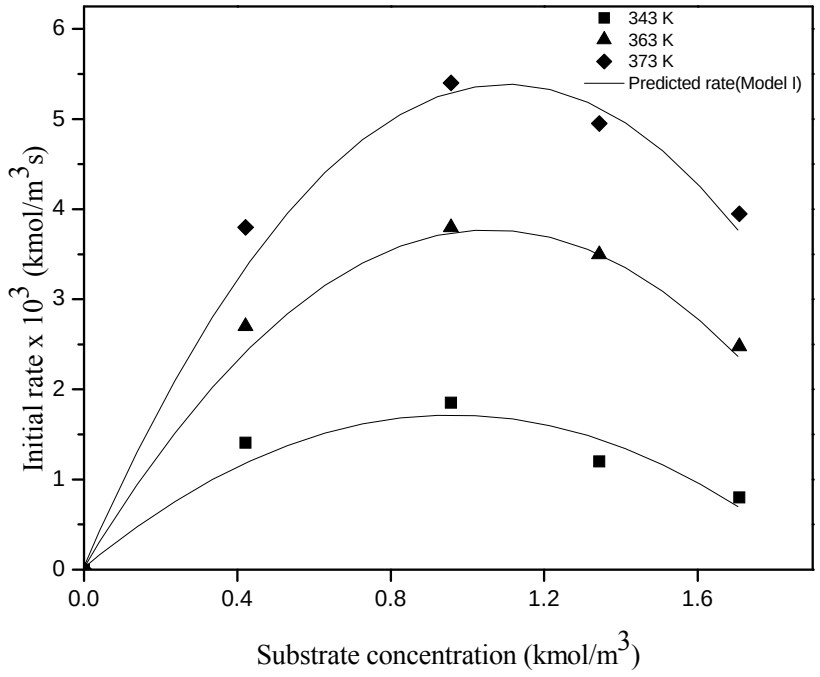

Figure 6.5. Effect of substrate concentration on rate of oxidation of *p*-cresol. Reaction conditions: NaOH : *p*-cresol, 4; catalyst loading, 1.5 kg/m^3; p_{O2}, 0.83 MPa; total reaction volume, 7.2 x 10^{-5} m^3.

It was found that initially the rate of reaction increased with increase in the substrate concentration from 0-1.01 kmol/m^3 and then decreased with further increase in the concentration, indicating the possibility of substrate inhibition kinetics at higher concentrations. Such types of substrate concentration dependence were also observed in case of catalytic hydrogenation reactions and have been successfully accounted for in the kinetic models to be described below [6, 18].

6.3.2.3. Kinetic model

Based on the observed reaction trends with respect to the oxygen partial pressure and the *p*-cresol concentration on the initial rate of reaction and by assuming the conventional Langmuir-Hinshelwood type mechanism, we could propose several forms of rate equations, as given in Table 6.4.

Table 6.4. Various forms of rate expressions

Reaction Mechanism	Formation of alcohol is rate controlling (Surface reaction controlling)	Formation of aldehydes is rate controlling (Surface reaction controlling)
Single Site (Eley- Rideal)	$r = \frac{wk_1K_AC_AC_B}{(1+K_AC_A)}$ *Model I*	$r = \frac{wK_2C_BC_D}{K_D(1+K_AC_A)}$ *Model II*
Dual site LH	$r = \frac{wk_1K_AK_B^{1/2}C_AC_B^{1/2}}{\left(1+K_AC_A+\sqrt{K_BC_B}+\frac{C_D}{K_D}+\frac{C_E}{K_E}\right)^2}$ *Model III*	$r = \frac{w(k_2/K_D)K_B^{1/2}C_B^{1/2}C_D}{\left(1+K_AC_A+\sqrt{K_BC_B}+\frac{C_D}{K_D}+\frac{C_E}{K_E}\right)^2}$ *Model IV*
Dual site LH	$r = \frac{wk_1K_AK_BC_AC_B}{\left(1+K_AC_A+K_BC_B+\frac{C_D}{K_D}+\frac{C_E}{K_E}\right)}$ *Model V*	

The power-law types of rate equations were avoided because the substrate showed an inhibition effect [19]. In order to discriminate the several rate equations listed in Table 6.4, a nonlinear regression analysis was performed using polymath software for each rate equation to obtain the best values of the rate parameters. For this purpose, an optimization program based on the Gauss-Jordan elimination method was used. The objective function was chosen as follows:

$$F = \sum_{j=i}^{N} \left(R'_{Ai} - R_{Ai} \right)_j^2 \qquad (6.4)$$

Where F is the objective function to be minimized (Φ_{min}), representing the sum of squares of the differences between the observed and the predicted rates; N is the number of experimental data; R'_{Ai} and R_{Ai} represents predicted and experimental rates, respectively.

Using the data under kinetic regime, we present the optimized values of rate parameters obtained for 95% confidence and Φ_{min} in Table 6.5.

Table 6.5. Kinetic parameters for different rate models

Model No.	Temp K	k^a	K_A m^3 / kmol	K_B m^3 / kmol	Φ_{min}
I	343	0.169×10^{-4}	1.153		1.813×10^{-13}
	363	0.183×10^{-4}	0.910		1.809×10^{-13}
	373	0.215×10^{-4}	0.882		1.820×10^{-13}
II	343	0.164×10^{-4}	1.153		1.913×10^{-13}
	363	0.179×10^{-4}	0.910		1.809×10^{-13}
	373	0.190×10^{-4}	0.882		1.820×10^{-13}
III	343	-10.11	-0.98×10^3	5.82×10^7	2.310×10^{-14}
	363	-9.37	-1.12×10^3	4.97×10^7	1.893×10^{-14}
	373	-8.83	-1.51×10^3	4.88×10^7	2.632×10^{-15}
IV	343	1.133×10^4	-0.98×10^3	5.82×10^7	1.236×10^{-10}
	363	1.279×10^4	-1.12×10^3	4.97×10^7	2.162×10^{-11}
	373	1.339×10^4	-1.51×10^3	4.88×10^7	2.702×10^{-11}
V	343	-5.69×10^{-4}	-0.972×10^3	18.32	1.772×10^{-11}
	363	-4.41×10^{-4}	-0.832×10^3	15.2	2.832×10^{-12}
	373	-3.41×10^{-4}	-1.186×10^3	14.19	2.702×10^{-11}

[a] Units of k are m^3/kg.s for model I; $(m^3)^2$/(kmol . kg. s) for models II and IV; (kmol/kg. s) for models III and V.

For the purpose of model discrimination, other criteria suggested by Froment and Bischoff were also considered [20]. It was found that the values of rate parameters were less than zero for models III and V; hence, these models were rejected. In the cases of models IV and V, the values of Φ_{min} were higher than those for other models. Models I and II satisfied the criteria and were found to fit the data with almost equal degrees of accuracy, as indicated by the Φ_{min} values. Both these models were developed using the reaction scheme 6.1 involving the reaction between single site adsorption of *p*-cresol with molecular of O_2 from the bulk liquid (Eley-Rideal mechanism). However, in case of model I, formation of PHB-alcohol is a rate-controlling step (no. 2, scheme 6.2) while for model II, formation of PHB-aldehyde is a rate-controlling step (no. 4, scheme 6.2). It was observed that the rates predicted by model I matched well with the experimental values for different reaction conditions (Figures 6.4, 6.5). The suitability of the rate model (I) was further confirmed by comparing the predicted and experimental concentration vs. time data, by developing a semi-batch reactor model discussed below. The temperature dependence of rate parameters is shown in Figure 6.6, from which the activation energy was estimated as 39.6 kJ/mol.

1) A + s ⇌ A.s

2) A.s + B → D.s

3) D.s ⇌ D + s

4) D.s + B → E.s + H_2O

5) E.s ⇌ E + s

6) E.s + B → F.s

7) F.s ⇌ F + s

8) D + C → G

Scheme 6.2. Single site adsorption of *p*-cresol, followed by its reaction with O_2 in the bulk liquid.

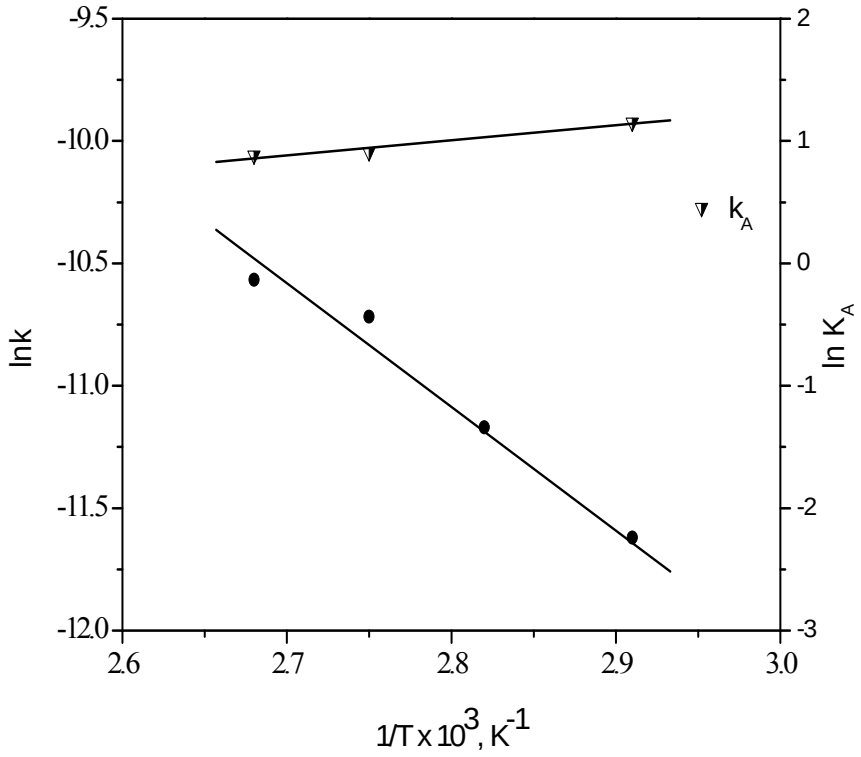

Figure 6.6. Temperature dependence of kinetic parameters.

The adsorption coefficient (K_A) obtained for model I showed the usual trend of decrease in the values of adsorption coefficient with temperature (Table 6.5).

6.3.2.4. Semi batch reactor model

The suitability of the proposed rate model I was further verified under integral conditions also. For this purpose, the experimental data on the liquid phase concentrations of *p*-cresol, PHB-alcohol and PHB-aldehyde as a function of time were also obtained. The variation of *p*-cresol concentration can be represented by the following mass balance equation:

$$-\frac{dC_A}{dt} = \frac{wk_1 K_A C_A C_B}{\left(1 + K_A C_A\right)} \tag{6.5}$$

with initial conditions,

$$t = 0, \quad C_A = 0 \tag{6.6}$$

Formation of PHB-alcohol using reaction stoichiometry can be represented by the following equation:

$$\frac{dC_D}{dt} = \frac{dC_A}{dt} = \left[\frac{wk_1 K_A C_A C_B}{\left(1 + K_A C_A\right)}\right] \tag{6.7}$$

with initial conditions,

$$t = 0, \quad C_D = 0 \tag{6.8}$$

Formation of PHB-aldehyde can be represented by the following equation:

$$\frac{dC_E}{dt} = \frac{dC_A}{dt} = \left[\int_0^{t_1} \frac{dC_A}{dt} + \int_{t_1}^{t_2} \frac{wk_1 K_A C_A C_B}{\left(1 + K_A C_A\right)^{1.2}} \right] \tag{6.9}$$

with initial conditions,

$$t = 0, \quad C_E = 0 \tag{6.10}$$

Equations (6.5- 6.9) were solved numerically using a Runge-Kutta method to obtain the concentrations of *p*-cresol, PHB-alcohol and PHB-aldehyde as a function of time. The intrinsic rate parameters given in Table 6.5 were used for model I in Eqs. 6.5-6.9. The predictions for model I were compared with the experimental concentration-time data and the results are presented in Figure 6.7, from which it is clear that the prediction results of model I match very well with the experimental data.

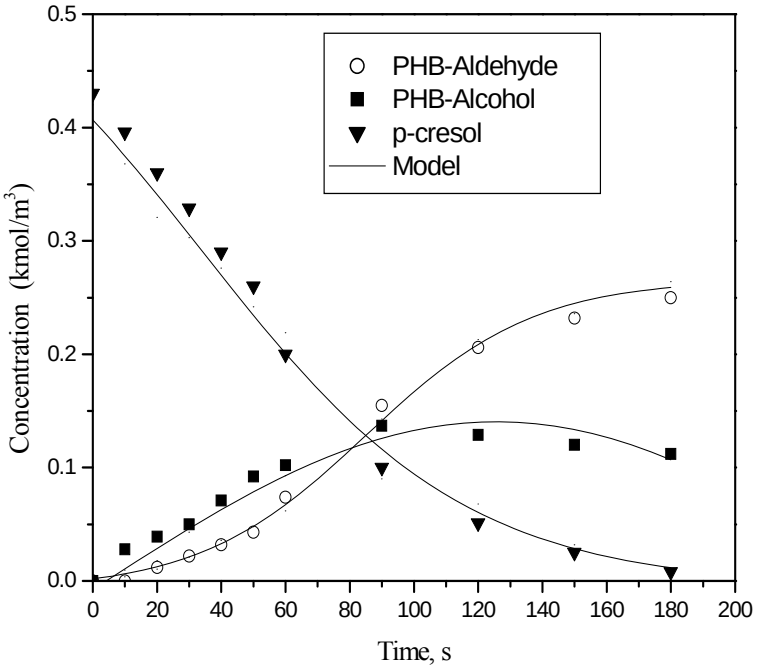

Figure 6.7. Concentration-time profile predicted by the model I
Reaction conditions: temperature, 373 K; NaOH : *p*-cresol, 4; catalyst loading, 1.5 kg/m^3; agitation, 900 rpm; total reaction volume 7.2 x 10^{-5} m^3; p_{O2}, 0.1 MPa.

6.4. Conclusions

Liquid phase air oxidation of *p*-cresol was studied in a slurry reactor over Co_3O_4 catalyst. This catalyst was found to give complete conversion of *p*-cresol with > 95% selectivity to *p*-hydroxybenzaldehyde. A systematic study on the effects of major reaction parameters like O_2 pressure, substrate concentration and temperature on the initial rate of *p*-cresol oxidation was carried out. The initial rate of reaction was found to be first order with respect to the oxygen partial pressure, while it was initially first-order and then became negative-order at higher substrate (*p*-cresol) concentration. Quantitative assessment of

external mass transfer resistances showed that these resistances were unimportant under the conditions used for kinetic study. Based on the trends observed, several L-H type rate equations were proposed and the selected rate model was verified under integral reactor conditions. The model predictions and the experimental data were found to be in good agreement over a wide range of conditions, and hence, can be useful for the design purposes.

6.5. Nomenclature

A	*p*-cresol
B	oxygen
C_A	concentrations of *p*-cresol, kmol/m^3
C_B	concentrations of oxygen, kmol/m^3
C_D	concentrations of PHB-alcohol, kmol/m^3
C_E	concentrations of PHB-aldehydes, kmol/m^3
D	PHB-alcohol
De	Effective diffusivity, m^2/s
dp	Catalyst particle diameter, m
E	PHB-aldehyde
F	PHB-acid
G	PHBME
k_1	reaction rate constants, m^3/kg.s
K_A, K_B, K_C,	adsorption equilibrium constants, m^3/kmol
R_{Ai}	initial reaction rate of *p*-cresol oxidation

R'_{Ai}	predicted initial reaction rate of *p*-cresol oxidation
r	rate of oxidation of *p*-cresol, kmol/m^{3}s
t	time, s
T	temperature, K
w	catalyst loading, kg/m^3

6.6. References

1. C.V. Rode, M.V. Sonar, J.M. Nadgeri, R.V. Chaudhari, *Org. Proc. Res. Dev*. **2004**, *8*, 873.
2. C. V. Rode, V. S. Kshirsagar, J. M. Nadgeri, K. R. Patil *Ind. Eng. Chem. Res*. **2007**, *46,* 8413.
3. V. S. Kshirsagar, S. Vijayanand, H. S. Potdar, P. A. Joy, K. R. Patil, C. V. Rode, *Chem. Lett*. **2008**, *37*, 310.
4. V. S. Kshirsagar, K. R. Patil, M. Shirai, C. V. Rode, *Top. Catal*. **2009** *52,* 784.
5. V. S. Kshirsagar, A. C. Garade, K. R. Patil, R. K. Jha, C. V. Rode, *Ind. Eng. Chem. Res* **2009** (*10.1021/ie801941e*)
6. M. Oku, K. Hirokawa, *J. Electron Spectrsc*. **1976**, *8*, 475.
7. A. Bielanski, J. Haber *Catal. Rev.-Sci. Eng*. **1979**, *19*, 1.
8. F. Wang, J. Xu, S. Liao, *Chem. Commun*. **2002**, *6*, 626.
9. D. Grier, G. MacCarthy, JCPDS-ICDD, PDF database, **1991**.

10. C.M. Shen, Y.K. Su, H.T. Yang, T.Z. Yang, H.J. Gao, *Chem. Phys. Lett*. **2003**, *373*, 39.

11. C.V. Rode, M.M. Telkar, R. Jaganathan, R.V. Chaudhari, *J. Mol. Catal. A: Chem*. **2003,** *200*, 279.

12. R.V. Malayala, C.V. Rode, M. Arai, S. G. Hegde, R. V. Chaudhari, *Appl. Catal. A: Gen*. **2000**, *193*, 71.

13. C.V. Rode, R.V. Chaudhari, *Ind. Eng. Chem. Res*. **1994**, *33*, 1645.

14. R.V. Chaudhari, R.V. Gholap, G. Emig, H. Hofmann, *Can. J. Chem. Eng*. **1987**, *65*, 774.

15. Y. Sano, N. Yamaguchi, T. Adachi, *J. Chem. Eng. Jpn*. **1974**, *1*, 255.

16. C.R. Wilke, P. Chang, *AIChE J*. **1995**, *1*, 264.

17. K. Radhakrishnan, P.A. Ramachandran, P.H. Brahme, R.V. Chaudhari, *J. Chem. Eng. Data*, **1983**, *28*, 1.

18. M. M. Telkar, C.V. Rode, V.H. Rane, R. Jaganathan, R.V. Chaudhari, *Appl. Catal. A: Gen*. **2001**, *216*, 13.

19. S.P. Gupte, R.V. Chaudhari, *Ind. Eng. Chem. Res*. **1992**, *31*, 2069.

20. G. F. Froment, K.B. Bischoff *Chemical Reactor Analysis and Design*; Wiley: New York, **1979**, p. 264.

7. Summary and conclusion

In this work following three types of cobalt based catalysts were developed and thoroughly characterized by physico-chemical methods. All these catalysts were found to catalyze the liquid phase oxidation of *p*-cresol using air as a primary oxidant.

1) Among various cobalt and manganese Schiff base complexes intercalated into the clay materials, Co(salen)-mont catalyst gave the highest activity for *p*-cresol oxidation. The complexes were intercalated in montmorillonite, saponite type clays. Intercalation of the cobalt salen was confirmed mainly by DRUV, FT-IR, XPS, XAFS, XANES, DT-TGA techniques. A distinct shift in decomposition temperature for cobalt-salen intercalated into montmorillonite as well as the formation of an additional Co-O bond (bond length of 0.199 nm) as observed from EXAFS studies confirmed the host-guest relationship between cobalt-salen and montmorillonite clay. The cobalt-salen intercalated into montmorillonite catalyst gave a TON as high as 150 as against TON 29 for homogeneous catalyst with a selectivity of 90 % to the oxyfunctionalized products for air oxidation of *p*-cresol under ambient pressure conditions. This catalyst was found to be an efficient catalyst for air oxidation of *p*-cresol under very mild conditions (338 K and ambient pressure) and the selectivity ratio of *p*-hydoxybenzaldehyde to *p*-hydroxybenzyl alcohol could be manipulated by varying the reaction parameter such as air flow rate. Formation of *p*-hydroxybenzoic acid and other non-oxidation products could be significantly minimized with our catalyst.

2) Second cobalt based catalyst developed was cobalt saponite which becomes a nanocomposite of Co phases over aluminosilicate support. A very interesting and novel finding while using this as a catalyst for liquid phase oxidation of *p*-cresol was that the role of lattice oxygen coordinating with Co^{2+}, first oxidizing the substrate and the vacancy being filled with molecular oxygen under oxidation conditions. Further experimental work involving oxidation with oxygen labeling, kinetic studies and evaluation of the solid state diffusion parameters for lattice oxygen is necessary for proving the Mars van Krevelene pathway for liquid phase oxidation over a solid catalyst.
3) Third type of cobalt catalyst developed was the nanostructured spinel Co_3O_4. This nano structured catalyst was prepared by controlling the aggregation of cobalt-hydroxycarbonate precursor particles by novel simultaneous co-precipitation/digestion technique. This was the first report of highly efficient heterogeneous nano-structured Co_3O_4 (6-8nm) having high surface area ($95 m^2/g$) developed for selective liquid phase air oxidation of *p*-cresol under atmospheric pressure conditions. Nanostructured Co_3O_4 catalyst showed highest TOF ($31\ h^{-1}$)) as compared to its bulk counterpart ($8\ h^{-1}$) under identical reaction conditions. Also the selectivity to oxidation products could be altered by varying the digestion time during preparation of the catalyst. Catalyst reuse studies and leaching test confirmed no leaching of cobalt occurred under the reaction conditions. The approach of work allows the preparation of nano size metal oxides with controlled morphology as efficient catalysts for various other reactions.

In addition to the novel cobalt catalysts developed for Liquid phase air oxidation of *p*-cresol as summarized above, a detailed kinetics of this reaction was also investigated using a commercially available Co_3O_4 catalyst in a slurry reactor using initial rate data. Quantitative assessment of external mass transfer resistances showed that these resistances were unimportant under the conditions used for kinetic study. The initial rate data showed first order dependence on the oxygen partial pressure while it showed negative order dependence at higher concentration of *p*-cresol. Based on the trends observed, several L-H type rate equations were proposed and the selected rate model was verified under integral reactor conditions. The model predictions and the experimental data were found to be in good agreement over a wide range of conditions.

List of publications

Research papers published/communicated in Peer Reviewed International Journals

1. Cobalt-salen Intercalated Montmorillonite Catalyst for Air Oxidation of *p*-Cresol under Mild Conditions

   C. V. Rode, **V. S. Kshirsagar**, J. M. Nadgeri, K. R. Patil *Ind. Eng. Chem. Res*. **2007**, *46*, 8413-8419

2. Reaction kinetics of liquid phase air oxidation of *p*-cresol to *p*-hydroxybenzaldehyde

   V. S. Kshirsagar, J. M. Nadgeri, P. R. Tayade, C. V. Rode *Appl. Catal. A: Gen.* **2008**, *339*, 28-35.

3. Highly Active Nanostructured Co_3O_4 Catalyst with Tunable Selectivity for Liquid Phase Air Oxidation of *p*-Cresol

   V. S. Kshirsagar, S. Vijayanand, H. S. Potdar, P. A. Joy, K. R. Patil, C. V. Rode, *Chem. Lett.* **2008**, *37*, 310-311.

4. Selective hydroxyalkylation of phenol to bisphenol F over dodecatungstophosphoric acid (DTP) impregnated on fumed silica

   A. C. Garade, **V. S. Kshirsagar,** C. V. Rode, *Appl. Catal. A: Gen.* **2009**, *354*, 176-182.

5. Liquid Phase Oxidation of *p*-Cresol over Cobalt Saponite

   V. S. Kshirsagar, K. R. Patil, M. Shirai, C. V. Rode, *Top. Catal.* **2009**, *52*, 784-788.

6. Heterogeneous Cobalt-Saponite Catalyst for Liquid Phase Air Oxidation of *p*-Cresol

   V. S. Kshirsagar, A. C. Garade, K. R. Patil, R. K. Jha, C. V. Rode, *Accepted ,in Ind. Eng. Chem. Res* **2009**.*(* doi *10.1021/ie801941e).*

7. Characterization of Clay Intercalated Cobalt Salen Catalyst for the Oxidation of *p*-Cresol

   V. S. Kshirsagar, A. C. Garade, K. R. Patil, A. Yamaguchi, M. Shirai, C. V. Rode *under revision Appl. Catal. A: Gen.* **2009**.

8. γ-Irradiation-induced synthesis of cobalt nanoparticles for liquid phase air oxidation of *p*-cresol.

   V. S. Kshirsagar, A. C. Garade, K. Navinkumar, A. A. Athavale, C. V. Rode, *to be communicated* in *ACS Nano* **2009**.

Posters/oral presentation for national/international symposium

1. Montmorillonite intercalated cobalt complexes for liquid phase oxidation of *p*-cresol to *p*-hydroxybenzaldehyde.

   C. V. Rode, **V. S. Kshirsagar,** J. M. Nadgeri, M. Shirai, *Fifth Tokyo Conference on Advanced Catalytic Science and Technology* July 23rd-July 28th , 2006 Tokyo, Japan.

2. Selective liquid phase oxidation of *p*-cresol to *p*-hydroxybenzaldehyde using solid catalysts.

   V. S. Kshirsagar, and C. V. Rode, *Science day poster presentation at National Chemical Laboratory*, Pune February 2006 (POSTER presentation)

3. Smectite clay intercalated transition metal complexes for liquid phase oxidation of *p*-cresol to *p*-hydroxybenzaldehyde.

   C. V. Rode, **V. S. Kshirsagar**, J. M. Nadgeri *The sixth International Symposium on Catalysis in Multiphase Reactors (CAMURE-6) and the fifth International Symposium on Multifunctional Reactors (ISMR-5)*, 14-16 JAN 2007, Pune, India (ORAL presentation)

4. Modified palladium catalyst for selective hydrogenation of styrene oxide to 2-phenethylalcohol.

   V. S. Kshirsagar, C. V. Rode and M. M. Telkar, *The sixth International Symposium on Catalysis in Multiphase Reactors (CAMURE-6) and the fifth International Symposium on Multifunctional Reactors (ISMR-5),* 14-16 JAN 2007, Pune, India (POSTER presentation)

5. Modified palladium catalyst for selective hydrogenation of styrene oxide to 2-2-phenethylalcohol.

   V. S. Kshirsagar, and C. V. Rode, Science day poster presentation at National Chemical Laboratory, Pune February 2007 (POSTER presentation)

6. Catalytic transfer hydrogenation of styrene oxide to 2-phenyl ethanol: a kinetic study in a batch slurry reactor.

   Rode C. V, **Kshirsagar V. S**., Rane V. H. and Chaudhari R. V presented in ***ChemCon' 2003****, Indian Chemical Engineers Association*, in Bhubaneswar, Orissa (India).

7. Atmospheric air oxidation of *p*-cresol catalyzed by Co (II) complexes intercalated between silicate layers of smectite

   V. S. Kshirsagar, M. Shirai, C. V. Rode, Poster presented in *CATWORKSHOP 2008*, organized *Catalysis Society of India*, Bhubaneswar, Orissa (India)
8. Liquid phase atmospheric air oxidation of *p*-cresol catalyzed by heterogeneous Co (II) oxo complexes.

   V. S. Kshirsagar, and C. V. Rode, Science day poster presentation at National Chemical Laboratory, Pune February 2008 (POSTER presentation)
9. Liquid phase air oxidation of *p*-cresol over Co-saponite catalyst

   V. S. Kshirsagar, V. R. Mate, M. Shirai, C. V. Rode, poster presented in Pre-ICC2008 International Symposium organized by *The Catalysis Society of Japan, KYOTO (JAPAN).*
10. Selectivity tuning using nanostructured Co_3O_4 catalyst for liquid phase air oxidation of p-cresol.

    V. S. Kshirsagar, S. Vijayanand, H. S. Potdar, C. V. Rode, **ORAL** presentation in *CATSYMP-19*, organized by *Catalysis Society of India*, Pune, Maharashtra (India) during 18-21 January 2009
11. Batch air oxidation of *p*-cresol in solution over solid catalyst

    V. S. Kshirsagar, and C. V. Rode, Science day poster presentation at National Chemical Laboratory, Pune February 2009 (POSTER presentation)
12. Reaction kinetics of liquid phase air oxidation of *p*-cresol to *p*-hydroxybenzaldehyde

    V. S. Kshirsagar, C. V. Rode, POSTER presentation in ACEPT2009 organized by National Chemical Laboratory, Pune during 4-6 June 2009.